

AperTO - Archivio Istituzionale Open Access dell'Università di Torino

Petrogenesis and tectonic significance of Neoproterozoic meta-basites and meta-granitoids within the central Dabie UHP zone, China: Geochronological and geochemical constraints

This is the author's manuscript

Original Citation:

Availability:

This version is available <http://hdl.handle.net/2318/1736045> since 2024-12-14T16:56:52Z

Published version:

DOI:10.1016/j.gr.2019.08.005

Terms of use:

Open Access

Anyone can freely access the full text of works made available as "Open Access". Works made available under a Creative Commons license can be used according to the terms and conditions of said license. Use of all other works requires consent of the right holder (author or publisher) if not exempted from copyright protection by the applicable law.

(Article begins on next page)

1 1 **Petrogenesis and tectonic significance of Neoproterozoic**
2
3 2 **meta-basites and meta-granitoids within the central Dabie**
4
5 3 **UHP zone, China: Geochronological and geochemical**
6
7 4 **constraints**
8
9

10
11 5
12 6 Yuan Li ^a, Yi-Can Liu ^{a,*}, Yang Yang ^a, F. Rolfo ^{b,c} and C. Groppo ^b

13 7 ^a CAS Key Laboratory of Crust-Mantle Materials and Environments, School of Earth and Space
14 8 Sciences, University of Science and Technology of China, Hefei 230026, China

15
16 9 ^b Department of Earth Sciences, University of Torino, Via Valperga Caluso 35, 1-10125 Torino,
17 10 Italy

18 11 ^c C.N.R. – I.G.G., Section of Torino, Via Valperga Caluso 35, 1-10125 Torino, Italy
19
20
21

22
23
24
25
26
27
28
29
30
31
32
33
34
35
36
37 18
38 19 *Corresponding author. Tel./fax: +86 551 63600367.

39 20 *E-mail address:* liuyc@ustc.edu.cn (Y.-C. Liu)
40
41 21
42
43
44
45
46
47
48
49
50
51
52
53
54
55
56
57
58
59
60
61
62
63
64
65

Abstract

A combined geochemical (whole-rock elements and Sr-Nd-Pb isotopes, zircon trace elements and Hf isotopes) and geochronological (zircon U-Pb ages) study was carried out on the relatively low-grade meta-basites and meta-granitoids from Longjingguan within the central Dabie ultrahigh-pressure (UHP) metamorphic zone, east-central China. Zircon investigations indicate that the meta-basites were formed at ~772 Ma and subsequently experienced granulite-facies metamorphism at ~768 Ma and a later thermal overprint at ~746 Ma, while the meta-granitoids recorded three groups of zircon ages at ca. 819 Ma, 784 Ma and 746 Ma. The meta-granitoids can be subdivided into low-Si and high-Si types, and they were derived from mid-Neoproterozoic partial melting of the Neoproterozoic and Paleoproterozoic metamorphic basement rocks of the South China Block, respectively. These Neoproterozoic zircon ages are consistent with the protolith ages of the Dabie Triassic UHP meta-igneous rocks. In addition, the low-grade rocks have bulk-rock Pb isotope compositions overlapping with the UHP meta-igneous rocks. Therefore, the low-grade meta-basites and meta-granitoids could be interpreted as counterparts of the UHP meta-igneous rocks in this area, suggesting the same petrogenesis for their protoliths in the Neoproterozoic.

Trace element patterns indicate that the low-grade rocks have better preserved their protolith compositions than their equivalent UHP rocks, and thus they are more suitable for elucidating the Neoproterozoic evolution of the northern margin of the South China Block. Zircon ages combined with geochemical features strongly suggest that the protoliths of the meta-granitoids and meta-basites were formed in a magmatic arc and a continental rifting setting, respectively. More specifically, the granitoids derived from partial melting of Neoproterozoic and Paleoproterozoic basement materials at ~819 Ma in a magmatic arc setting, whereas the precursors of the meta-basites are products of a continental rifting event at about 784 to 772 Ma. The obtained results provide new geochronological and geochemical constraints for the Neoproterozoic evolution of the northern margin of the South China Block, which can further

1 51 contribute to the understanding of the breakup of the supercontinent Rodinia.

2 52

3
4 53 **Keywords:** Neoproterozoic evolution; meta-basite and meta-granitoid; Rodinia

5
6 54 assembly and break-up; continental rifting; continental collision

7
8 55

9
10
11
12
13
14
15
16
17
18
19
20
21
22
23
24
25
26
27
28
29
30
31
32
33
34
35
36
37
38
39
40
41
42
43
44
45
46
47
48
49
50
51
52
53
54
55
56
57
58
59
60
61
62
63
64
65

1. Introduction

The Dabie orogen located in central China is a continental collision belt with the exposed largest area of coesite- and diamond-bearing ultrahigh-pressure (UHP) metamorphic rocks in the world, and thus it has attracted great research interest in the geologic community during the past decades (e.g., Okay et al., 1989, 1993; Wang et al., 1989; Xu et al., 1992a,b, 2003; Li et al., 1993, 2000; Ames et al., 1996; Rowley et al., 1997; Hacker et al., 1998, 2000; Rolfo et al., 2000, 2004; Zheng et al., 2006; Liu et al., 2007a,b, 2011a,b, 2015; Groppo et al., 2015). Previous studies focused mainly on the Triassic UHP metamorphism and related processes, whereas less attention has been paid to the nature and origin of the protoliths of the UHP rocks (e.g., Ames et al., 1996; Hacker et al., 1998; Zheng et al., 2006). U-Pb dating in magmatic zircon cores demonstrated that the protoliths of the UHP meta-igneous rocks in the Dabie orogen were formed in the Neoproterozoic (e.g., Rowley et al., 1997; Hacker et al., 1998; Liu et al., 2007a,b), likely under a continental rifting setting related to the breakup of the supercontinent Rodinia (Li et al., 2003a,b,c). However, the detailed Neoproterozoic evolutionary processes of the area have not been well understood, and the precise onset of the continental rifting is still not well constrained. UHP rocks usually experience complex evolution including interaction with melt and/or fluids that can significantly modify the elemental and isotopic characteristics of the rocks (e.g., Kessel et al., 2005; Hermann et al., 2006; Zheng et al., 2011), making it challenging to reveal their protolith nature and origin.

Apart from the UHP rocks, relatively low-grade metamorphosed rocks have been identified in several localities within the UHP metamorphic zone in the Dabie orogen (e.g., Dong et al., 1997; Gao et al., 2006); these rocks occur as interlayers or tectonic blocks within the UHP units, but yield much lower peak-metamorphic temperatures and pressures. If these rocks can be proved to be counterparts of the UHP rocks that escaped UHP metamorphism, they should be good candidates to reveal the Neoproterozoic evolution of the area. Previous studies about the rocks in the Dabie orogen mainly concentrated on geochronology investigations, while their elemental

1 85 and isotopic signatures have not been studied in detail so far, and their petrogenesis
2 86 and tectonic setting are still not well constrained.

3
4 87 Recently, some relatively low-grade meta-basites and meta-granitoids have been
5
6 88 for the first time recognized at Longjingguan, within the central Dabie UHP
7
8 89 metamorphic zone (Fig. 1). In this paper we perform integrated investigations on their
9
10 90 mineral compositions, whole-rock elements and Pb isotopes, as well as zircon
11
12 91 SHRIMP U-Pb dating, REE and Hf isotopes. The aim of the study is to investigate
13
14 92 whether the rocks are counterparts of the UHP meta-igneous rocks and, if so, whether
15
16 93 the rocks preserved their protolith compositions better than the UHP rocks. These new
17
18 94 data are crucial for better understanding the formation and tectonic evolution of the
19
20 95 Precambrian basement of the South China Block (SCB), especially the events related
21
22 96 to the Neoproterozoic breakup of the supercontinent Rodinia.
23
24
25 97

27 98 **2. Geological setting and samples**

28 99 *2.1. Geological setting*

29
30 100 The Dabie orogen located in the middle portion of the
31
32 101 Qinling–Tongbai–Dabie–Sulu orogenic belt is formed by the Triassic subduction of
33
34 102 the SCB beneath the North China Block (NCB) and exposed the largest area of UHP
35
36 103 rocks in the world. The widespread occurrence of coesite- (Okay et al., 1989; Wang et
37
38 104 al., 1989) and diamond-bearing (Xu et al., 1992b) rocks in the orogen provides an
39
40 105 excellent natural laboratory for investigating evolutionary processes of the orogen, as
41
42 106 well as formation and exhumation mechanisms of UHP rocks. The orogen is generally
43
44 107 divided into five fault-bounded rock units with different metamorphic grades and
45
46 108 histories, which are from south to north: the Susong complex zone (SZ), the South
47
48 109 Dabie low-T eclogite zone (SDZ), the Central Dabie UHP zone (CDZ), the North
49
50 110 Dabie complex zone (NDZ) and the Beihuaiyang zone (BZ) (Xu et al., 2003, 2005;
51
52 111 Liu et al., 2005, 2007a,b, 2011a,b; Zheng et al., 2005; Liu and Li, 2008; Li et al.,
53
54 112 2017). These five units are separated by the near E-W trending Taihu–Shanlong,
55
56 113 Hualiangting–Mituo, Wuhe–Shuihou and Xiaotian–Mozitan faults, respectively (Fig.

1
2
3
4
5
6
7
8
9
10
11
12
13
14
15
16
17
18
19
20
21
22
23
24
25
26
27
28
29
30
31
32
33
34
35
36
37
38
39
40
41
42
43
44
45
46
47
48
49
50
51
52
53
54
55
56
57
58
59
60
61
62
63
64
65

114 1). Although the meta-igneous rocks in the five units exhibit different metamorphic
115 histories, they have similar Neoproterozoic protolith ages reflecting a regional-scale
116 magmatism related to the Rodinia break-up (e.g., Ames et al., 1996; Rowley et al.,
117 1997; Hacker et al., 1998; Liu et al., 2007a,b, 2011a).

118 UHP index minerals like coesite and diamond were found in different lithologies
119 from the CDZ (e.g., Okay et al., 1989; Wang et al., 1989; Xu et al., 1992b; Schertl et
120 al., 1994; Su et al., 1996; Rolfo et al., 2000, 2004), demonstrating that the CDZ was
121 involved in a deep subduction and experienced **Triassic** UHP metamorphism as a
122 coherent unit (Xu et al., 1992b, 2003; Li et al., 1993, 2000; Hacker et al., 1998; Rolfo
123 et al., 2004; Liu and Li, 2008). Evidence of UHP metamorphism like coesite
124 pseudomorphs were later discovered also in the low-T eclogites from the SDZ (Li et
125 al., 2004). Eclogites (Wei et al., 1998; Xu et al., 2000; Liu et al., 2001) or eclogite
126 relics (Tsai and Liou, 2000; Xiao et al., 2001) were also recognized in the NDZ,
127 together with diamond inclusion within zircon and other clues of UHP metamorphism
128 (Tsai et al., 2000; Xu et al., 2000, 2003, 2005; Liu et al., 2007b, 2011b). Moreover,
129 the NDZ (Liu et al., 2000; Xie et al., 2001; Liu et al., 2005, 2007a,b, 2011a) and the
130 SDZ (Li et al., 2004) were confirmed to be segments of the Triassic subducted
131 continental crust of the SCB. This implies that the three eclogite-bearing units in the
132 Dabie orogen all experienced the Triassic deep subduction, although they have
133 different lithological and isotopic compositions and metamorphic histories (Liu and Li,
134 2008).

135 In recent years, relatively low-grade meta-igneous rocks with Neoproterozoic
136 protolith ages and Triassic metamorphic ages have been recognized within the
137 Dabie-Sulu UHP belt. For example, some meta-igneous rocks in Ganghe provided
138 Rb-Sr isochronal ages of 232 ± 8 Ma and Ar-Ar ages of 770-780 Ma, as well as
139 magmatic zircon U-Pb ages of 760–800 Ma (Dong et al., 1997; Gao et al., 2006).
140 These ages indicate that these rocks formed in the Neoproterozoic and experienced
141 Triassic metamorphism, with peak metamorphic temperatures between the closure
142 temperatures of Rb-Sr and Ar-Ar isotopic systems. Different from the UHP rocks,
143 they experienced a relatively low-grade metamorphism (greenschist- to

1 144 low-amphibolite-facies) during the Triassic (Dong et al., 1997; Liu et al., 2017 and
2 145 references therein), indicating that they were exhumed from much shallower depths.
3
4 146 Similar granitic gneisses/meta-granites, meta-basites with Neoproterozoic protolith
5
6 147 ages have also been recognized in the BZ, the northern sector of the Dabie orogen
7
8 148 (e.g., Hacker et al., 2000; Xie et al., 2002; Chen et al., 2003; Jiang et al., 2005; Zheng
9
10 149 et al., 2005; Liu et al., 2006a, 2010, 2011c, 2017; Wu et al., 2007). These rocks have
11
12 150 identical amphibole Ar-Ar (Hacker et al., 2000) and zircon U-Pb ages (Jiang et al.,
13
14 151 2005; Liu et al., 2010, 2017) of ~750 Ma, suggesting that their peak metamorphic
15
16 152 temperatures during the Triassic were lower than the closure temperatures of the
17
18 153 amphibole Ar-Ar dating system (<500 °C). These protolith ages are in agreement with
19
20 154 those of the UHP eclogites and orthogneisses (e.g., Ames et al., 1996; Rowley et al.,
21
22 155 1997; Hacker et al., 1998; Liu et al., 2007a,b, 2011a), as well as the Neoproterozoic
23
24 156 mafic dykes and granites widely distributed along the northern margin of the SCB,
25
26 157 thus they are generally considered to be closely related (Zhao and Zhou, 2009; Hong
27
28 158 et al., 2009; Xue et al., 2011; Wang et al., 2013). It is consequently thought that these
29
30 159 Neoproterozoic meta-granites and meta-basites were once skin layers of the SCB,
31
32 160 detached from the subducted slab during the initial stages of the subduction, and
33
34 161 overthrust onto the southern margin of the NCB (e.g., the BZ), or into the UHP
35
36 162 metamorphic zone (e.g., Ganghe) during the Triassic continental collision.
37
38

39 163 In addition to the locations described above, the relatively low-grade
40
41 164 meta-basites and meta-granitoids have been discovered at Longjingguan within the
42
43 165 central Dabie UHP zone (Fig. 1). So far, their petrogenesis, emplacement time and
44
45 166 relationship with the adjacent UHP rocks have not been studied in detail.
46
47

48 167

49 168 2.2. Petrography and mineral chemistry

50
51 169 Fourteen samples were collected from the Longjingguan area, including six
52
53 170 meta-basites (samples 11LJG3-4-5-6-7-8) and eight meta-granitoids (samples 11LJG2,
54
55 171 1202LJG3, 1209LJG5, 1303LJG2, 1303LJG4, 1209LJG1, 1209LJG3 and 1209LJG4).
56
57 172 Their outcrops are concentrated within an area of few tens of square meters marked
58
59 173 by the black star in Figure 1. All the samples were collected as far as possible from
60
61
62
63
64
65

174 the contact with different lithologies, to avoid possible interaction between them.

175 The meta-basites occur as tectonic lenses within meta-granitoids (Fig. 2), with
176 the margins slightly deformed; the surface is locally characterized by few
177 light-coloured, weakly deformed spots of about 0.5 mm in size. The meta-basite
178 generally contains fine-grained symplectites mainly consisting of plagioclase and
179 amphibole. **The symplectite composed of plagioclase and amphibole points to the**
180 **replaced former mineral, rather than derived** from magma crystallization. Accessory
181 minerals are rutile, titanite, ilmenite and magnetite. A few amphibole porphyroblasts
182 occur in the meta-basites, and they contain inclusions of plagioclase, plagioclase +
183 rutile, rutile, rutile + ilmenite and rutile + titanite (Figs. 3a & b).

184 Electron microprobe analyses were carried out on representative minerals of three
185 samples 11LJG7, 1209LJG5 and 1209LJG1, which represent the **meta-basites**, low-Si
186 meta-granitoids and high-Si meta-granitoids, respectively. The results are listed in
187 **Supplementary** Table 1.

188 The meta-granitoids are subdivided into two types, named low-Si and high-Si
189 meta-granitoids, respectively, according to their bulk-rock SiO₂ content
190 (**Supplementary** Table 2). The low-Si meta-granitoid is mainly composed of
191 plagioclase (with K-feldspar exsolutions), quartz, and biotite, with minor amphibole
192 and apatite (Fig. 3c-d), while the high-Si meta-granitoid is dominated by quartz and
193 K-feldspar, with rare allanite, muscovite and amphibole (Figs. 3e-f). Minerals in the
194 meta-granitoids vary from few tens of microns to hundreds of microns in size,
195 significantly coarser than those in the matrix of the meta-basites. The structure varies
196 from gneissic, with a poorly developed foliation (Fig. 3c-d), to granoblastic (Figs.
197 3e-f).

198

199 2.2.1. 11LJG7

200 In this meta-basite sample, amphibole occurs as fine grains in the symplectitic
201 matrix or as porphyroblasts. Both porphyroblasts and the fine-grained amphibole in
202 the matrix are magnesiohornblende: the porphyroblasts have lower Mg[#] values
203 (72~73) and higher TiO₂ contents (0.26~0.35 wt%) than the fine grains in the matrix

1 204 (Mg[#]=79~81; TiO₂=0.02~0.13 wt%). Plagioclase is an oligoclase (Supplementary
2 205 Table 1). Two rutile inclusions within amphibole porphyroblast have Zr contents of
3 206 277 and 735 ppm, respectively. Rutile inclusions in Neoproterozoic metamorphic
4 207 zircon domains (see Section 4.2) have higher Zr contents, in the range 2107-2519 ppm
5
6 208 (Supplementary Table 3).
7
8
9

10 209

11 210 2.2.2. 1209LJG5

12 211 This low-Si meta-granitoid sample exhibits a weak foliation defined by biotite
13 212 and amphibole preferred orientation (Figs. 3c-d). Plagioclase is oligoclase (An₁₉₋₃₀)
14 213 and contains K-feldspar (Or₉₂₋₉₆) exsolutions. Amphibole is a ferro-edenite /
15 214 ferropargasite, with X_{Ca}=0.76–0.77 [X_{Ca}=Ca/(Ca+Na+K)] and X_{Fe}=0.66–0.68
16 215 [X_{Fe}=Fe/(Fe+Mg)]. Biotite has low Mg[#] (~36) and variable TiO₂ contents (3.68 to
17 216 4.12 wt%).
18
19
20
21
22
23
24
25
26

27 217

28 218 2.2.3. 1209LJG1

29 219 This high-Si meta-granitoid sample consists mainly of K-feldspar and quartz,
30 220 with minor allanite (Fig. 3e). The K-feldspar contains about 6% albite end-member
31 221 component.
32
33
34
35
36

37 222

38 223 2.3. Thermobarometry

39 224 Thermobarometric methods were applied on the meta-basite sample 11LJG7. The
40 225 main amphibole–plagioclase symplectitic assemblage gives a P-T range of
41 226 478-541 °C, 2.2-3.4 kbar (i.e. lower-T boundary of the amphibolite-facies) based on
42 227 the amphibole-plagioclase thermometer (Holland and Blundy, 1994) and the
43 228 Al^{Tot}-in-amphibole barometer (Schmidt, 1992).
44
45
46
47
48
49

50 229 Rutile inclusions within amphibole porphyroblast yield temperatures of
51 230 651-737 °C based on their Zr contents (Tomkins et al., 2007), with the pressure set to
52 231 ~12 kbar according to the coexistence of rutile, ilmenite and titanite (Bohlen and
53 232 Liotta, 1986; Angiboust and Harlov, 2017). Rutile inclusions in Neoproterozoic
54 233 metamorphic zircon domains (see Section 4.2) yield significantly higher temperatures
55
56
57
58
59
60
61
62
63
64
65

1 234 of about 850-870 °C. In the application of Zr-in-rutile thermometer, rutile
2 235 measurements with Si > 200 ppm should be excluded from further analysis if the Zr
3 236 concentration is substantially higher than that of other rutiles in the same sample
4
5 237 (Zack et al., 2004); accordingly, data of three analytical spots (No. 2, 3 and 4,
6
7 238 Supplementary Table 4) were excluded. In addition, the analytical spot No. 1
8
9 239 (Supplementary Table 4) was also excluded because of extremely low total contents.

10
11
12 240 Overall, thermobarometric results suggest that rutile inclusions within
13 241 Neoproterozoic metamorphic zircon domains preserve evidence of a HT,
14 242 granulite-facies metamorphic event (840-860°C, ~12 kbar), completely overprinted by
15 243 a later amphibolite-facies event (480-540 °C, 2.2-3.4 kbar), responsible for the
16 244 formation of the amphibole + plagioclase symplectites in the matrix. The
17 245 Neoproterozoic granulite-facies metamorphic event is also supported by the previous
18 246 investigations from the deeply subducted NDZ in Liu et al. (2007a). Rutile inclusions
19 247 within amphibole porphyroblasts were likely partially reequilibrated during the late
20 248 amphibolite-facies metamorphic event, due to the lack of protection by rigid
21 249 "container" such as zircon, thus indicating temperatures (652-737 °C) lower than
22 250 those preserved by rutiles included in zircons.

251 252 **3. Analytical methods**

253 Rock-crushing and powdering were performed at the Langfang Laboratory,
254 Hebei Bureau of Geological and Mineral Resources. Zircon grains were separated by
255 the procedures of crushing, heavy-liquid separation, magnetic separation. After that,
256 zircon grains were further selected by hand-picking under a binocular microscope,
257 and mounted in an epoxy mount, which was polished to section the crystals for
258 analyses, with a zircon U–Pb standard TEM (417 Ma) (Black et al., 2003) at Beijing
259 SHRIMP Center, Chinese Academy of Geological Sciences (CAGS).

260 Whole-rock major element composition was analyzed by wet chemical methods
261 at the Langfang Laboratory, Hebei Bureau of Geological and Mineral Resources.
262 Analytical uncertainties have a range from ±1 to ±5% for major elements. Trace

1 263 elements analysis was carried out at the CAS Key Laboratory of Crust-Mantle
2 264 Materials and Environments, University of Science and Technology of China (USTC)
3
4 265 in Hefei, by an Elan DRCII ICP-MS, with analytical uncertainties ranging from $\pm 5\%$
5
6 266 to $\pm 10\%$. Detailed analytical procedures and instrument parameters for trace element
7
8 267 analyses are documented in Hou and Wang (2007). Zircon SHRIMP U–Pb dating was
9
10 268 carried out at the Beijing SHRIMP Center, with transmitted and reflected light
11
12 269 micrographs and CL imaging as a guide to selection of U–Pb dating spot. The detailed
13
14 270 analytical method was described by Compston et al. (1992) and Williams (1998).
15
16 271 Common Pb corrections were made using measured ^{204}Pb , and the data were treated
17
18 272 following Compston et al. (1992) with the ISOPLOT program of Ludwig (2001).
19

20
21 273 Zircon trace elements analyses were performed by LA-ICP-MS at the CAS Key
22
23 274 Laboratory of Crust-Mantle Materials and Environments, USTC in Hefei and the
24
25 275 State Key Laboratory of Continental Dynamics, Northwest University in Xi'an. The
26
27 276 analyses were carried out with pulse rate of 10 Hz, beam energy of 10 J/cm^2 , and spot
28
29 277 diameter of $32 \mu\text{m}$. The detailed parameters of the instrument are similar to those
30
31 278 described by Yuan et al. (2004) and Liu et al. (2011a). Element contents of zircons
32
33 279 were calculated by using Pepita software with the zircon SiO_2 as internal standard and
34
35 280 the NIST610 as external standard. Precision and accuracy of analyses are 2–5% for
36
37 281 REE, Y, Rb, Sr, Nb, Ta, Hf, Th and U at the ppm concentration level, and from 8% to
38
39 282 10% for P, Ti and Pb. The detection limit for the different REE varies from 0.02 to
40
41 283 0.09 ppm.
42

43 284 In situ zircon Lu–Hf isotope analysis were conducted at the Institute of Geology
44
45 285 and Geophysics, the Chinese Academy of Sciences in Beijing, and the School of Earth
46
47 286 Sciences and Engineering, Nanjing University, each using a Neptune multi-collector
48
49 287 ICPMS, with a Geolas 193 nm laser ablation system. Instrumental parameters and
50
51 288 data acquisition followed those described by Wu et al. (2006a). The detailed processes
52
53 289 were shown in Liu et al. (2012). Initial Hf isotope ratios are denoted as $\epsilon_{\text{Hf}}(t)$ values
54
55 290 that are calculated with the reference to the chondritic reservoir (CHUR) at the time of
56
57 291 zircon crystallization. Parameters adopted in this study are: $1.865 \times 10^{-11} \text{ yr}^{-1}$ for the
58
59 292 decay constant of ^{176}Lu (Scherer et al., 2001), 0.282772 and 0.0332 for the $^{176}\text{Hf}/^{177}\text{Hf}$
60
61
62
63
64
65

1
2
3
4
5
6
7
8
9
10
11
12
13
14
15
16
17
18
19
20
21
22
23
24
25
26
27
28
29
30
31
32
33
34
35
36
37
38
39
40
41
42
43
44
45
46
47
48
49
50
51
52
53
54
55
56
57
58
59
60
61
62
63
64
65

293 and $^{176}\text{Lu}/^{177}\text{Hf}$ ratios of the chondrite (Blichert-Toft and Albarede, 1997). Single
294 stage model ages (T_{DMI}) were calculated referred to the depleted mantle with a
295 present day $^{176}\text{Hf}/^{177}\text{Hf}$ ratio of 0.28325, similar to that of the average MORB (Nowell
296 et al., 1998) and $^{176}\text{Lu}/^{177}\text{Hf}$ ratio of 0.0384 (Griffin et al., 2000).

297 Mineral inclusions in zircon were identified using Raman spectroscopy at the
298 CAS Key Laboratory of Crust–Mantle Materials and Environments, University of
299 Science and Technology of China in Hefei, and analyzed using the electron
300 microprobe (EMP) at the Institute of Mineral Resources, CAGS in Beijing. The
301 analytical conditions of the Raman and EMP were reported by Liu et al. (2009). The
302 compositions of the representative minerals in thin sections were detected by EMP at
303 the Department of Resource and Environment Engineering, Hefei University of
304 Technology in Hefei. The accelerating voltage and beam current were 15 kV and
305 15nA, respectively.

306 Rb-Sr, Sm-Nd, and Pb isotopic analyses were performed at the Laboratory for
307 Radiogenic Isotope Geochemistry, in USTC according to the methods of Chen et al.
308 (2000, 2007). Sm, Nd, Rb, and Sr concentrations were determined by isotopic dilution
309 using ^{149}Sm , ^{150}Nd , ^{84}Sr , and ^{85}Rb tracers. The isotopic abundance ratios were
310 determined on a Finnigan MAT 262. Sr and Nd isotopic ratios were corrected for mass
311 fractionation relative to $^{86}\text{Sr}/^{88}\text{Sr} = 0.1194$ and $^{146}\text{Nd}/^{144}\text{Nd} = 0.7219$, respectively.
312 NBS987 and La Jolla standard solutions analyzed along with samples yielded
313 $0.710250 \pm 12 (2\sigma)$ for $^{87}\text{Sr}/^{86}\text{Sr}$ and $0.511860 \pm 12 (2\sigma)$ for $^{143}\text{Nd}/^{144}\text{Nd}$. Measured Pb
314 isotopic ratios were then corrected for instrumental mass fractionation using a value
315 of 0.11% per atomic mass unit inferred from analysis of the reference material
316 NBS981.

317 318 **4. Results**

319 *4.1. Major and trace elements*

320 Whole-rock major and trace elemental compositions of the studied meta-basites
321 and meta-granitoids are listed in **Supplementary** Table 2.

322

323 *4.1.1. Meta-basites*

324 The meta-basite samples 11LJG3-4-5-6-7-8 have uniform bulk-rock
325 compositions. The SiO₂ contents range from 45.72 to 51.81 wt%, Al₂O₃ from 12.46 to
326 14.30 wt%, and MgO from 4.37 to 13.29 wt%. They have high FeO^T (11.47–14.99
327 wt%) and Mg[#] values of 34–67. The TiO₂ contents are also relatively high (2.01–3.42
328 wt%). They are alkalic with Na₂O contents of 1.74–3.55 wt%, K₂O contents of
329 0.77–1.80 wt% and Na₂O/K₂O ratios of 1.25–4.14. Element pairs that have similar
330 bulk D values (solid/melt partition coefficient for modal melting), for example Y-Ho
331 and Eu-Sm, are correlated during magmatic processes (e.g., Workman and Hart, 2005).
332 In the Y vs. Ho and Eu vs. Sm plots (no attachment), all the studied meta-mafic rocks
333 fall along a linear trend, suggesting that they were derived from the same source.

334 In the TAS (Le Bas et al., 1986) and Zr/TiO₂ vs Nb/Y (Winchester and Floyd,
335 1977) diagrams (Fig. 4), the meta-mafic rocks plot very close to the boundary
336 between fields of alkaline and sub-alkaline series. The primitive mantle normalized
337 spider diagram (Fig. 5b) shows that they are enriched in incompatible elements
338 compared to MORB, and have negative anomalies of Sr, Nb and Ta, positive or
339 slightly negative Pb anomalies. They have uniform C1 chondrite normalized REE
340 patterns (Fig. 5a) characterized by enrichment in LREE, slight depletion in HREE and
341 weakly positive or negative Eu anomaly (Eu/Eu*=0.80–1.06). Their (La/Yb)_N
342 (primitive mantle normalized) ratios range from 2.2 to 7.5 and (La/Sm)_N from 1.3 to
343 2.1. The UHP eclogites derived from basaltic protoliths have similar REE patterns and
344 related trace-element contents (Fig. 5c and d).

346 *4.1.2. Low-Si meta-granitoids*

347 The low-Si meta-granitoids (samples 11LJG2, 1209LJG5 and 1202LJG3) have
348 slightly inhomogeneous bulk compositions. The SiO₂ contents range from 60.45 to
349 61.50 wt%, Al₂O₃ from 14.18 to 14.96 wt%, TiO₂ from 1.16 to 1.38 wt% and MgO
350 from 1.60 to 1.86 wt%. They have high FeO^T (7.78–8.29 wt%) with Mg[#] values of
351 0.26–0.31. They have Na₂O ranging from 1.50 to 3.26 wt% and K₂O from 3.11 to

352 4.28 wt% with Na₂O/K₂O ratios of 0.35–1.05. In the TAS diagram, these rocks plot in
353 the field of andesite, close to the boundary with trachy-andesite; in the Zr/TiO₂ vs
354 Nb/Y diagram, they are distributed in the fields of dacite + rhyodacite and
355 trachyandesite. They exhibit significant depletion of HFSE including Nb, Ta, Ti and P,
356 as well as enrichment of Pb (Fig. 5b), which are typical features of crustal-sourced
357 rocks (Rudnick and Gao, 2003). They have identical C1 chondrite normalized REE
358 patterns (Fig. 5a) characterized by enrichment of LREE, weak depletion of HREE and
359 positive Eu anomalies (Eu/Eu* = 1.12–2.00). Their (La/Yb)_N ratios range from 9.59 to
360 17.49 and (La/Sm)_N from 2.77 to 4.02.

361

362 4.1.3. High-Si meta-granitoids

363 Compared to the meta-basites and low-Si meta-granitoids, the high-Si
364 meta-granitoids (samples 1303LJG2, 1303LJG4, 1209LJG1, 1209LJG3 and
365 1209LJG4) have more scattered bulk-rock compositions. The SiO₂ contents range
366 from 67.98 to 80.98 wt%, Al₂O₃ from 8.96 to 11.78 wt%, TiO₂ from 0.17 to 0.54 wt%
367 and MgO from 0.06 to 3.82 wt%. They have low FeO^T (2.09–4.30 wt%) contents with
368 varied Mg[#] values of 0.04–0.62. The Na₂O contents range from 1.12 to 2.99 wt% and
369 K₂O from 2.44 to 5.35 wt% with Na₂O/K₂O ratios of 0.29–0.98. In the TAS diagram,
370 four samples plot into the field of sub-alkaline rhyolite and one sample into that of
371 dacite; in the Zr/TiO₂ vs Nb/Y plot, the studied samples scatter among four categories:
372 comendite + pantellerite, rhyolite, rhyodacite + dacite and trachyandesite. They have
373 trace elements patterns comparable to those of the low-Si meta-granitoids (Fig. 5b),
374 and uniform C1 chondrite normalized REE patterns (Fig. 5a) characterized by
375 enrichment of LREE, slight depletion of HREE and strong negative Eu anomalies
376 (Eu/Eu* = 0.10–0.75). Their (La/Yb)_N ratios range from 10.29 to 49.87 and (La/Sm)_N
377 range from 3.64 to 5.41.

378

379 4.2. Zircon geochronology

380 4.2.1. Zircon morphology and mineral inclusions

381 Zircons from the meta-basites are anhedral to subhedral in shape with smooth

1 382 outlines, and their length-width ratios are generally smaller than 1.5. CL images show
2 383 that most of them have core, mantle and rim structures with clear boundaries between
3
4 384 them. The cores are grey colored with clear or weak oscillatory zoning while the
5
6 385 mantles are light colored and homogeneous (Fig. 6). Some zircon grains have a
7
8 386 mantle **domain** showing gradually darker luminance outwards. The rims are bright,
9
10 387 too thin to be analysed. According to the microstructures, the cores with oscillatory
11
12 388 zoning are interpreted to be of magmatic origin, while the homogeneous cores and
13
14 389 mantles are considered to be metamorphic zircon domains (e.g., Hanchar and Rudnick,
15
16 390 1995; Gebauer et al., 1997; Hermann et al., 2001). Most of the zircon cores exhibit
17
18 391 rounded shapes, suggesting that they were partially resorbed after crystallization,
19
20
21 392 maybe during the formation of the zircon mantles.

22
23 393 As opposed to the meta-basites, zircons from the meta-granitoids exhibit more
24
25 394 regular crystal shapes. Some of the zircons from the meta-granitoids are euhedral in
26
27 395 shape with clear oscillatory zones, indicative of magmatic origin. Other zircons show
28
29 396 core and mantle structures, wherein the cores are dark grey with clear oscillatory
30
31 397 zoning or no zoning, while the mantles are light grey with weak or no oscillatory
32
33 398 zonings. Similarly, the zircons in the meta-granitoids can also be divided into
34
35 399 magmatic (with oscillatory zoning) and metamorphic (no zoning) domains. Generally,
36
37 400 the metamorphic zircon domains from both the meta-**basites** and the meta-granitoids
38
39 401 are granular, platy and prismatic in shape with smooth boundaries, and some of them
40
41 402 retain plenty of mineral inclusions (Fig. 7), which are powerful tools to link zircon
42
43 403 growth to precise metamorphic events (e.g., Gebauer et al., 1997; Hermann et al.,
44
45 404 2001; Liu et al., 2007b, 2011a). The metamorphic zircons in the meta-**basite** sample
46
47 405 11LJG3 contain quartz, plagioclase, apatite, hornblende, K-feldspar, chlorite, epidote,
48
49 406 biotite, rutile, ilmenite and titanite, while those from the meta-granitoid sample
50
51 407 11LJG2 contain K-feldspar, muscovite, epidote and quartz. The compositions of
52
53 408 typical mineral inclusions in metamorphic zircons were detected by electron
54
55 409 microprobe, with the results listed in **Supplementary** Table 3. Biphase inclusions
56
57 410 composed of rutile + titanite or of titanite + ilmenite are recognized in a few
58
59 411 metamorphic zircons from sample 11LJG3.

1 412

2 413 *4.2.2. Zircon REE patterns*

3
4 414 Representative zircon REE contents of the meta-basites (samples 11LJG3 and
5
6 415 11LJG7) and the meta-granitoids (samples 11LJG2, 1202LJG3, 1303LJG2 and
7
8 416 1209LJG5) are listed in **Supplementary** Table 5 (all the analyzed results for zircon
9
10 417 rare earth elements in **Supplementary** Table 6). Zircon cores have almost identical
11
12 418 steep HREE patterns, positive Ce anomalies and negative Eu anomalies (Fig. 8),
13
14 419 typical of magmatic zircon (Hoskin and Ireland, 2000). On the contrary, the REE
15
16 420 patterns of metamorphic zircons are varied. In the meta-basites, most metamorphic
17
18 421 zircons (the cyan lines, Fig. 8a) exhibit higher REE contents than, but similar REE
19
20 422 patterns with, the magmatic zircons, except for one spot that show slightly positive Eu
21
22 423 anomaly; besides, a metamorphic zircon (the black line, Fig. 8a) has almost the same
23
24 424 La, Ce and HREE contents with the magmatic zircons, but it exhibits significantly
25
26 425 higher Pr, Nd, Sm and Eu. In the meta-granitoids, most metamorphic zircons exhibit
27
28 426 similar REE patterns with the magmatic cores, whereas some analyses exhibit higher
29
30 427 REE contents and/or higher LREE/HREE ratios than the magmatic zircons (Fig. 8b-d),
31
32 428 or exhibit no anomaly of Eu.

33
34
35 429
36
37 430 *4.2.3. Zircon SHRIMP U-Pb ages*

38
39 431 In-situ analyses have been performed on different zircon domains, with the
40
41 432 U-Th-Pb data listed in **Supplementary** Table 7 and U-Pb concordia diagram illustrated
42
43 433 in Figure 9.

44
45 434 Magmatic zircon cores from the meta-basite sample 11LJG3 yield a cluster of
46
47 435 concordant $^{206}\text{Pb}/^{238}\text{U}$ age averaging at 772 ± 4 Ma (MSWD=2.0, n=7; Fig. 9a), while
48
49 436 the metamorphic domains give a concordant $^{206}\text{Pb}/^{238}\text{U}$ age group of 768 ± 7 Ma
50
51 437 (MSWD=2.9, n=11; Fig. 9a). In another meta-basite sample 11LJG7, magmatic zircon
52
53 438 domains yield a cluster of concordant $^{206}\text{Pb}/^{238}\text{U}$ age of 772 ± 7 Ma (MSWD=2.5, n=5;
54
55 439 Fig. 9b), and the metamorphic domains give a concordant $^{206}\text{Pb}/^{238}\text{U}$ age group of 746
56
57 440 ± 4 Ma (MSWD=2.6, n=9; Fig. 9b). Summing up, the magmatic zircons yield a
58
59 441 cluster of concordant $^{206}\text{Pb}/^{238}\text{U}$ age at ~ 772 Ma (Ma domains), and the metamorphic

1 442 zircons yield two groups of concordant $^{206}\text{Pb}/^{238}\text{U}$ age at ~768 Ma (Me1 domains) and
2 443 ~746 Ma (Me2 domains), corresponding to magmatism, metamorphism and thermal
3
4 444 overprinting events, respectively.
5

6 445 Zircon cores in the low-Si meta-granitoids (samples 11LJG2, 1202LJG3,
7 446 1209LJG5) have a wide age spectrum spreading from ~800 Ma to ~2500 Ma.
8 447 Analytical spots on zircon cores in sample 11LJG2 are distributed along the concordia
9 448 curve or on a Pb loss line, yielding two upper intercept ages of 1940 ± 140 Ma
10 449 (MSWD=2.1; Fig. 9d) and 2529 ± 38 Ma (MSWD=3.1; Fig. 9d), respectively. Six
11 450 magmatic zircon spots give a concordant $^{206}\text{Pb}/^{238}\text{U}$ age cluster of 838 ± 18 Ma
12 451 (MSWD=0.73, n=6; Fig. 9e), while twelve metamorphic zircon analyses yield two
13 452 concordant $^{206}\text{Pb}/^{238}\text{U}$ age clusters averaging at 797 ± 7 Ma (MSWD=0.54, n=9; Fig.
14 453 10e) and 762 ± 22 Ma (MSWD=0.25, n=3; Fig. 9e), respectively. Zircons in sample
15 454 1209LJG5 plot along the concordia curve, or on a Pb loss line with an upper intercept
16 455 age of 1999 ± 57 Ma and a lower intercept age of 779 ± 49 Ma (MSWD=4.8; Fig. 9g).
17 456 Neoproterozoic magmatic zircons give a concordant $^{206}\text{Pb}/^{238}\text{U}$ age of 839 ± 7 Ma
18 457 (MSWD=0.99, n=6; Fig. 9h), and two analyses on metamorphic zircon yield
19 458 concordant $^{206}\text{Pb}/^{238}\text{U}$ ages of 785 ± 6 Ma and 744 ± 16 Ma, respectively. Three near
20 459 concordant $^{206}\text{Pb}/^{238}\text{U}$ age clusters were obtained from sample 1202LJG3: one age of
21 460 819 ± 12 Ma (MSWD=2.3, n=3; Fig. 9c) from magmatic zircon cores, and two ages
22 461 of 772 ± 7 Ma (MSWD=1.14, n=3; Fig. 9c) and 751 ± 6 Ma (MSWD=0.39, n=3; Fig.
23 462 9c) from metamorphic zircon domains.
24
25
26
27
28
29
30
31
32
33
34
35
36
37
38
39
40
41
42

43 463 Magmatic zircons from the high-Si meta-granitoid sample 1303LJG2 give an
44 464 average concordant $^{206}\text{Pb}/^{238}\text{U}$ age of 813 ± 5 Ma (MSWD=0.99, n=7; Fig. 9f), while
45 465 metamorphic zircons yield two concordant age clusters of 784 ± 7 Ma and 732 ± 6 Ma
46 466 (Fig. 9f). The zircon dating results indicate that the protoliths of the low-Si and
47 467 high-Si meta-granitoids were formed at about 819 ± 12 Ma and 813 ± 5 Ma,
48 468 respectively. The zircons yielding older ages are thus inherited from their source rocks,
49 469 with their original ages preserved or reset by Pb loss, corresponding to the apparent
50 470 concordant or discordant ages.
51
52
53
54
55
56
57
58
59
60
61
62
63
64
65

1 471

2
3 472 *4.3. Zircon Hf isotopes*

4
5 473 Zircon $\epsilon_{\text{Hf}}(t)$ values and T_{DM} ages of two meta-basites (samples 11LJG3 and
6
7 474 11LJG7), three low-Si meta-granitoids (samples 11LJG2, 1209LJG5 and 1202LJG3)
8
9 475 and one high-Si meta-granitoid (sample 1303LJG2) are listed in **Supplementary** Table
10
11 476 8.

12
13 477 The zircons in the meta-basites have $\epsilon_{\text{Hf}}(780 \text{ Ma})$ values from +2.6 to +7.9 (Fig.
14
15 478 10), and corresponded single stage model ages (T_{DM1}) of 1033 to 1248 Ma, slightly
16
17 479 older than their zircon U-Pb ages.

18
19 480 Six inherited zircon cores from low-Si meta-granitoids have $\epsilon_{\text{Hf}}(t)$ values of +7.1
20
21 481 to -6.6, with corresponding T_{DM1} ages of 2359 to 2702 Ma, and T_{DM2} ages of 2506 to
22
23 482 2823 Ma, respectively (Fig. 10). The Neoproterozoic zircon domains in the low-Si
24
25 483 meta-granitoids yield a relatively wide $\epsilon_{\text{Hf}}(800 \text{ Ma})$ spectrum of -3.2 to -12.0, with
26
27 484 T_{DM1} ages of 1513~1819 Ma and T_{DM2} ages of 1893~2446 Ma. Zircons from the
28
29 485 high-Si meta-granitoid have $\epsilon_{\text{Hf}}(800 \text{ Ma})$ values ranging from -7.5 to +1.4, with T_{DM1}
30
31 486 ages of 1313~1679 Ma, and T_{DM2} ages of 1618~2172 Ma. Neoproterozoic zircons
32
33 487 from low-Si and high-Si meta-granitoids have overlapped $\epsilon_{\text{Hf}}(t)$ values and T_{DM} ages,
34
35 488 but the high-Si rocks have slightly higher average $\epsilon_{\text{Hf}}(t)$ values and younger Hf model
36
37 489 ages.

38
39
40 490
41
42 491 *4.4. Sr-Nd-Pb isotope compositions*

43
44 492 The Rb-Sr, Sm-Nd and Pb contents and isotopic compositions of the
45
46 493 meta-basites are listed in **Supplementary** Tables 9 and 10, respectively. The
47
48 494 meta-basites have Rb and Sr contents of 16.0–62.9 and 87–320 ppm, and measured
49
50 495 $^{87}\text{Rb}/^{86}\text{Sr}$ and $^{87}\text{Sr}/^{86}\text{Sr}$ ratios of 0.1423–1.6997 and 0.705386–0.709376, Sm and Nd
51
52 496 contents of 4.15–9.64 and 13.1–35.9 ppm, and measured $^{147}\text{Sm}/^{144}\text{Nd}$ and $^{143}\text{Nd}/^{144}\text{Nd}$
53
54 497 ratios of 0.1515–0.1888 and 0.512511–0.512674. Sr and Nd isotopic compositions
55
56 498 were back calculated to $t=230 \text{ Ma}$, and thus the $(^{87}\text{Sr}/^{86}\text{Sr})_t$, $\epsilon_{\text{Nd}}(t)$ values and T_{DM2}
57
58 499 ages are 0.7023–0.7067, -1.8–+1.8 and 862–1156 Ma. The meta-basites have U, Th

1 500 and Pb contents of 0.34–0.70, 1.27–2.34 and 2.36–10.20 ppm, and measured
2 501 $^{206}\text{Pb}/^{204}\text{Pb}$, $^{207}\text{Pb}/^{204}\text{Pb}$ and $^{208}\text{Pb}/^{204}\text{Pb}$ ratios of 17.046–17.308, 15.403–15.467 and
3
4 502 38.119–38.344. Pb isotopic compositions were back calculated to $t=230$ Ma, and thus
5
6 503 the $(^{206}\text{Pb}/^{204}\text{Pb})_i$, $(^{207}\text{Pb}/^{204}\text{Pb})_i$ and $(^{208}\text{Pb}/^{204}\text{Pb})_i$ values are 16.84–17.11, 15.39–15.46
7
8 504 and 37.81–38.06, respectively. The Dabie orogen experienced two major geological
9
10 505 events: the Neoproterozoic rifting-related magmatism and the Triassic
11
12 506 subduction-related metamorphism. In deed, we also tried to calculate the Sr, Nd and
13
14 507 Pb isotope compositions back to $t=800$ Ma, but obtained much more scattered results,
15
16 508 indicating that the meta-basites experienced metamorphism at the Triassic, during
17
18 509 which their isotopes were reseted.
19
20

21 510

22 511 **5. Discussion**

23 512 *5.1. The relationship between the studied rocks and the UHP rocks in the CDZ*

24 513 *5.1.1. Low-grade meta-basites and meta-granitoids vs. \pm retrograded UHP eclogites* 25 514 *and granitic gneisses*

26 515 The CDZ contains a variety of coesite- and/or diamond-bearing rock types,
27 516 including eclogites and granitic gneisses; these rocks experienced Triassic UHP
28 517 metamorphism and post-peak amphibolite-facies retrogression, responsible for the
29 518 widespread development of amphibolite-facies assemblages in some eclogites in the
30 519 area (Wang et al., 1989; Cong et al., 1995; Zhang et al., 2003; Rolfo et al., 2004; Liu
31 520 et al., 2006b). In some strongly retrograded eclogites, most garnets and omphacites
32 521 are replaced by symplectites or pseudomorphs; even though, mineral inclusions (e.g.
33 522 coesite, diamond, omphacite and rutile) within relict garnet preserve the evidence of
34 523 peak metamorphism at UHP conditions. Even in the most retrograded eclogites that
35 524 do not contain garnet relics, the former occurrence of garnet is suggested by
36 525 pseudomorphs of Pl + Amp + Bt that exhibit isometric shape typical of garnet (e.g.,
37 526 Zhang et al., 2003). In contrast, no garnet and/or other microstructural evidence that
38 527 could be related to eclogite-facies metamorphism have been observed in the studied
39 528 meta-basites, thus suggesting that the studied rocks have not been involved in the
40
41
42
43
44
45
46
47
48
49
50
51
52
53
54
55
56
57
58
59
60
61
62
63
64
65

1 529 deep subduction of the SCB in the Triassic.

2 530 In addition to the main rock-forming minerals, inclusions in metamorphic zircon
3
4 531 can be also used to reveal the peak metamorphic conditions in strongly retrograded
5
6 532 metamorphic rocks (e.g., Xu et al., 1992b; Nasdala and Massonne, 2000; Bauer et al.,
7
8 533 2007; Liu et al., 2007b, 2011b). This is because zircon behaves as a rigid “container”
9
10 534 that can protect the inclusions from the retrogression occurring in the matrix. Mineral
11
12 535 inclusions related to UHP conditions (e.g. coesite, diamond, omphacite and rutile)
13
14 536 have been identified in Triassic metamorphic zircons from the retrograded eclogites in
15
16 537 the CDZ, thus confirming that they experienced UHP metamorphism, although the
17
18 538 matrix of the rocks is dominated by amphibolite-facies mineral assemblages (Liu et
19
20 539 al., 2001, 2006a). On the contrary, no Triassic metamorphic zircon and related
21
22 540 eclogite-facies mineral inclusions have been identified in the studied meta-basites (see
23
24 541 section 4.2.1).

25
26
27 542 Different from UHP eclogites, felsic gneisses that underwent deep subduction
28
29 543 and UHP metamorphism commonly do not preserve evidence of the peak
30
31 544 metamorphic mineral assemblage. Nevertheless, their metamorphic zircons can trap
32
33 545 and preserve peak metamorphic minerals. In the CDZ, UHP inclusions (e.g. coesite
34
35 546 and diamond) have been recognized in Triassic metamorphic zircons from the felsic
36
37 547 gneisses (Tabata et al., 1998; Liu et al., 2001). On the contrary, no Triassic ages have
38
39 548 been obtained from the metamorphic zircons in the studied meta-granitoids, and no
40
41 549 eclogite-facies mineral inclusions have been observed therein (see section 4.2.1).

42
43
44 550 The overall observations and data clearly indicate that the studied meta-basites
45
46 551 and meta-granitoids were not involved in the Triassic deep subduction and UHP
47
48 552 eclogite-facies metamorphism, but underwent lower-grade metamorphism, i.e., at
49
50 553 amphibolite-facies conditions as suggested by the mineral assemblages and estimated
51
52 554 temperatures of the meta-basites (see sections 2.2 and 2.3). The age of this low-grade
53
54 555 metamorphic event has not been directly constrained due to the lack of related
55
56 556 metamorphic zircon, which may be attributed to the relatively low temperatures (<541
57
58 557 °C, section 2.3). Nevertheless, similar low-grade rocks from the same region showing
59
60 558 identical Neoproterozoic protolith ages, yield Triassic whole-rock Rb-Sr isochronal

1 559 ages of 232 ± 8 Ma (Dong et al., 1997; Gao et al., 2006). We therefore suggest that
2 560 during the Triassic, the studied meta-basites and meta-granitoids underwent a shallow
3
4 561 subduction associated with amphibolite-facies metamorphism, nearly synchronous
5
6 562 with the deep subduction of the CDZ.
7

8 563

10 564 *5.1.2. The same source and crustal levels indicated by zircon Hf and bulk-rock*
11
12 565 *Sr-Nd-Pb isotopes*

14 566 *Zircon Hf isotopes*

16 567 Because Hf is more incompatible than Lu, the continental crust acquired a
17
18 568 Lu/Hf ratio much lower than that in the primitive mantle, when it differentiated from
19
20 569 the primitive mantle. As a result, the $^{176}\text{Hf}/^{177}\text{Hf}$ ratio in the continental crust increases
21
22 570 slower than in the depleted mantle and thus its $\epsilon_{\text{Hf}}(t)$ value becomes more and more
23
24 571 negative with time, whereas the depleted mantle develops more and more positive
25
26 572 $\epsilon_{\text{Hf}}(t)$ values (Rudnick and Gao, 2003; Kelemen et al., 2003; Salters and Stracke, 2004;
27
28 573 Palme and O'Neill, 2003). When a zircon crystallized from a crustal-derived melt, the
29
30 574 $^{176}\text{Hf}/^{177}\text{Hf}$ ratio in the melt was timely imprinted in the zircon, because Hf content in
31
32 575 zircon is several orders of magnitude higher than Lu content, and thus the change of
33
34 576 $^{176}\text{Hf}/^{177}\text{Hf}$ ratio in zircon with time is negligible; moreover, zircon $^{176}\text{Hf}/^{177}\text{Hf}$ ratio is
35
36 577 resistant to the influence of later processes such as weathering, fluid alteration and
37
38 578 metamorphic recrystallization (Patchett et al., 1984; Wu et al., 2006b; Zheng et al.,
39
40 579 2008; Hanyu et al., 2006; Carpentier et al., 2009; Hoffmann et al., 2011; Roux et al.,
41
42 580 2009; Yu et al., 2009; Chen et al., 2010; Tappe et al., 2011; Choi and Mukasa, 2012).
43
44 581 In this way, the $\epsilon_{\text{Hf}}(t)$ value of zircon reflects the mass source of the host rocks: given
45
46 582 the same zircon U-Pb age, the more negative zircon $\epsilon_{\text{Hf}}(t)$ value is, the higher
47
48 583 proportion of ancient continental crustal material the host rock contains. In principle,
49
50 584 the most positive $\epsilon_{\text{Hf}}(t)$ values correspond to the youngest single-stage Hf model ages
51
52 585 (T_{DM1}) that represent the maximum time of the emplacement of the mantle-derived
53
54 586 magma, while the most negative $\epsilon_{\text{Hf}}(t)$ values correspond to the oldest T_{DM1} ages that
55
56 587 represent the minimum time of the formation of the involved crust.
57

58 588 The UHP eclogites and gneisses in the CDZ exhibit varied zircon Hf isotope
59
60
61
62
63
64
65

1 589 compositions, indicating both source mixing and crustal contamination along an
2 590 active rifting zone, with varying degrees of mixing between different ages of crustal
3 591 materials at ~750 Ma. Therein, the youngest zircon T_{DM1} ages from the eclogites are
4 592 in agreement with the Neoproterozoic zircon U-Pb ages of ~750 Ma, while the oldest
5 593 zircon T_{DM2} ages from the gneisses are close to the Paleoproterozoic zircon U-Pb ages
6 594 of ~2.15 Ga, indicating growth and immediate reworking of juvenile crust at
7 595 Paleoproterozoic (~2.15 Ga) and Neoproterozoic (~750 Ma), respectively (e.g., Zheng
8 596 et al., 2006).

9 597 The studied meta-basites and meta-granitoids have varied zircon Hf isotope
10 598 compositions (Supplementary Table 8) which are in agreement with the UHP
11 599 eclogites and orthogneisses in the CDZ (e.g., Zheng et al., 2006) (Fig. 10), indicating
12 600 different degrees of mixing between Neoproterozoic depleted mantle materials and
13 601 Paleoproterozoic crustal components. The meta-basites have positive $\epsilon_{Hf}(t)$ values of
14 602 +2.6~+7.9 and young T_{DM1} ages of about 1.2~1.5 Ga, slightly older than their zircon
15 603 U-Pb ages, reflecting incongruent contamination of crustal materials during the
16 604 emplacement of their parental magmas. Inherited zircons from the low-Si
17 605 meta-granitoids exhibit overlapped T_{DM1} ages of 2359~2702 Ma and T_{DM2} ages of
18 606 2506~2823 Ma from late Archean to Paleoproterozoic, representing the time of the
19 607 formation of continental crust from the mantle. For the Neoproterozoic zircons with
20 608 negative $\epsilon_{Hf}(t)$ values, T_{DM2} can better reflect their origin than T_{DM1} . Neoproterozoic
21 609 zircons in the low-Si meta-granitoids exhibit negative $\epsilon_{Hf}(t)$ values of -3.2~-12.0 and
22 610 younger T_{DM2} ages of 1893~2446 resulting from mixing between depleted mantle
23 611 materials and late Archean continental crust at Neoproterozoic. Compared to the
24 612 low-Si meta-granitoids, the high-Si rocks do not contain ancient (late Archean)
25 613 inherited zircon, and have higher $\epsilon_{Hf}(t)$ values of -7.5~+1.4 and younger T_{DM2} ages of
26 614 1618~2172 Ma, indicating that they were mainly derived from remelting of younger
27 615 continental crust formed at early Paleoproterozoic. These clusters of T_{DM2} age of the
28 616 meta-granitoids are consistent with multiple episodes of crust growth of the South
29 617 China Block from the late Archean to Paleoproterozoic (Greentree et al., 2006; Zhang
30 618 et al., 2006a,b; Liu et al., 2008; Wang et al., 2010; Zhao and Cawood, 2012).

619 As a summary, the studied meta-basites and meta-granitoids derived from the
620 same sources as the UHP eclogites and felsic gneisses in the CDZ. Therein the
621 meta-basites were formed from depleted mantle upwelling and mafic magmatic
622 activities during the Neoproterozoic, with incongruent mixing with the Yangtze
623 crustal materials; the mafic magmatic activities remelted the basement of the South
624 China Block, which comprises the Archean and early Paleoproterozoic crustal rocks,
625 and generated the low-Si and high-Si meta-granitoids.

626

627 *Bulk-rock Sr-Nd-Pb isotopes*

628 Because Rb is more incompatible than Sr, and Nd is more incompatible than Sm,
629 melts will have higher Rb/Sr but lower Sm/Nd ratios than residues during partial
630 melting. Therefore, when the primitive mantle differentiated to form the crust and
631 depleted mantle, the crust acquired higher Rb/Sr and lower Sm/Nd ratios than the bulk
632 earth, while the depleted mantle acquired lower Rb/Sr and higher Sm/Nd ratios. Then
633 the $^{87}\text{Sr}/^{86}\text{Sr}$ of the crust will be more and more higher than the bulk earth, but the
634 $\epsilon_{\text{Nd}}(t)$ will be more and more negative with time; on the contrary, the $^{87}\text{Sr}/^{86}\text{Sr}$ and
635 $\epsilon_{\text{Nd}}(t)$ of the depleted mantle will evolve in the opposite direction. The meta-basites
636 have initial $^{87}\text{Sr}/^{86}\text{Sr}$ ratios of 0.7023–0.7067 (calculated to $t=230$ Ma), $\epsilon_{\text{Nd}}(230$ Ma)
637 values from -1.8 to +1.8 and T_{DM2} ages of 862–1156 Ma. In the $\epsilon_{\text{Nd}}(t)$ vs $(^{87}\text{Sr}/^{86}\text{Sr})_i$
638 diagram (Fig. 11), the meta-basites plot around the composition of the bulk silicate
639 earth and slightly toward lower continental crust, indicating that the meta-basites were
640 derived mainly from the mantle, with minor addition of lower continental crust. This
641 conclusion is also supported by their two-stage Nd model ages (T_{DM2}) of 862–1156
642 Ma, which are slightly older than their magmatic zircon U-Pb ages (~ 772 Ma).

643 U is more incompatible than Pb. This being the case, we would therefore predict
644 that continental crust should be more enriched in radiogenic Pb than the average of the
645 bulk-earth, while the depleted mantle should be depleted in radiogenic Pb. Upper
646 continental crustal rocks do have higher $^{206}\text{Pb}/^{204}\text{Pb}$ and $^{207}\text{Pb}/^{204}\text{Pb}$ ratios as expected, but
647 surprisingly, most mantle-derived rocks also exhibit higher Pb isotope ratios than the
648 average of the bulk-earth, whereas a majority of lower crustal rocks are relatively

1 649 depleted in radiogenic Pb. This phenomenon is known as the Pb paradox and it implies
2 650 that other processes apart from magmatism may have played key roles in the
3
4 651 differentiation of the U-Pb element pair.
5

6 652 In addition, Pb isotopes can be used to trace the crust affinity of given rocks from
7
8 653 upper or lower crust, i.e., upper crustal rocks commonly have higher radiogenic Pb
9
10 654 isotopes than lower crustal rocks (Zartman and Doe, 1981; Taylor and McLennan, 1985).
11
12 655 For example, Liu and Li (2008) concluded that the NDZ is of lower crustal origin, while
13
14 656 the CDZ and the SDZ are slices from middle to upper crust, according to their different
15
16 657 radiogenic Pb isotope compositions. As shown in Figure 12, the Pb isotope compositions
17
18 658 of the studied meta-basites fall into the range of the UHP meta-igneous rocks from the
19
20 659 CDZ, and are significantly higher than that of the UHP meta-igneous rocks from the NDZ.
21
22 660 This indicates that the studied meta-basites and the associated meta-granitoids were at
23
24 661 middle to upper crustal depths, consistent with the UHP meta-igneous rocks from the
25
26 662 CDZ.
27

28
29 663 Summing up, both zircon Hf and bulk-rock Sr-Nd-Pb isotopic data demonstrate
30
31 664 that the studied meta-basites and meta-granitoids are low-grade metamorphosed
32
33 665 counterparts of the UHP eclogites and orthogneisses in the CDZ; these rocks did not
34
35 666 experience deep subduction and UHP metamorphism during the Triassic, but were
36
37 667 detached from the subducting plate and exhumed from shallower depths, experiencing
38
39 668 amphibolite-facies metamorphic peak conditions.
40

41 669
42
43 670 *5.1.3. The studied rocks as the best candidates for elucidating the Neoproterozoic*
44
45 671 *evolution of the South China Block*
46

47 672 The UHP meta-igneous rocks in the CDZ consist mainly of granitic gneisses and
48
49 673 eclogites, which are generally considered to be transformed from bimodal igneous
50
51 674 rocks derived from rift magmatism in Neoproterozoic (e.g., Ames et al., 1996; Rowley
52
53 675 et al., 1997; Hacker et al., 1998). The studied meta-basites and meta-granitoids at
54
55 676 Longjingguan have consistent Neoproterozoic protolith ages and zircon Hf isotopic
56
57 677 compositions with those from the UHP meta-igneous rocks, most likely indicating that
58
59 678 they were derived from the same rifting events, during which depleted mantle
60
61

1 679 materials were added to the crust, and caused remelting of existing old crust and
2 680 generated bimodal magmas (Liu et al., 2007a). In addition, the bulk-rock Pb isotopic
3 681 compositions of the studied rocks fall into the range of the UHP meta-igneous rocks in
4 682 the CDZ (Fig.12), suggestive of upper crustal origin (Liu et al., 2017). In this regard,
5 683 the studied rocks are likely counterparts of the UHP rocks in the region, and both of
6 684 them were formed from partial melting of ancient crust in the Neoproterozoic.
7 685 Moreover, during the Triassic the studied rocks experienced lower-grade and
8 686 lower-pressure metamorphism with respect to their UHP counterpart. Therefore, we
9 687 suggest that the rocks could likely have better preserved their protolith compositions
10 688 than the UHP rocks, which often experienced interactions with melt and/or
11 689 supercritical fluids during UHP metamorphism (e.g., Zheng et al., 2011). In order to
12 690 test this hypothesis, the trace element patterns of the studied meta-basites are
13 691 compared to those of the UHP eclogites derived from **basites** (data from Tang et al.,
14 692 2007), as shown in Fig. 5: the studied meta-basites have identical REE and trace
15 693 element patterns, while the UHP eclogites exhibit similar REE patterns but
16 694 significantly varied large ion lithophile element (LILE) contents. This is consistent
17 695 with the fact that LILE have significantly higher mobilities than REE in hydrous
18 696 fluids during UHP metamorphism (Kessel et al., 2005; Hermann et al., 2006; Zheng et
19 697 al., 2011). As a conclusion, the rocks here have better preserved their protolith
20 698 compositions than their UHP counterparts, and thus they are more suitable for
21 699 elucidating the Neoproterozoic evolution in the area.

22 700

23 701 *5.2. Neoproterozoic magmatic and metamorphic events*

24 702 *5.2.1. Meta-basites*

25 703 Zircons in the meta-**basites** (samples 11LJG3 and 11LJG7) give a concordant
26 704 magmatic age cluster of ~772 Ma (Ma) and two concordant metamorphic age clusters
27 705 of ~768 Ma (Me1) and ~746 Ma (Me2) (see section 4.2.3). As mentioned above, the
28 706 magmatic zircons exhibit clear oscillatory zoning and REE patterns typical of
29 707 magmatic genesis, thus the age of ~772 Ma represents a magmatic event. As to the
30 708 metamorphic zircons, they formed during metamorphic events characterized by the

1 709 circulation of REE-enriched fluids controlled by fractures. In addition, most
2 710 metamorphic zircons exhibit slightly higher Nb + Ta, U and Th contents than the
3 711 magmatic zircons (Supplementary Table 5), thus suggesting that the metamorphic
4 712 fluids were also enriched in Nb+Ta, U and Th. These REE-, Nb+Ta-, U- and Th-
5 713 enriched fluids favoured the precipitation of minerals rich in these elements, such as
6 714 epidote, rutile, ilmenite and titanite (Figs. 7a-i), observed as inclusions in the
7 715 metamorphic zircons (e.g., sample 11LJG3; Me1 domains). Thermobarometric
8 716 estimates (see Section 2.3) based on rutile inclusions indicate that metamorphic zircon
9 717 domains Me1 grew at about 850-870 °C, 12 kbar. No rutile or other inclusions
10 718 suitable for thermometric estimates have been recognized in the Me2 domain of
11 719 zircons in sample 11LJG7, thus the temperatures of the late thermal overprinting at
12 720 ~746 Ma has not been estimated. Summing up, the meta-basites were formed at ca.
13 721 772 Ma (Me domains) and experienced subsequent granulite-facies (850-870 °C)
14 722 metamorphism at ca. 768 Ma (Me1 domains), followed by a thermal overprinting
15 723 event at ~746 Ma (Me2 domains). The almost overlapped magmatic and metamorphic
16 724 zircon ages (772 ± 4 and 768 ± 7 Ma, respectively) suggest that the Neoproterozoic
17 725 magmatism in this area occurred in pulse, and that the later magma underplating
18 726 warmed the already solidified rocks (e.g., Liu et al., 2007a; Liu et al., 2015) resulting
19 727 in granulite-facies metamorphism. The thermal overprinting age of ~746 Ma is
20 728 comparable with the emplacement age of some mafic rocks in the Dabie orogen, for
21 729 example the meta-basites in the BZ located in the northern part of the Dabie orogen
22 730 (Liu et al., 2017), indicating that a later magma emplacement at that time in the area
23 731 may have been the heat source of the thermal overprinting. Moreover, these ages are
24 732 in agreement with the time of Rodinia breakup indicated by large volumes of mafic
25 733 and felsic magmatism along the northern margin of the Yangtze Block (Li et al., 2002;
26 734 Li et al., 2003a,b,c; Zhou et al., 2002a,b, 2006a,b; Zhao and Zhou, 2007a,b, 2008),
27 735 suggesting that the studied rocks are generated from several episodes of magmatic
28 736 event related to the Rodinia breakup.

29 737

30 738 5.2.2. *Meta-granitoids*

1 739 Compared to the meta-**basites**, the low-Si meta-granitoids exhibit a more complex
2 740 zircon U-Pb age spectrum. Few inherited zircon cores preserve two groups of age at
3 741 ~2.0 and ~2.5 Ga, timely consistent with two episodes of Precambrian crustal growth
4 742 and immediate reworking event of the SCB (e.g., Zhang et al., 2006a,b,c; Liu et al.,
5 743 2008; Wang et al., 2010; Zhao and Cawood, 2012). Same for these inherited zircon
6 744 cores, the zircons in the studied rocks are distinguished into two types: magmatic
7 745 zircon domains yielding concordant ages of ca. 819 Ma (Ma domains) and
8 746 metamorphic zircon domains with concordant ages at ca. 784 (Me1 domains) and 746
9 747 Ma (Me2 domains). The latter are discriminated from the former by weaker or no
10 748 oscillatory zonings, lighter brightness in CL image and enrichment of mineral
11 749 inclusion. A typical zircon with magmatic zircon core and metamorphic mantle in
12 750 meta-granitoid sample 11LJG2 (Me1) is shown (Figs. 7j-l): the core is dark with
13 751 obvious oscillatory zoning, while the mantle is light and homogeneous in CL image;
14 752 the core is free of mineral inclusion, while the mantle contains K-feldspar +
15 753 muscovite inclusion; and there is a clear boundary between the core and the mantle.
16 754 Two analytical spots on metamorphic zircon domains exhibit significantly higher
17 755 LREE patterns than the magmatic zircons (Figs. 8b,c), therein a spot also exhibit
18 756 higher REE contents than the magmatic zircons. Moreover, muscovite + K-feldspar
19 757 inclusion is identified in metamorphic zircon (Fig. 7k), indicating that the
20 758 metamorphic zircons were formed in the presence of LREE-enriched fluid, in
21 759 agreement with the metamorphic zircons in the meta-**basites**. Therefore, the low-Si
22 760 meta-granitoids experienced two episodes of metamorphism at ~784 Ma and ~746 Ma,
23 761 respectively. It is worth noting that, the ~784 Ma metamorphic zircon ages are
24 762 comparable with the forming (i.e. magmatic) ages of the meta-**basites** (~772 Ma)
25 763 within error, suggesting that the emplacement of the basic magmas may be the heat
26 764 source for the metamorphism of the low-Si meta-granitoids. The thermal overprinting
27 765 of ~746 Ma is timely in agreement with the ca. 750 Ma forming age of the
28 766 meta-granitoids and meta-**basites** in the BZ (Jiang et al., 2005; Wu et al., 2007; Liu et
29 767 al., 2010, 2017), indicating that the low-Si meta-granitoids and the meta-basites in the
30 768 region experienced a coeval thermal event as a consequence of the emplacement of

1 769 the meta-basites within the BZ.

2 770 The high-Si meta-granitoids exhibit nearly the same Neoproterozoic magmatic
3
4 771 and metamorphic zircon ages with the low-Si type, indicating that they were
5
6 772 generated from the same or adjacent magmatic events and then jointly experienced the
7
8 773 same metamorphic processes during the Neoproterozoic. However, the two types of
9
10 774 meta-granitoids are likely derived from different sources: (i) the low-Si type contains
11
12 775 inherited zircons with two age clusters at ~2.5 Ga and ~2.0 Ga, suggesting that its
13
14 776 source could be a late Archean basement that experienced metamorphic reworking
15
16 777 during the Paleoproterozoic, whereas (ii) the high-Si type does not contain ancient
17
18 778 inherited zircon, and the oldest zircon Hf model age (T_{DM2}) is 2172 Ma, suggesting
19
20 779 that a derivation from the juvenile crust formed during the Paleoproterozoic. This
21
22 780 hypothesis can well explain the compositional gap, especially the different Si contents,
23
24 781 between the two types of meta-granitoids (see section 4.1), and also the slightly higher
25
26 782 zircon $\varepsilon_{Hf}(t)$ values and younger Hf model ages of the high-Si meta-granitoids (see
27
28 783 section 4.3).

29
30 784 The meta-basites and meta-granitoids with similar mid- to late-Neoproterozoic
31
32 785 ages have been reported from other localities within the Dabie orogen, for example,
33
34 786 Ganghe within the CDZ (Dong et al., 1997), Yuexi within the NDZ (Gao et al., 2006),
35
36 787 and Huwan, Sujiahe and Luzhenguan within the BZ (Jiang et al., 2005; Wu et al.,
37
38 788 2007; Liu et al., 2010, 2017). In addition, extensive mid- to late-Neoproterozoic mafic
39
40 789 dyke swarms and granitic bodies (Zhao and Zhou, 2009; Hong et al., 2009; Xue et al.,
41
42 790 2011; Wang et al., 2013) are exposed in Suizhou-Zaoyang of the Hubei province,
43
44 791 along the northern margin of the SCB. Moreover, the forming ages of these rocks are
45
46 792 clearly comparable with the protolith ages of the UHP eclogites and orthogneisses
47
48 793 (Rowley et al., 1997; Hacker et al., 1998; Liu et al., 2007a,b, 2011a; and references
49
50 794 therein) in the Dabie orogen. In this regard, these rocks, including those from
51
52 795 Longjingguan in this study, should be counterparts of the UHP meta-igneous rocks in
53
54 796 the Dabie orogen, implying that the protoliths of the latter could have been formed
55
56 797 during the same Neoproterozoic magmatic events, and could have experienced the
57
58 798 same Neoproterozoic metamorphism.

799

800 *5.3. Petrogenesis and tectonic setting*

801 *5.3.1. Meta-basites*

802 Mantle-normalized trace element patterns are frequently used to infer
803 petrogenesis and tectonic settings of igneous rocks, because the same rock type
804 formed in different tectonic settings can display significantly different trace element
805 patterns. For example, the **basites** of mid-ocean ridges (MORB) are formed from the
806 depleted mantle within a narrow depth interval, and thus have a uniform chemical
807 composition, while the island-arc basalts (IAB) and within-plate basalts (WPB)
808 exhibit large variation in trace element contents and patterns, and generally
809 enrichment in LILE and LREE compared to MORB, depending on addition
810 component of crustal materials. The strong negative Sr anomalies, together with
811 slightly positive or negative anomalies of HFSE elements of the studied meta-basites
812 (Fig. 5b) indicate that they are unlikely IAB or post-collision basic rocks (PCB),
813 which commonly exhibit positive Sr anomalies and strong depletion of the HFSE.
814 WPB fits better with the studied meta-basites, with respect to the mantle-normalized
815 trace element pattern (e.g., Velikoslavinsky and Krylov, 2014 and references therein),
816 thus the meta-basites were most likely formed in a within-plate environment. To
817 reinforce the hypothesis, the discrimination diagrams proposed by Velikoslavinsky
818 and Krylov (2014) were applied (Fig. 13). Nearly all major elements as well as many
819 trace elements are involved in the discriminant functions of these diagrams; hence
820 they include comprehensive information of the geochemical characteristics of basalts.
821 In this way, the average weighted uncertainty of IAB, MORB, and WPB identification
822 is substantially small as compared with previously elaborated plots. All of the studied
823 meta-basites plot into the category of WPB in the $DF_1(x)$ range (Fig. 13a) and most of
824 them fall into continental WPB field with only a small percentage of OIB in the $DF_3(x)$
825 range (Fig. 13b). In addition, the $DF_5(x)$ values of the meta-basites are coincident with
826 most WPB but only few post-collision basic rocks (PCB) (Fig. 13c). As a
827 consequence, the studied meta-basites are most likely continental WPB not related to
828 post-collision processes, but rather involved in mantle plume or continental rifting.

1 829 This conclusion is highly in agreement with the zircon Hf isotopic features of the
2 830 meta-basites (see section 5.1), which demonstrate mixing between the depleted mantle
3
4 831 and the crust.
5

6 832

8 833 *5.3.2. Meta-granitoids*

9
10 834 Various binary discrimination diagrams were applied to constrain the tectonic
11 835 setting of the meta-granitoids in Longjingguan. The diagrams employing Ga/Al
12
13 836 (Whalen et al., 1987) show that the meta-granitoids have similar geochemical features
14
15 837 with A-type granites (Fig. 14). A-type granite was firstly proposed to be related to
16
17 838 anorogenic environments (Chappell and White, 1974), but afterwards more and more
18
19 839 studies suggest that A-type granite may form under different environments (Whalen et
20
21 840 al., 1987; Eby, 1990; Wu et al., 2002; Bonin, 2007). Nevertheless, it is widely
22
23 841 accepted that high melting temperatures (>830 °C) are required to generate A-type
24
25 842 granite magmas (Clemens et al., 1986), probably through the emplacement of
26
27 843 mantle-derived mafic magmas into the lower crust. In this study, the meta-granitoids
28
29 844 are spatially and temporally associated with meta-basites, indicating that they were
30
31 845 formed under a geodynamic setting characterized by asthenosphere upwelling and
32
33 846 basic magmatism, which can provide sufficient heat to generate high-T granitoids.
34
35 847 Zircon Hf isotopic compositions of the meta-granitoids (see section 5.1) also suggest
36
37 848 addition of the depleted mantle materials into the felsic magmas.
38
39

40
41 849 Trace elements and REE patterns are frequently used in identifying petrogenesis
42
43 850 and tectonic setting of granitoids. The significant depletion of HREE, Nb, Ta, and Ti
44
45 851 of the studied meta-granitoids (Fig. 5b) is in agreement with adakite and arc-related
46
47 852 ADR (andesite, dacite and rhyolite) (see Castillo, 2006 for an overview). Adakite and
48
49 853 arc-related ADR are generally associated to slab subducting and mantle convecting,
50
51 854 consistent with the aforementioned high temperature characteristics of the studied
52
53 855 meta-granitoids. However, the high Sr, low Yb and high Sr/Y characteristics of
54
55 856 adakite are in contrast with the studied meta-granitoids, which exhibit low Sr (13-275
56
57 857 ppm), high Y (19-46 ppm) and low Sr/Y (0.34-10.39). In the Sr/Y vs Y diagram (Fig.
58
59 858 15), which is usually used to discriminate adakites and TTGs from typical arc
60
61
62
63
64
65

1 859 calc-alkaline rocks (Drummond and Defant, 1990), all the studied meta-granitoids
2 860 plot into the field of typical arc rocks. Therefore, based on the geochemical
3 861 characteristics, zircon U-Pb ages and Hf isotopic compositions described above, the
4 862 studied meta-granitoids most likely formed under magmatic arc setting, in agreement
5 863 with the previous investigations on the Neoproterozoic igneous rocks in the periphery
6 864 of the SCB (Zheng et al., 2007; Zhao et al., 2018 and references therein); and the
7 865 low-Si and high-Si types are mainly derived from partial melting of late-Archean and
8 866 Paleoproterozoic continental crustal materials, respectively, with various degrees of
9 867 addition of mantle materials.

10 868 In summary, the meta-granitoids were formed at ca. 819 Ma by partial melting of
11 869 ancient continental crustal materials in an arc setting, whereas the meta-basites were
12 870 derived mainly from the depleted mantle at ca. 772 Ma in a rifting setting. Thus, the
13 871 studied rocks witness the transition from a convergent to an extensional tectonic
14 872 setting, and provide new constraints for the beginning of the Neoproterozoic rifting in
15 873 northern SCB, which can further help to better understand the breakup of the
16 874 supercontinent Rodinia.

17 875

18 876 **6. Conclusions**

19 877 (1) The meta-basites and meta-granitoids in Longjingguan are relatively low-grade
20 878 metamorphosed counterparts of the UHP eclogites and orthogneisses within the
21 879 CDZ; they were detached from the subducted crust of the SCB and exhumed from
22 880 shallow depths during subduction, and subsequently thrust over the CDZ during
23 881 collisional orogenesis.

24 882 (2) The precursors of the studied meta-granitoids and meta-basites were formed at ca.
25 883 819 Ma and 772–784 Ma, respectively. They jointly experienced a granulite-facies
26 884 metamorphism at ca. 768 Ma and a thermal overprinting at ca. 746 Ma resulted
27 885 from underplating of mafic magmas, strongly pointing to **multiple episodes of**
28 886 continental rifting during the Neoproterozoic.

29 887 (3) The meta-granitoids are derived mainly from partial melting of ancient continental

1 888 crustal materials of the SCB in an arc setting. The low-Si meta-granitoids were
2 889 derived from the late Archean basement rocks that underwent Paleoproterozoic
3
4 890 metamorphic reworking, while the high-Si meta-granitoids mainly come from the
5
6 891 Paleoproterozoic juvenile crust. The meta-basites were derived from the depleted
7
8 892 mantle in a rifting environment. The studied rocks thus witness the transition from
9
10 893 a convergent to an extensional tectonic setting, and provide new time constraints
11
12 894 for the beginning of the Neoproterozoic rifting in northern SCB, which can further
13
14 895 help to better understand the breakup of the supercontinent Rodinia.
15
16
17 896

18 19 897 **Acknowledgements**

20
21
22 898 This study is financially supported by the National Basic Research Program of
23
24 899 China (2015CB856104) and the National Natural Science Foundation of China
25
26 900 (41273036 and 41773020). We thank B. Song and Q. Yang for their help in SHRIMP
27
28 901 U-Pb dating, P. Sun for Hf-isotope and Z.H. Hou and X.M. Liu for trace-element
29
30 902 analysis on zircon, F.-K. Chen for Sr-Nd-Pb isotope and Raman analysis, and Z.-Y.
31
32 903 Chen and Y.H. Shi for electron microprobe analysis. Many suggestions and
33
34 904 constructive comments by Yunpeng Dong and three anonymous reviewers have
35
36 905 greatly improved the paper.
37
38 906

References

- Ames, L., Zhou, G.Z., Xiong, B.C., 1996. Geochronology and isotopic character of ultrahigh-pressure metamorphism with implications for the collision of the Sino-Korean and Yangtze cratons, central China. *Tectonics* 15, 472–489.
- Angiboust, S., Harlov, D., 2017. Ilmenite breakdown and rutile-titanite stability in metagranitoids: Natural observations and experimental results. *American Mineralogist* 102, 1696–1708.
- Bauer, C., Rubatto, D., Krenn, K., Proyer, A., Hoinkes, G., 2007. A zircon study from the rhodope metamorphic complex, n-greece: time record of a multistage evolution. *Lithos* 99(3), 207–228.
- Black, L.P., Kamo, S.L., Allen, C.M., Aleinikoff, J.N., 2003. TEMORA 1: a new zircon standard for phanerozoic U–Pb geochronology. *Chemical Geology* 200, 155–170.
- Blichert-Toft, J., Albarede, F., 1997. The Lu–Hf isotope geochemistry of chondrites and the evolution of the mantle–crust system. *Earth and Planetary Science Letters* 148, 243–258.
- Bohlen, S.R., Liotta, J.J., 1986. A Barometer for Garnet Amphibolites and Garnet Granulites. *Journal of Petrology* 27, 1025–1034.
- Bonin, B., 2007. A-type granites and related rocks: evolution of a concept, problems and prospects. *Lithos* 97(1–2), 1–29.
- Carpentier, M., Chauvel, C., Maury, R., Mattielli, N., 2009. The “zircon effect” as recorded by the chemical and Hf isotopic compositions of the Lesser Antilles forearc sediments. *Earth and Planetary Science Letters* 287, 86–99.
- Castillo, P.R., 2006. An overview of adakite petrogenesis. *Chinese Science Bulletin* 51(3), 257–268.
- Chappell, B.W., White, A.J.R., 1974. Two contrasting granite types. *Pacific Geology* 8, 173–174.
- Chemenda, A.I., Mattauer, M., Bokun, A.N., 1996. Continental subduction and a mechanism for exhumation of high-pressure metamorphic rocks: new modelling,

- 1 936 field data from Oman. *Earth and Planetary Science Letters* 143, 173–182.
- 2 937 Chen, F., Hegner, E., Todt, W., 2000. Zircon ages and Nd isotopic and chemical
3 compositions of orthogneisses from the Black Forest, Germany: evidence for a
4 938 Cambrian magmatic arc. *International Journal of Earth Sciences* 88, 791– 802.
- 5
6 939
7
8 940 Chen, F.K., Guo, J.H., Jiang, L.L., Siebel, W., Cong, B., Satir, M., 2003. Provenance
9 of the Beihuaiyang lower-grade metamorphic zone of the Dabie
10 941 ultrahigh-pressure collisional orogen, China: evidence from zircon ages. *Journal*
11 942 *of Asian Earth Science* 22(4), 343–352.
- 12
13 943
14
15 944 Chen, F., Li, X.H., Wang, X.L., Li, Q.L., Siebel, W., 2007. Zircon age and Nd-Hf
16 isotopic composition of the Yunnan Tethyan belt, southwestern China.
17 945 *International Journal of Earth Science* 96, 1179–1194.
- 18
19 946
20
21 947 Chen, R.X., Zheng, Y.F., Xie, L., 2010. Metamorphic growth and recrystallization of
22 zircon: distinction by simultaneous in-situ analyses of trace elements, U–Th–Pb
23 948 and Lu–Hf isotopes in zircons from eclogite-facies rocks in the Sulu orogen.
24 *Lithos* 114, 132–154.
- 25
26 949
27
28 950
29
30 951 Choi, S.H., Mukasa, S.B., 2012. Lu–Hf and Sm–Nd isotope systematic of Korean
31 spinel peridotites: a case for metasomatically induced Nd–Hf decoupling. *Lithos*
32 952 154, 263–276.
- 33
34 953
35
36 954 Chopin, C., 1984. Coesite and pure pyrope in high grade blueschists of the western
37 Alps: a first record and some consequences. *Contributions to Mineralogy and*
38 955 *Petrology* 86, 107–118.
- 39
40 956
41
42 957 Clemens, J.D., Holloway, J.R., White, A.J.R., 1986. Origin of an A-type granite:
43 experimental constraints. *American Mineralogist* 71, 317–324.
- 44
45 958
46
47 959 Compston, W., Williams, I.S., Kirschvink, J.L., 1992. Zircon U–Pb ages for the Early
48 Cambrian time-scale. *Journal of the Geological Society* 149, 171–184.
- 49
50 960
51
52 961 Cong, B., Zhai, M., Carswell, D.A., Wilson, R.N., Wang, Q., Zhao, Z., Windly, B.F.,
53 1995. Petrogenesis of ultrahigh-pressure rocks and their country rocks at
54 962 Shuanghe in Dabieshan, central China. *European Journal of Mineralogy* 7, 119–
55 138.
- 56
57 963
58
59 964
60
61 965 Dong, S.W., Wang, X.F., Huang, D.Z., 1997. Discovery of low grade metamorphic

1 966 volcanic rock sheets within UHP in Dabie Mts. and its implications. Chinese
2 Science Bulletin 42, 1199–1203.
3
4 968 Drummond, M.S., Defant, M.J., 1990. A model for trondhjemite–tonalite–dacite
5 genesis and crustal growth via slab melting: Archaean to modern comparisons.
6 Journal of Geophysical Research 95, 21503–21521.
7
8 970 Eby, G.N., 1990. The A-type granitoids: a review of their occurrence and chemical
9 characteristics and speculations on their petrogenesis. Lithos 26, 115–134.
10
11 971 Ernst, W.G., Maruyama, S., Wallis, S., 1997. Buoyancy-driven, rapid exhumation of
12 ultrahigh-pressure metamorphosed continental crust. Proceedings of the National
13 Academy of Science, USA 94, 9532–9537.
14
15 973 Gao, T.S., Tang, J.F., Sang, H.Q., Hu, S.L., Qian, C.C., 2006. Whole-rock Ar-Ar
16 dating for low-grade metavolcanics within the Dabie orogen and its geological
17 implications. Chinese Science Bulletin 51, 1197–1202.
18
19 974 Gebauer, D., Schertl, H.P., Brix, M., Schreyer, W., 1997. 35 Ma old ultrahigh-pressure
20 metamorphism and evidence for very rapid exhumation in the Dora Maira Massif,
21 Western Alps. Lithos 41, 5–24.
22
23 975 Greentree, M.R., Li, Z.X., Li, X.H., Wu, H., 2006. Late mesoproterozoic to earliest
24 neoproterozoic basin record of the sibao orogenesis in western south china and
25 relationship to the assembly of rodinia. Precambrian Research 151(1–2), 79–100.
26
27 976 Griffin, W.L., Pearson, N.J., Belousova, E., Jackson, S.E., van Achterbergh, E.,
28 O’Reilly, S.Y., Shee, S.R., 2000. The Hf isotope composition of cratonic mantle:
29 LAM-MC-ICPMS analysis of zircon megacrysts in kimberlites. Geochimica et
30 Cosmochimica Acta 64, 133–147.
31
32 981 Groppo, C., Rolfo, F., Liu, Y.C., Deng, L.P., Wang, A.D., 2015. P-T evolution of
33 elusive UHP eclogites from the Luotian dome (north Dabie zone, China): how
34 far can the thermodynamic modeling lead us? Lithos 226, 183–200.
35
36 982 Hacker, B.R., Ratschbacher, L., Webb, L., Ireland, T., Walker, D., Dong, S.W., 1998.
37 U/Pb zircon ages constrain the architecture of the ultrahigh-pressure
38 Qinling–Dabie orogen, China. Earth and Planetary Science Letters 161,
39 215–230.
40
41
42
43
44
45
46
47
48
49
50
51
52
53
54
55
56
57
58
59
60
61
62
63
64
65

- 1 996 Hacker, B.R., Ratschbacher, L., Webb, L., McWilliams, M.O., Ireland, T., Calvert, A.,
2
3 997 Dong, S.W., Wenk, H.R., Chateigner, D., 2000. Exhumation of ultrahigh-pressure
4
5 998 continental crust in east central China: Late Triassic-Early Jurassic tectonic
6
7 999 unroofing. *Journal of Geophysical Research* 105 (B6), 13339–13364.
- 8
9 1000 Hanchar, J.M., Rudnick, R.L., 1995. Revealing hidden structures: the application of
10
11 1001 cathodoluminescence and back-scattered electron imaging to dating zircons from
12
13 1002 lower crustal xenoliths. *Lithos* 36, 289–303.
- 14
15 1003 Hanyu, T., Tatsumi, Y., Nakai, S., Chang, Q., Miyazaki, T., Sato, K., Tani, K., Shi-bata,
16
17 1004 T., Yoshida, T., 2006. Contribution of slab melting and slab dehydration to
18
19 1005 magmatism in the NE Japan arc for the last 25 Myr: Constraints from
20
21 1006 geochemistry. *Geochemistry Geophysics Geosystems* 7, Q08002.
- 22
23 1007 Hermann, J., Rubatto, D., Korsakov, A., Shatsky, V.S., 2001. Multiple zircon growth
24
25 1008 during fast exhumation of diamondiferous, deeply subducted continental crust
26
27 1009 (Kokchetav massif, Kazakhstan). *Contributions to Mineralogy and Petrology* 141,
28
29 1010 66–82.
- 30
31 1011 Hermann, J., Spandlera, C., Hacka, A., Korsakovb, A.V., 2006. Aqueous fluids and
32
33 1012 hydrous melts in high-pressure and ultra-high pressure rocks: Implications for
34
35 1013 element transfer in subduction zones. *Lithos* 92, 399–417.
- 36
37 1014 Hoffmann, J.E., Münker, C., Polat, A., Rosing, M.T., Schulz, T., 2011. The origin of
38
39 1015 decoupled Hf–Nd isotope compositions in Eoarchean rocks from southern West
40
41 1016 Greenland. *Geochimica et Cosmochimica Acta* 75, 6610–6628.
- 42
43 1017 Holland, T., Blundy, J., 1994. Non-ideal interactions in calcic amphiboles and their
44
45 1018 bearing on amphibole-plagioclase thermometry. *Contributions to Mineralogy and*
46
47 1019 *Petrology* 116, 433–447.
- 48
49 1020 Hong, J.A., Ma, B., Huang, Q., 2009. The Dafushan meta-basic/ultrameta-basic
50
51 1021 complex and genesis of the related rutile ore deposit at Zaoyang, Hubei (in
52
53 1022 Chinese with English abstract). *Chinese Journal of Geology* 44, 231–244.
- 54
55 1023 Hoskin, P.W., Ireland, T.R., 2000. Rare earth element chemistry of zircon and its use
56
57 1024 as a provenance indicator. *Geology* 28(7), 627–630.
- 58
59 1025 Hou, Z.H., Wang, C.X., 2007. Determination of 35 trace elements in geological
60
61
62
63
64
65

- 1 1026 samples by inductively coupled plasma mass spectrometry (in Chinese with
2 English abstract). *Journal of University of Science and Technology of China* 37,
3 1027
4 940–944.
5 1028
- 6 1029 Jiang, L., Siebel, W., Chen, F., Liu, Y.C., Chu, D., 2005. U-Pb zircon ages for the
7 Luzhengan Complex in northern part of the eastern Dabie orogen. *Science*
8 1030
9 China (Series D) 48, 1357–1367.
10 1031
- 11 1032 Kelemen, P.B., Hanghoj, K., Greene, A.R., 2003. One view of the geochemistry of
12 subducted-related magmatic arcs, with an emphasis on primitive andesites and
13 1033
14 lower crust. *Treatise of Geochemistry* 3, 593–659.
15 1034
- 16 1035 Kessel, R., Schmidt, M.W., Ulmer, P., Pettke, T., 2005. Trace element signature of
17 subduction-zone fluids, melts and supercritical liquids at 120–180 km depth.
18 1036
19 *Nature* 437, 724–727.
20 1037
- 21 1038 Le Bas, M.J., Le Maitre, R.W., Streckeisen, A., Zanettin, B., 1986. A chemical
22 classification of volcanic rocks based on the total alkali-silica diagram. *Journal*
23 1039
24 of *Petrology* 27(3), 745–750.
25 1040
- 26 1041 Lee, C.A., Luffi, P., Plank, T., Dalton, H., Leeman, W.P., 2009. Constraints on the
27 depths and temperatures of basic magma generation on Earth and other terrestrial
28 1042
29 planets using new thermobarometers for mafic magmas. *Earth and Planetary*
30 1043
31 *Science Letters* 279, 20–33.
32 1044
- 33 1045 Li, S.G., Xiao, Y.L., Liou, D.L., Ge, N.J., Zhang, Z.Q., Sun, S.S., Cong, B.L., Zhang,
34 R.Y., Hart, S.R., Wang, S.S., 1993. Collision of the North China and Yangtze
35 1046
36 blocks and formation of coesite bearing eclogites: timing and processes.
37 1047
38 *Chemical Geology* 109, 89–111.
39 1048
- 40 1049 Li, S.G., Jagoutz, E., Chen, Y.Z., Li, Q.L., 2000. Sm–Nd and Rb–Sr isotope
41 1050
42 chronology of ultrahigh-pressure metamorphic rocks and their country rocks at
43 1051
44 Shuanghe in the Dabie Mountains, central China. *Geochimica et Cosmochimica*
45 1052
46 *Acta* 64, 1077–1093.
47 1053
- 48 1053 Li, S.Z., Kusky, T.M., Zhao, G.C., Liu, X.C., Zhang, G.W., Kopp, H., Wang, L., 2010.
49 1054
50 Two-stage Triassic exhumation of HP–UHP terranes in the western Dabie orogen
51 1055
52 of China: constraints from structural geology. *Tectonophysics* 490, 267–293.
53
54
55
56
57
58
59
60
61
62
63
64
65

- 1 1056 Li, X.H., Li, Z.X., Ge, W.C., Zhou, H.W., Li, W.X., Liu, Y., Wingate, M.T.D., 2003a.
2
3 1057 Neoproterozoic granitoids in South China: crustal melting above a mantle plume
4
5 1058 at ca 825 Ma? *Precambrian Research* 122, 45–83.
- 6 1059 Li, X.H., Li, Z.X., Zhou, H., Liu, Y., Liang, X., Li, W., 2003b. SHRIMP U–Pb zircon
7
8 1060 age, geochemistry and Nd isotope of the Guandaoshan pluton in SW Sichuan:
9
10 1061 petrogenesis and tectonic significance. *Science China (Series D)* 46, 73–83.
- 11 1062 Li, X.P., Zheng, Y., Wu, Y., Chen, F., Gong, B., Li, Y.L., 2004. Low-T eclogite in the
12
13 1063 Dabie terrane of China: petrological and isotopic constrains on fluid activity and
14
15 1064 radiometric dating. *Contributions to Mineralogy and Petrology* 148, 443–470.
- 16 1065 Li, Z.X., Li, X.H., Kinny, P.D., Wang, J., Zhang, S., Zhou, H., 2003c. Geochronology
17
18 1066 of Neoproterozoic syn-rift magmatism in the Yangtze Craton, South China and
19
20 1067 correlations with other continents: evidence for a mantle superplume that broke
21
22 1068 up Rodinia. *Precambrian Research* 122, 85–109.
- 23 1069 Li, S.G., Huang, F., Zhou, H.Y., Li, H.M., 2003d. U-Pb isotopic compositions of the
24
25 1070 ultrahigh pressure metamorphic (UHPM) rocks from Shuanghe and gneisses
26
27 1071 from Northern Dabie zone in the Dabie Mountains, central China: Constraint on
28
29 1072 the exhumation mechanism of UHPM rocks. *Science China (Series D)* 46(3),
30
31 1073 200–209.
- 32 1074 Li, Y., Liu, Y.C., Yang, Y., Deng, L.P., 2017. New U-Pb geochronological constraints
33
34 1075 on formation and evolution of the Susong complex zone in the Dabie orogen.
35
36 1076 *Acta Geologica Sinica* 91, 1915–1918.
- 37 1077 Liu, F., Gerdes, A., Xue, H., Liang, F., 2006a. SHRIMP U-Pb zircon dating from
38
39 1078 eclogite lenses in marble, Dabie-Sulu UHP terrane: restriction on the prograde,
40
41 1079 UHP and retrograde metamorphic ages. *Acta Petrologica Sinica* 22, 1761–1778.
- 42 1080 Liu, J., Ye, K., Maruyama, S., Cong, B., Fan, H., 2001. Mineral inclusions in zircon
43
44 1081 from gneisses in the ultrahigh-pressure zone of the Dabie Mountains, China.
45
46 1082 *Journal of Geology* 109, 523–535.
- 47 1083 Liu, X.C., Jahn, B.-M., Liu, D., Dong, S., Li, S., 2004. SHRIMP U-Pb zircon dating
48
49 1084 of a metagabbro and eclogites from western Dabieshan (Hong'an Block), China,
50
51 1085 and its tectonic implications. *Tectonophysics* 394, 171–192.

- 1 1086 Liu, X.M, Gao, S., Diwu, C.R, Ling, W.L., 2008. Precambrian crustal growth of
2 Yangtze Craton as revealed by detrital zircon studies. *American Journal of*
3 *Science* 308(4), 421–468.
4
5 1088
6 1089 Liu, Y.C., Deng, L.P., Gu, X.F., Groppo, C., Franco, R., 2015. Application of
7 Ti-in-zircon and Zr-in-rutile thermometers to constrain high-temperature
8 metamorphism in eclogites from the Dabie orogen, central China. *Gondwana*
9 *Research* 27, 410–423.
10
11 1091
12 1092
13 1093 Liu, Y.C., Gu, X.F., Li, S.G., Hou, Z.F., Song, B., 2011a. Multistage metamorphic
14 events in granulitized eclogites from the North Dabie complex zone, central
15 China: evidence from zircon U-Pb age, trace element and mineral inclusion.
16 *Lithos* 122, 107–121.
17
18 1094
19 1095
20 1096
21 1097 Liu, Y.C., Gu, X.F., Rolfo, F., Chen, Z.Y., 2011b. Ultrahigh-pressure metamorphism
22 and multistage exhumation of eclogite from the Luotian dome, North Dabie
23 Complex Zone (central China): Evidence from mineral inclusions and
24 decompression texture. *Journal of Asian Earth Science* 42, 607–617.
25
26 1098
27 1099
28 1100
29 1101 Liu, Y.C., Li, S.G., 2005. Lower crustal rocks from the Dabie Mountains and their
30 subduction. *Acta Petrologica Sinica* 21, 1059–1066.
31
32 1102
33 1103 Liu, Y.C., Li, S.G., 2008. Detachment within subducted continental crust and
34 multi-plate successive exhumation of ultrahigh-pressure metamorphic rocks:
35 Evidence from the Dabie-Sulu orogenic belt. *Chinese Science Bulletin* 53,
36 3105–3119.
37
38 1104
39 1105
40 1106
41 1107 Liu, Y.C., Li, S.G., Gu, X.F., Hou, Z.H., 2006b. Zircon SHRIMP U-Pb dating for
42 olivine gabbro at Wangmuguan in the Beihuaiyang zone and its geological
43 significance. *Chinese Science Bulletin* 51, 2500–2506.
44
45 1108
46 1109
47 1110 Liu, Y.C., Li, S.G., Gu, X.F., Xu, S.T., Chen, G.B., 2007a. Ultrahigh-pressure eclogite
48 transformed from mafic granulite in the Dabie orogen, east-central China.
49 *Journal of Metamorphic Geology* 25, 975–989.
50
51 1111
52 1112
53 1113 Liu, Y.C., Li S.G., Xu, S.T., 2007b. Zircon SHRIMP U-Pb dating for gneiss in
54 northern Dabie high T/P metamorphic zone, central China: Implication for
55 decoupling within subducted continental crust. *Lithos* 96, 170–185.
56
57 1114
58 1115
59
60
61
62
63
64
65

- 1 1116 Liu, Y.C., Li, S.G., Xu, S.T., John, B., Zheng, Y.F., Zhang, Z.Q., Jiang, L.L., Chen,
2 G.B., Wu, W.P., 2005. Geochemistry and geochronology of eclogites from the
3 northern Dabie Mountains, central China. *Journal of Asian Earth Science* 25,
4 431–443.
5
6 1119
7
8 1120 Liu, Y.C., Liu, L.X., Gu, X.F., Li, S.G., Liu, J., Song, B., 2010. Occurrence of
9 Neoproterozoic low-grade metagranite in the western Beihuaiyang zone, the
10 Dabie orogen. *Chinese Science Bulletin* 55, 3490–3498.
11
12 1122
13 1123 Liu, Y.C., Liu, L.X., Li, Y., Gu, X.F., Song, B., 2017. Zircon U-Pb geochronology and
14 petrogenesis of metabasites from the western Beihuaiyang zone in the Hong’an
15 orogen, central China: Implications for detachment within subducting continental
16 crust at shallow depths. *Journal of Asian Earth Science* 145, 74–90.
17
18 1126
19 1127 Liu, Y.C., Wang, A.D., Rolfo, F., Groppo, C., Gu, X.F., Song, B., 2009.
20 Geochronological and petrological constraints on Palaeoproterozoic granulite
21 facies metamorphism in southeastern margin of the North China Craton. *Journal*
22 *of Metamorphic Geology* 27, 125–138.
23
24 1128
25 1129
26 1130
27 1131 Liu, Y.S., Gao, S., Yuan, H.L., Zhou, L., Liu, X.M., Wang, X.C., Hu, Z.C., Wang, L.S.,
28 2004. U–Pb zircon ages and Nd, Sr, and Pb isotopes of lower crustal xenoliths
29 from North China Craton: insights on evolution of lower continental crust.
30 *Chemical Geology* 211, 87–109.
31
32 1132
33 1133
34 1134
35 1135 Ludwig, K.R., 2001. Users Manual for Isoplot/Ex (rev. 2.49): A Geochronological
36 Toolkit for Microsoft Excel. Berkeley Geochronology Center, Special
37 Publication No. 1a, 55 p.
38
39 1137
40 1138 Maruyama, S., Liou, J.G., Terabayashi, M., 1996. Blueschists and eclogites of the
41 world, and their exhumation. *International Geology Review* 38, 485–594.
42
43 1139
44 1140 Nasdala, L., Massonne, H.J., 2000. Microdiamonds from the Saxonian Erzgebirge,
45 Germany: in situ micro-Raman characterisation. *European Journal of Mineralogy*
46 12, 495–498.
47
48 1141
49 1142
50 1143 Nowell, G.M., Kempton, P.D., Noble, S.R., Fitton, J.G., Saunders, A.D., Mahoney, J.J.,
51 Taylor, R.N., 1998. High precision Hf isotope measurements of MORB and OIB
52 by thermal ionisation mass spectrometry: insights into the depleted mantle.
53
54 1144
55 1145
56
57
58
59
60
61
62
63
64
65

1 1146 Chemical Geology 149, 211–233.

2 1147 Okay, A.I., Xu, S.T., Sengör, A.M.C., 1989. Coesite from the Dabie Shan eclogites,
3
4 1148 central China. *European Journal of Mineralogy* 1, 595–598.

5
6 1149 Okay, A.I., Sengör, A.M.C., 1992. Evidence for intracontinental thrust-related
7
8 1150 exhumation of the ultra-high-pressure rocks in China. *Geology* 20, 411–414.

9
10 1151 Okay, A.I., Sengör, A.M.C., Satir, M., 1993. Tectonics of an ultrahigh-pressure
11
12 1152 metamorphic terrane: the Dabie Shan/Tongbai orogen, China. *Tectonics* 12,
13
14 1153 1320–1334.

15
16 1154 Palme, H., O'Neill, H.St.C., 2003. Cosmochemical constraints of mantle composition.
17
18 1155 *Treatise of Geochemistry* 2, 1–38.

19
20 1156 Patchett, P.J., White, W.M., Feldmann, H., Kienlinczuk, S., Hofmann, A.W., 1984.
21
22 1157 Hafnium/rare earth element fractionation in the sedimentary system and crustal
23
24 1158 recycling into the Earth's mantle. *Earth and Planetary Science Letters* 1984,
25
26 1159 365–378.

27
28 1160 Rolfo, F., Compagnoni, R., Xu, S., Jiang, L., 2000. First report of felsic whiteschist in
29
30 1161 the ultrahigh-pressure metamorphic belt of Dabie Shan, China. *European Journal*
31
32 1162 *of Mineralogy* 12, 883–898.

33
34 1163 Rolfo, F., Compagnoni, R., Wu, W.P., Xu, S.T., 2004. A coherent lithostratigraphic
35
36 1164 unit in the coesite–eclogite complex of Dabie Shan, China: geologic and
37
38 1165 petrologic evidence. *Lithos* 73, 71–94.

39
40 1166 Roux, V.L., Bodinier, J.L., Alard, O., O'Reilly, S.Y., Griffin, W.L., 2009. Isotopic
41
42 1167 decoupling during porous melt flow: a case-study in the Lherzperidotite. *Earth*
43
44 1168 *and Planetary Science Letters* 279, 76–85.

45
46 1169 Rowley, D.B., Xue, F., Tucker, R.D., Peng, Z.X., Baker, J., Davis, A., 1997. Ages of
47
48 1170 ultrahigh pressure metamorphism and protolith orthogneisses from the eastern
49
50 1171 Dabie Shan: U/Pb zircon geochronology. *Earth and Planetary Science Letters*
51
52 1172 151, 191–203.

53
54 1173 Rudnick, R.L., Gao, S., 2003. Composition of the continental crust. *Treatise on*
55
56 1174 *Geochemistry* 3, 1–64.

57
58 1175 Salters, V.J.M., Stracke, A., 2004. Composition of the depleted mantle. *Geochemistry*
59
60
61
62
63
64
65

1 1176 Geophysics Geosystems 5, Q05004.

2 1177 Scherer, E., Munker, C., Mezger, K., 2001. Calibration of the lutetium–hafnium clock.

3 1178 Science 293, 683–687.

4 1179 Schertl, H.P., Okay, A.I., 1994. A coesite inclusion in dolomite in Dabie Shan, China;

5 1180 petrological and rheological significance. European Journal of Mineralogy 6,

6 1181 995–1000.

7 1182 Schmidt, M.W., 1992. Amphibole composition in tonalite as a function of pressure: an

8 1183 experimental calibration of the Al-in-hornblende barometer. Contributions to

9 1184 Mineralogy and Petrology 110, 304–310.

10 1185 Smith, D.C., 1984. Coesite in clinopyroxene in the Caledonides and its implications

11 1186 for geodynamics. Nature 310, 641–644.

12 1187 Sobolev, N.V., Shatsky, V.S., 1990. Diamond inclusions in garnets from metamorphic

13 1188 rocks: a new environment for diamond formation. Nature 343, 742–746.

14 1189 Su, W., Xu, S., Jiang, L., Liu, Y.C., 1996. Coesite from quartz jadeitite in the Dabie

15 1190 Mountains, Eastern China. Mineralogical Magazine 60, 659–662.

16 1191 Sun, S.S., McDonough, W.F., 1989. Chemical and isotopic systematics of oceanic

17 1192 basalts: implications for mantle composition and processes. In: Saunders, A.D.,

18 1193 Norry, M.J. (Eds.), Magmatism in the ocean basins. Geological Society, London,

19 1194 Special Publications 42, pp. 313–345.

20 1195 Tabata, H., Yamauchi, K., Maruyama, S., Liou, J.G., 1998. Tracing the Extent of a

21 1196 UHP Metamorphic Terrane: Mineral-Inclusion Study of Zircons in Gneisses from

22 1197 the Dabie Shan. In: Hacker, B.R., Liou, J.G. (Eds), When Continents Collide:

23 1198 Geodynamics and Geochemistry of Ultrahigh-Pressure Rocks. Springer

24 1199 Netherlands 10, pp. 261–273.

25 1200 Tang, H.F., Liu, C.Q., Nakai, S., Orihashi, Y., 2007. Geochemistry of eclogites from

26 1201 the Dabie–Sulu terrane, eastern china: new insights into protoliths and trace

27 1202 element behaviour during UHP metamorphism. Lithos 95, 441–457.

28 1203 Tang, J., Zheng, Y.F., Wu, Y. B., Gong, B., 2006. Zircon SHRIMP U–Pb dating, C and

29 1204 O isotopes for impure marbles from the Jiaobei terrane in the Sulu orogen:

30 1205 Implication for tectonic affinity. Precambrian Research 144, 1–18.

- 1 1206 Tappe, S., Pearson, D.G., Nowell, G., Nielsen, T., Milstead, P., Muehlenbachs, K.,
2 1207 2011. A fresh isotopic look at Greenland kimberlites: cratonic mantle lithosphere
3
4 1208 imprint on deep source signal. *Earth and Planetary Science Letters* 305, 235–248.
5
6 1209 Taylor, S.R., McLennan, S.M., 1985. *The Continental Crust: Its Composition and*
7
8 1210 *Evolution*. Blackwell Scientific Publications, Oxford.
9
10 1211 Tomkins, H.S., Powell, R., Ellis, D.J., 2007. The pressure dependence of the
11
12 1212 zirconium-in-rutile thermometer. *Journal of Metamorphic Geology* 25, 703–713.
13
14 1213 Tsai, C.H., Liou, J.G., 2000. Eclogite-facies relics and inferred ultrahigh-pressure
15
16 1214 metamorphism in the North Dabie Complex, central-eastern China. *American*
17
18 1215 *Mineralogist* 85, 1–8.
19
20 1216 Velikoslavinsky, S.D., Krylov, D.P. 2014. Geochemical discrimination of basalts
21
22 1217 formed in major geodynamic settings. *Geotectonics* 48(6), 427–439.
23
24 1218 Wang, L.J., Griffin, W.L., Yu, J.H., O'Reilly, S.Y., 2010. Precambrian crustal
25
26 1219 evolution of the Yangtze Block tracked by detrital zircons from Neoproterozoic
27
28 1220 sedimentary rocks. *Precambrian Research* 177(1), 131–144.
29
30 1221 Wang, M.X., Wang, C.Y., Zhao, J.H., 2013. Zircon U/Pb dating and Hf-O isotopes of
31
32 1222 the Zhouan ultramafic intrusion in the northern margin of the Yangtze Block, SW
33
34 1223 China: Constraints on the nature of mantle source and timing of the
35
36 1224 supercontinent Rodinia breakup. *Chinese Science Bulletin* 58(7), 777–787.
37
38 1225 Wang, X., Liou, J.G., Mao, H.K., 1989. Coesite-bearing eclogites from the Dabie
39
40 1226 Mountains in central China. *Geology* 17, 1085–1088.
41
42 1227 Whalen, J.B., Currie, K.L., Chappell, B.W., 1987. A-type granites: geochemical
43
44 1228 characteristics, discrimination and petrogenesis. *Contributions to Mineralogy and*
45
46 1229 *Petrology* 95, 407–419.
47
48 1230 Whitney, J.A., Stormer, J.C., 1977. Two-feldspar geothermometry, geobarometry in
49
50 1231 mesozonal granitic intrusions: three examples from the Piedmont of Georgia.
51
52 1232 *Contributions to Mineralogy and Petrology* 63(1), 51–64.
53
54 1233 Williams, I.S., 1998. U–Th–Pb geochronology by ion microprobe. Applications of
55
56 1234 Microanalytical Techniques to Understanding Mineralizing Processes. In:
57
58 1235 McKibben, M.A., Shanks III, W.C., Ridley, W.I. (Eds.), *Reviews in Economic*
59
60
61
62
63
64
65

- 1 1236 Geology 7, pp. 1–35.
- 2 1237 Winchester, J.A., Floyd, P.A., 1977. Geochemical discrimination of different magma
- 3 series and their differentiation products using immobile elements. Chemical
- 4 1238
- 5
- 6 1239 Geology 20, 325–343.
- 7
- 8 1240 Workman, R.K., Hart, S.R., 2005. Major and trace element composition of the
- 9
- 10 1241 depleted MORB mantle (DMM). Earth and Planetary Science Letters 231,
- 11
- 12 1242 53–72.
- 13
- 14 1243 Wu, F.Y., Sun, D.Y., Li, H., Jahn, B.M., Wilde, S., 2002. A-type granites in
- 15
- 16 1244 northeastern china: age and geochemical constraints on their petrogenesis.
- 17
- 18 1245 Chemical Geology 187, 143–173.
- 19
- 20 1246 Wu, Y.B., Zheng, Y.F., Zhao, Z.F., Gong, B., Liu, X.M., Wu, F.Y., 2006a. U–Pb, Hf
- 21
- 22 1247 and O isotope evidence for two episodes of fluid-assisted zircon growth in
- 23
- 24 1248 marble-hosted eclogites from the Dabie orogen. Geochimica et Cosmochimica
- 25
- 26 1249 Acta 70, 3743–3761.
- 27
- 28 1250 Wu, R.X., Zheng, Y.F., Wu, Y.B., Zhao, Z.F., Zhang, S.B., Liu, X.M., Wu, F.Y., 2006b.
- 29
- 30 1251 Reworking of juvenile crust: element and isotope evidence from Neoproterozoic
- 31
- 32 1252 granodiorite in South China. Precambrian Research 146, 179–212.
- 33
- 34 1253 Wu, Y.B., Zheng, Y.F., Tang, J., Gong, B., Zhao, Z.F., Liu, X., 2007. Zircon U–Pb
- 35
- 36 1254 dating of water–rock interaction during Neoproterozoic rift magmatism in South
- 37
- 38 1255 China. Chemical Geology 246, 65–86.
- 39
- 40 1256 Xiao, Y., Hoefs, J., van den Kerkhof, A.M., Li, S.G., 2001. Geochemical constraints of
- 41
- 42 1257 the eclogite and granulite facies metamorphism as recognized in the Raobazhai
- 43
- 44 1258 complex from North DabieShan, China. Journal of Metamorphic Geology 19,
- 45
- 46 1259 3–19.
- 47
- 48 1260 Xu, S.T., Jiang, L.L., Liu, Y.C., Zhang, Y., 1992a. Tectonic Framework and Evolution
- 49
- 50 1261 of the Dabie Mountains in Anhui, Eastern China. Acta Geologica Sinica 5,
- 51
- 52 1262 221–238.
- 53
- 54 1263 Xu, S.T., Okay, A.I., Ji, S.Y., Sengör, A.M.C., Su, W., Liu, Y.C., Jiang, L.L., 1992b.
- 55
- 56 1264 Diamond from the Dabie Shan metamorphic rocks and its implication for
- 57
- 58 1265 tectonic setting. Science 256, 80–82.
- 59
- 60
- 61
- 62
- 63
- 64
- 65

- 1 1266 Xu, S.T., Liu, Y.C., Su, W., Wang, R.C., Jiang, L.L., Wu, W.P., 2000. Discovery of the
2 eclogite and its petrography in the Northern Dabie Mountains. Chinese Science
3 Bulletin 45, 273–278.
4
5 1268
6 1269 Xu, S.T., Liu, Y.C., Chen, G.B., Compagnoni, R., Rolfo, F., He, M.C., Liu, H.F., 2003.
7
8 1270 New finding of micro-diamonds in eclogites from Dabie-Sulu region in
9
10 1271 central-eastern China. Chinese Science Bulletin 48, 988–994.
11
12 1272 Xu, S.T., Liu, Y.C., Chen, G.B., Ji, S.Y., Ni, P., Xiao, W.S., 2005. Microdiamonds,
13
14 1273 their classification and tectonic implications for the host eclogites from the Dabie
15
16 1274 and Su-Lu regions in central eastern China. Mineralogical Magazine 69,
17
18 1275 509–520.
19
20 1276 Xue, H.M., Ma, F., Song, Y.Q., 2011. Geochemistry and SHRIMP zircon U-Pb data of
21
22 1277 Neoproterozoic meta-magmatic rocks in the Suizhou-Zaoyang area, northern
23
24 1278 margin of the Yangtze Craton, Central China. Acta Petrologica Sinica 27,
25
26 1279 1116–1130.
27
28 1280 Yu, S.Y., Xu, Y.G., Huang, X.L., Ma, J.L., Ge, W.C., Zhang, H.H., Qin, X.F., 2009.
29
30 1281 Hf–Nd isotopic decoupling in continental mantle lithosphere beneath Northeast
31
32 1282 China: effects of pervasive mantle metasomatism. Journal of Asian Earth Science
33
34 1283 35, 554–570.
35
36 1284 Yuan, H.L., Gao, S., Liu, X.M., Gunther, D., Wu, F.Y., 2004. Accurate U–Pb age and
37
38 1285 trace element determinations of zircon by laser ablation-inductively coupled
39
40 1286 plasma mass spectrometry. Geostandards and Geoanalytical Research 28,
41
42 1287 353–370.
43
44 1288 Zack, T., Moraes, R., Kronz, A., 2004. Temperature dependence of Zr in rutile:
45
46 1289 empirical calibration of a rutile thermometer. Contributions to Mineralogy and
47
48 1290 Petrology, 148, 471–488.
49
50 1291 Zartman, R.E., 1981. Plumbotectonics—the model. Tectonophysics 75, 135–162.
51
52 1292 Zhang, H.F., Gao, S., Zhang, Z.Q., Zhang, B.R., Zhang, L., Hu, S.H., 2002.
53
54 1293 Geochemical and Sr-Nd-Pb isotopic compositions of Cretaceous granitoids:
55
56 1294 constraints on tectonic framework and crustal structure of the Dabieshan
57
58 1295 ultrahigh-pressure metamorphic belt, China. Chemical Geology 186, 281–299.
59
60
61
62
63
64
65

- 1 1296 Zhang, R.Y., Liou, J.G., Zheng, Y.F., Fu, B., 2003. Transition of UHP eclogites to
2 1297 gneissic rocks of low-amphibolite facies during exhumation: evidence from the
3 1298 Dabie terrane, central China. *Lithos*, 70, 269–291.
- 4 1299 Zhang, S.B., Zheng, Y.F., Wu, Y.B., Zhao, Z.F., Gao, S., Wu, F.Y., 2006a. Zircon
5 1300 isotope evidence for ≥ 3.5 Ga continental crust in the Yangtze craton of China.
6 1301 *Precambrian Research* 146, 16–34.
- 7 1302 Zhang, S.B., Zheng, Y.F., Wu, Y.B., Zhao, Z.F., Gao, S., Wu, F.Y., 2006b. Zircon
8 1303 U–Pb age and Hf–O isotope evidence for Paleoproterozoic metamorphic event in
9 1304 South China. *Precambrian Research* 151, 265–288.
- 10 1305 Zhang, S.B., Zheng, Y.F., Wu, Y.B., Zhao, Z.F., Gao, S., Wu, F.Y., 2006c. Zircon
11 1306 U–Pb age and Hf isotope evidence for 3.8 Ga crustal remnant and episodic
12 1307 reworking of Archean crust in South China. *Earth and Planetary Science Letters*
13 1308 252, 56–71.
- 14 1309 Zhao, G.C., Cawood, P.A., 2012. Precambrian geology of China. *Precambrian*
15 1310 *Research* 222–223, 13–54.
- 16 1311 Zhao, J.H., Zhou, M.F., 2009. Secular evolution of the Neoproterozoic lithospheric
17 1312 mantle underneath the northern margin of the Yangtze Block, South China.
18 1313 *Lithos* 107, 152–168.
- 19 1314 Zhao, J.H., Li, Q.W., Liu, H., Wang, W., 2018. Neoproterozoic magmatism in the
20 1315 western and northern margins of the Yangtze Block (South China) controlled by
21 1316 slab subduction and subduction-transform-edge-propagator. *Earth-Science*
22 1317 *Reviews* 187, 1–18.
- 23 1318 Zheng, Y.F., Zhou, J.B., Wu, Y.B., Xie, Z., 2005. Low-grade metamorphic rocks in the
24 1319 Dabie-Sulu orogenic belt: a passive-margin accretionary wedge deformed during
25 1320 continent subduction. *International Geology Review* 47, 851–871.
- 26 1321 Zheng, Y.F., Zhao, Z.F., Wu, Y.B., Zhang, S.B., Liu, X.M., Wu, F.Y., 2006. Zircon
27 1322 U–Pb age, Hf and O isotope constraints on protolith origin of ultrahigh-pressure
28 1323 eclogite and gneiss in the Dabie orogen. *Chemical Geology* 231, 135–158.
- 29 1324 Zheng, Y.F., Zhang, S.B., Zhao, Z.F., Wu, Y.B., Li, X.H., Li, Z.X., Wu, F.Y., 2007.
30 1325 Contrasting zircon Hf and O isotopes in the two episodes of Neoproterozoic

1 1326 granitoids in South China: implications for growth and reworking of continental
2 1327 crust. *Lithos* 96, 127–150.
3
4 1328 Zheng, Y.F., Wu, R.X., Wu, Y.B., Zhang, S.B., Yuan, H.L., Wu, F.Y., 2008. Rift
5
6 1329 melting of juvenile arc-derived crust: geochemical evidence from
7
8 1330 Neoproterozoic volcanic and granitic rocks in the Jiangnan Orogen, South China.
9
10 1331 *Precambrian Research* 163, 351–383.
11
12 1332 Zheng, Y.F., Xia, Q.X., Chen, R.X., Gao, X.Y., 2011. Partial melting, fluid
13
14 1333 supercriticality and element mobility in ultrahigh-pressure metamorphic rocks
15
16 1334 during continental collision. *Earth Science Reviews* 107, 342–374.
17
18 1335 Zhou, M.F., Kennedy, A.K., Sun, M., Malpas, J., Lesher, C.M., 2002a. Neoproterozoic
19
20 1336 arc-related mafic intrusions in the northern margin of South China: implications
21
22 1337 for accretion of Rodinia. *The Journal of Geology* 110, 611–618.
23
24 1338 Zhou, M.F., Yan, D.P., Kennedy, A.K., Li, Y.Q., Ding, J., 2002b. SHRIMP zircon
25
26 1339 geochronological and geochemical evidence for Neo-proterozoic arc-related
27
28 1340 magmatism along the western margin of the Yangtze Block, South China. *Earth
29
30 1341 and Planetary Science Letters* 196, 51–67.
31
32 1342 Zhou, M.F., Ma, Y.X., Yan, D.P., Xia, X.P., Zhao, J.H., Sun, M., 2006a. The Yanbian
33
34 1343 Terrane (Southern Sichuan Province, SW China): a Neoproterozoic arc
35
36 1344 assemblage in the western margin of the Yangtze Block. *Precambrian Research*
37
38 1345 144, 19–38.
39
40 1346 Zhou, M.F., Yan, D.P., Wang, C.L., Qi, L., Kennedy, A., 2006b. Subduction related
41
42 1347 origin of the 750 Ma Xuelongbao adakitic complex (Sichuan Province, China):
43
44 1348 implications for the tectonic setting of the giant Neoproterozoic magmatic event
45
46 1349 in South China. *Earth and Planetary Science Letters* 248, 286–300.
47
48 1350 Zindler, A., Hart, S., 1986. Chemical geodynamics. *Annual Review of Earth and
49
50 1351 Planetary Science* 14, 493–571.
51
52 1352
53
54
55
56
57
58
59
60
61
62
63
64
65

Figure captions

1 1353

2
3 1354 **Figure 1** Schematic geological map of the Dabie orogen. The inset shows its location
4
5 1355 within the Triassic Qinling–Dabie–Sulu collision orogen in central China (modified
6
7 1356 from Liu et al., 2007a). Sample locality is marked by a red star. BZ = Beihuaiyang
8
9 1357 zone, NDZ = North Dabie high-T/UHP complex zone, CDZ = Central Dabie
10
11 1358 mid-T/UHP metamorphic zone, SDZ = South Dabie low-T eclogite zone, SZ =
12
13 1359 Susong complex zone, HMZ = Huwan mélangé zone, HZ = Hong'an low-T eclogite
14
15 1360 zone, DC = amphibolite-facies Dabie complex, XMF = Xiaotian-Mozitan fault, WSF
16
17 1361 = Wuhe-Shuihou fault, HMF = Hualiangting-Mituo fault, TSF = Taihu-Shanlong fault,
18
19 1362 TLF = Tan-Lu fault.

21 1363

22
23 1364 **Figure 2** Field photograph showing meta-basite lens tectonically enclosed within
24
25 1365 meta-granitoid.

26 1366

27
28
29 1367 **Figure 3** Photomicrographs of plane- and corresponding cross-polarized images for
30
31 1368 the meta-basite sample 11LJG7 (a & b), low-Si meta-granitoid sample 1209LJG5 (c
32
33 1369 & d), high-Si meta-granitoid sample 1209LJG1 (e & f). Pl: plagioclase; Rt: rutile;
34
35 1370 Amp: amphibole; Bt: biotite; Qz: quartz; Ap: apatite; Kfs: K-feldspar; Aln: allanite.

36 1371

37
38
39 1372 **Figure 4** TAS (total alkalis versus silica) diagram (Le Bas et al., 1986) (a) and
40
41 1373 Zr/TiO₂ vs Nb/Y (Winchester and Floyd, 1977) (b) plots for the studied rocks in
42
43 1374 Longjingguan. **Green** circles: meta-basites; **red** circles: low-Si granitoids; **blue** circles:
44
45 1375 high-Si granitoids; Pc: picrobasalt; B: basalt; O1: basaltic andesite; O2: andesite; O3:
46
47 1376 dacite; R: rhyolite; S1: trachybasalt; S2: basaltic trachyandesite; S3: trachyandesite; T:
48
49 1377 trachyte; U1: basanite; U2: phonotephrite; U3: tephriphonolite; Ph: phonolite; F:
50
51 1378 foidite. **Symbols used for different types of samples are the same as in the following**
52
53 1379 **figures.**

54 1380

55
56
57 1381 **Figure 5** Chondrite-normalized REE patterns (a) and primitive mantle-normalized

1 1382 trace element patterns (b) for the studied rocks in Longjingguan and for the UHP
2 1383 eclogites (c & d) in the CDZ. Normalized values and the data of the N-MORB and
3 1384 E-MORB are from Sun and McDonough (1989), the elemental data of the UHP
4 1385 eclogites are from Tang et al. (2007).

5 1386

6 1387 **Figure 6** Representative CL images of zircons from the meta-basites (samples
7 1388 11LJG3 and 11LJG7), low-Si meta-granitoids (samples 11LJG2, 1209LJG5 and
8 1389 1202LJG3) and high-Si meta-granitoid (sample 1303LJG2) in Longjingguan. The red
9 1390 circles locate the SHRIMP analysis spots, and the red numbers are the corresponding
10 1391 $^{206}\text{Pb}/^{238}\text{U}$ ages.

11 1392

12 1393 **Figure 7** Mineral inclusions within metamorphic zircon domains from samples
13 1394 11LJG3 (a-i) and 11LJG2 (j-l). Hbl, hornblende; Rt, rutile; Qz, quartz; Ap, apatite;
14 1395 Kfs, K-feldspar; Mus, muscovite; Ep, epidote; Ttn, titanite; Ilm, ilmenite.

15 1396

16 1397 **Figure 8** Zircon rare earth element (REE) patterns for the meta-basites (samples
17 1398 11LJG3 and 11LJG7) and meta-granitoids (samples 1209LJG5, 11LJG2, 1303LJG2
18 1399 and 1202LJG3) in Longjingguan. Normalized values are from Sun and McDonough
19 1400 (1989).

20 1401

21 1402 **Figure 9** SHRIMP zircon U-Pb ages for the meta-basites (a & b), low-Si
22 1403 meta-granitoids (c, d, e, g & h) and high-Si meta-granitoid (f) in Longjingguan. (e)
23 1404 and (h) correspond to the dashed squares in (d) and (g), respectively.

24 1405

25 1406 **Figure 10** Zircon $\varepsilon_{\text{Hf}}(t)$ vs U-Pb age of the studied meta-basites and meta-granitoids,
26 1407 as well as the UHP eclogites and gneisses (data from Zheng et al., 2006) from the
27 1408 CDZ. The evolution trendlines of the depleted mantle (DMM) and chondrite are from
28 1409 Griffin et al. (2000).

29 1410

30 1411

1 1412 **Figure 11** Plot of Nd vs Sr isotopes for the meta-basites (samples 11LJG3 to 11LJG8)
2 1413 from Longjingguan. MORB: mid-ocean ridge basalt; UCC: upper continental crust;
3
4 1414 LCC: lower continental crust.
5

6 1415
7
8 1416 **Figure 12** ($^{207}\text{Pb}/^{204}\text{Pb}$)_i vs ($^{206}\text{Pb}/^{204}\text{Pb}$)_i and ($^{208}\text{Pb}/^{204}\text{Pb}$)_i vs ($^{206}\text{Pb}/^{204}\text{Pb}$)_i plots for
9 1417 the meta-basites (samples 11LJG3 to 11LJG8) from Longjingguan. The initial Pb
10 1418 isotopes data of the meta-basites are calibrated with t=230 Ma, the blue-green and
11 1419 grey areas in the diagrams represent the UHP orthogneiss and eclogites in the North
12 1420 Dabie (NDZ) and Central Dabie (CDZ) terranes, respectively (data from Zhang et al.,
13 1421 2002; Li et al., 2003d). The initial Pb isotope data of MORB, EMI and EMII are from
14 1422 Zindler and Hart. (1986), and that of lower crust (LC) is from Liu et al. (2004).
15 1423 ($^{207}\text{Pb}/^{204}\text{Pb}$)_{NHRL}=0.1084×($^{206}\text{Pb}/^{204}\text{Pb}$)_i + 13.401; ($^{208}\text{Pb}/^{204}\text{Pb}$)_{NHRL}=1.209×($^{206}\text{Pb}/$
16 1424 ^{204}Pb)_i + 15.627.
17
18 1425

19 1426 **Figure 13** Tectonic discrimination diagrams (Velikoslavinsky and Krylov, 2014) for
20 1427 the meta-basites in Longjingguan. Values of the discriminant functions DF₁(x), DF₂(x),
21 1428 DF₃(x) and DF₅(x) have been calculated from formula: D(x) = Σa_i*x_i + constant,
22 1429 where a_i is coefficient at corresponding variable; x_i is value of variable (oxide content,
23 1430 wt %; trace element content, ppm). In the DF₁(x) – DF₂(x) diagram (a), the
24 1431 meta-basites (green circles) plot in the field of WPB. In the DF₃(x) – frequency (%) (b)
25 1432 and DF₅(x) – frequency (%) (c) diagrams, the rocks (the red rectangles with dashed
26 1433 oblique lines) have function values coincident with the majority population of WPB.
27
28 1434

29 1435 **Figure 14** Plots employing Ga/Al (Whalen et al., 1987) for the meta-granitoids in
30 1436 Longjingguan. I & S: I-type and S-type granite; A: A-type granite.
31
32 1437

33 1438 **Figure 15** (Sr/Y) vs. Y diagram discriminating adakite and TTG from typical arc
34 1439 calc-alkaline rocks (Drummond and Defant, 1990).
35
36 1440

1 1 **Petrogenesis and tectonic significance of Neoproterozoic**
2
3 2 **meta-basites and meta-granitoids within the central Dabie**
4
5 3 **UHP zone, China: Geochronological and geochemical**
6
7 4 **constraints**
8
9

10
11 5
12 6 Yuan Li ^a, Yi-Can Liu ^{a,*}, Yang Yang ^a, F. Rolfo ^{b,c} and C. Groppo ^b

13 7 ^a CAS Key Laboratory of Crust-Mantle Materials and Environments, School of Earth and Space
14 8 Sciences, University of Science and Technology of China, Hefei 230026, China

15
16 9 ^b Department of Earth Sciences, University of Torino, Via Valperga Caluso 35, 1-10125 Torino,
17
18 10 Italy

19
20 11 ^c C.N.R. – I.G.G., Section of Torino, Via Valperga Caluso 35, 1-10125 Torino, Italy

21
22
23
24
25
26
27
28
29
30
31
32
33
34
35
36
37
38 19 *Corresponding author. Tel./fax: +86 551 63600367.

39
40 20 *E-mail address:* liuyc@ustc.edu.cn (Y.-C. Liu)

Abstract

A combined geochemical (whole-rock elements and Sr-Nd-Pb isotopes, zircon trace elements and Hf isotopes) and geochronological (zircon U-Pb ages) study was carried out on the relatively low-grade meta-basites and meta-granitoids from Longjingguan within the central Dabie ultrahigh-pressure (UHP) metamorphic zone, east-central China. Zircon investigations indicate that the meta-basites were formed at ~772 Ma and subsequently experienced granulite-facies metamorphism at ~768 Ma and a later thermal overprint at ~746 Ma, while the meta-granitoids recorded three groups of zircon ages at ca. 819 Ma, 784 Ma and 746 Ma. The meta-granitoids can be subdivided into low-Si and high-Si types, and they were derived from mid-Neoproterozoic partial melting of the Neoproterozoic and Paleoproterozoic metamorphic basement rocks of the South China Block, respectively. These Neoproterozoic zircon ages are consistent with the protolith ages of the Dabie Triassic UHP meta-igneous rocks. In addition, the low-grade rocks have bulk-rock Pb isotope compositions overlapping with the UHP meta-igneous rocks. Therefore, the low-grade meta-basites and meta-granitoids could be interpreted as counterparts of the UHP meta-igneous rocks in this area, suggesting the same petrogenesis for their protoliths in the Neoproterozoic.

Trace element patterns indicate that the low-grade rocks have better preserved their protolith compositions than their equivalent UHP rocks, and thus they are more suitable for elucidating the Neoproterozoic evolution of the northern margin of the South China Block. Zircon ages combined with geochemical features strongly suggest that the protoliths of the meta-granitoids and meta-basites were formed in a magmatic arc and a continental rifting setting, respectively. More specifically, the granitoids derived from partial melting of Neoproterozoic and Paleoproterozoic basement materials at ~819 Ma in a magmatic arc setting, whereas the precursors of the meta-basites are products of a continental rifting event at about 784 to 772 Ma. The obtained results provide new geochronological and geochemical constraints for the Neoproterozoic evolution of the northern margin of the South China Block, which can further

1 51 contribute to the understanding of the breakup of the supercontinent Rodinia.

2 52

3
4 53 **Keywords:** Neoproterozoic evolution; meta-basite and meta-granitoid; Rodinia

5
6 54 assembly and break-up; continental rifting; continental collision

7
8 55

9
10
11
12
13
14
15
16
17
18
19
20
21
22
23
24
25
26
27
28
29
30
31
32
33
34
35
36
37
38
39
40
41
42
43
44
45
46
47
48
49
50
51
52
53
54
55
56
57
58
59
60
61
62
63
64
65

1. Introduction

The Dabie orogen located in central China is a continental collision belt with the exposed largest area of coesite- and diamond-bearing ultrahigh-pressure (UHP) metamorphic rocks in the world, and thus it has attracted great research interest in the geologic community during the past decades (e.g., Okay et al., 1989, 1993; Wang et al., 1989; Xu et al., 1992a,b, 2003; Li et al., 1993, 2000; Ames et al., 1996; Rowley et al., 1997; Hacker et al., 1998, 2000; Rolfo et al., 2000, 2004; Zheng et al., 2006; Liu et al., 2007a,b, 2011a,b, 2015; Groppo et al., 2015). Previous studies focused mainly on the Triassic UHP metamorphism and related processes, whereas less attention has been paid to the nature and origin of the protoliths of the UHP rocks (e.g., Ames et al., 1996; Hacker et al., 1998; Zheng et al., 2006). U-Pb dating in magmatic zircon cores demonstrated that the protoliths of the UHP meta-igneous rocks in the Dabie orogen were formed in the Neoproterozoic (e.g., Rowley et al., 1997; Hacker et al., 1998; Liu et al., 2007a,b), likely under a continental rifting setting related to the breakup of the supercontinent Rodinia (Li et al., 2003a,b,c). However, the detailed Neoproterozoic evolutionary processes of the area have not been well understood, and the precise onset of the continental rifting is still not well constrained. UHP rocks usually experience complex evolution including interaction with melt and/or fluids that can significantly modify the elemental and isotopic characteristics of the rocks (e.g., Kessel et al., 2005; Hermann et al., 2006; Zheng et al., 2011), making it challenging to reveal their protolith nature and origin.

Apart from the UHP rocks, relatively low-grade metamorphosed rocks have been identified in several localities within the UHP metamorphic zone in the Dabie orogen (e.g., Dong et al., 1997; Gao et al., 2006); these rocks occur as interlayers or tectonic blocks within the UHP units, but yield much lower peak-metamorphic temperatures and pressures. If these rocks can be proved to be counterparts of the UHP rocks that escaped UHP metamorphism, they should be good candidates to reveal the Neoproterozoic evolution of the area. Previous studies about the rocks in the Dabie orogen mainly concentrated on geochronology investigations, while their elemental

1 85 and isotopic signatures have not been studied in detail so far, and their petrogenesis
2 86 and tectonic setting are still not well constrained.

3
4 87 Recently, some relatively low-grade meta-basites and meta-granitoids have been
5
6 88 for the first time recognized at Longjingguan, within the central Dabie UHP
7
8 89 metamorphic zone (Fig. 1). In this paper we perform integrated investigations on their
9
10 90 mineral compositions, whole-rock elements and Pb isotopes, as well as zircon
11
12 91 SHRIMP U-Pb dating, REE and Hf isotopes. The aim of the study is to investigate
13
14 92 whether the rocks are counterparts of the UHP meta-igneous rocks and, if so, whether
15
16 93 the rocks preserved their protolith compositions better than the UHP rocks. These new
17
18 94 data are crucial for better understanding the formation and tectonic evolution of the
19
20 95 Precambrian basement of the South China Block (SCB), especially the events related
21
22 96 to the Neoproterozoic breakup of the supercontinent Rodinia.
23
24
25 97

27 98 **2. Geological setting and samples**

28 99 *2.1. Geological setting*

29
30 100 The Dabie orogen located in the middle portion of the
31
32 101 Qinling–Tongbai–Dabie–Sulu orogenic belt is formed by the Triassic subduction of
33
34 102 the SCB beneath the North China Block (NCB) and exposed the largest area of UHP
35
36 103 rocks in the world. The widespread occurrence of coesite- (Okay et al., 1989; Wang et
37
38 104 al., 1989) and diamond-bearing (Xu et al., 1992b) rocks in the orogen provides an
39
40 105 excellent natural laboratory for investigating evolutionary processes of the orogen, as
41
42 106 well as formation and exhumation mechanisms of UHP rocks. The orogen is generally
43
44 107 divided into five fault-bounded rock units with different metamorphic grades and
45
46 108 histories, which are from south to north: the Susong complex zone (SZ), the South
47
48 109 Dabie low-T eclogite zone (SDZ), the Central Dabie UHP zone (CDZ), the North
49
50 110 Dabie complex zone (NDZ) and the Beihuaiyang zone (BZ) (Xu et al., 2003, 2005;
51
52 111 Liu et al., 2005, 2007a,b, 2011a,b; Zheng et al., 2005; Liu and Li, 2008; Li et al.,
53
54 112 2017). These five units are separated by the near E-W trending Taihu–Shanlong,
55
56 113 Hualiangting–Mituo, Wuhe–Shuihou and Xiaotian–Mozitan faults, respectively (Fig.

1
2
3
4
5
6
7
8
9
10
11
12
13
14
15
16
17
18
19
20
21
22
23
24
25
26
27
28
29
30
31
32
33
34
35
36
37
38
39
40
41
42
43
44
45
46
47
48
49
50
51
52
53
54
55
56
57
58
59
60
61
62
63
64
65

114 1). Although the meta-igneous rocks in the five units exhibit different metamorphic
115 histories, they have similar Neoproterozoic protolith ages reflecting a regional-scale
116 magmatism related to the Rodinia break-up (e.g., Ames et al., 1996; Rowley et al.,
117 1997; Hacker et al., 1998; Liu et al., 2007a,b, 2011a).

118 UHP index minerals like coesite and diamond were found in different lithologies
119 from the CDZ (e.g., Okay et al., 1989; Wang et al., 1989; Xu et al., 1992b; Schertl et
120 al., 1994; Su et al., 1996; Rolfo et al., 2000, 2004), demonstrating that the CDZ was
121 involved in a deep subduction and experienced Triassic UHP metamorphism as a
122 coherent unit (Xu et al., 1992b, 2003; Li et al., 1993, 2000; Hacker et al., 1998; Rolfo
123 et al., 2004; Liu and Li, 2008). Evidence of UHP metamorphism like coesite
124 pseudomorphs were later discovered also in the low-T eclogites from the SDZ (Li et
125 al., 2004). Eclogites (Wei et al., 1998; Xu et al., 2000; Liu et al., 2001) or eclogite
126 relics (Tsai and Liou, 2000; Xiao et al., 2001) were also recognized in the NDZ,
127 together with diamond inclusion within zircon and other clues of UHP metamorphism
128 (Tsai et al., 2000; Xu et al., 2000, 2003, 2005; Liu et al., 2007b, 2011b). Moreover,
129 the NDZ (Liu et al., 2000; Xie et al., 2001; Liu et al., 2005, 2007a,b, 2011a) and the
130 SDZ (Li et al., 2004) were confirmed to be segments of the Triassic subducted
131 continental crust of the SCB. This implies that the three eclogite-bearing units in the
132 Dabie orogen all experienced the Triassic deep subduction, although they have
133 different lithological and isotopic compositions and metamorphic histories (Liu and Li,
134 2008).

135 In recent years, relatively low-grade meta-igneous rocks with Neoproterozoic
136 protolith ages and Triassic metamorphic ages have been recognized within the
137 Dabie-Sulu UHP belt. For example, some meta-igneous rocks in Ganghe provided
138 Rb-Sr isochronal ages of 232 ± 8 Ma and Ar-Ar ages of 770-780 Ma, as well as
139 magmatic zircon U-Pb ages of 760–800 Ma (Dong et al., 1997; Gao et al., 2006).
140 These ages indicate that these rocks formed in the Neoproterozoic and experienced
141 Triassic metamorphism, with peak metamorphic temperatures between the closure
142 temperatures of Rb-Sr and Ar-Ar isotopic systems. Different from the UHP rocks,
143 they experienced a relatively low-grade metamorphism (greenschist- to

1 144 low-amphibolite-facies) during the Triassic (Dong et al., 1997; Liu et al., 2017 and
2 145 references therein), indicating that they were exhumed from much shallower depths.
3
4 146 Similar granitic gneisses/meta-granites, meta-basites with Neoproterozoic protolith
5
6 147 ages have also been recognized in the BZ, the northern sector of the Dabie orogen
7
8 148 (e.g., Hacker et al., 2000; Xie et al., 2002; Chen et al., 2003; Jiang et al., 2005; Zheng
9
10 149 et al., 2005; Liu et al., 2006a, 2010, 2011c, 2017; Wu et al., 2007). These rocks have
11
12 150 identical amphibole Ar-Ar (Hacker et al., 2000) and zircon U-Pb ages (Jiang et al.,
13
14 151 2005; Liu et al., 2010, 2017) of ~750 Ma, suggesting that their peak metamorphic
15
16 152 temperatures during the Triassic were lower than the closure temperatures of the
17
18 153 amphibole Ar-Ar dating system (<500 °C). These protolith ages are in agreement with
19
20 154 those of the UHP eclogites and orthogneisses (e.g., Ames et al., 1996; Rowley et al.,
21
22 155 1997; Hacker et al., 1998; Liu et al., 2007a,b, 2011a), as well as the Neoproterozoic
23
24 156 mafic dykes and granites widely distributed along the northern margin of the SCB,
25
26 157 thus they are generally considered to be closely related (Zhao and Zhou, 2009; Hong
27
28 158 et al., 2009; Xue et al., 2011; Wang et al., 2013). It is consequently thought that these
29
30 159 Neoproterozoic meta-granites and meta-basites were once skin layers of the SCB,
31
32 160 detached from the subducted slab during the initial stages of the subduction, and
33
34 161 overthrust onto the southern margin of the NCB (e.g., the BZ), or into the UHP
35
36 162 metamorphic zone (e.g., Ganghe) during the Triassic continental collision.
37
38

39 163 In addition to the locations described above, the relatively low-grade
40
41 164 meta-basites and meta-granitoids have been discovered at Longjingguan within the
42
43 165 central Dabie UHP zone (Fig. 1). So far, their petrogenesis, emplacement time and
44
45 166 relationship with the adjacent UHP rocks have not been studied in detail.
46
47

48 167

49 168 *2.2. Petrography and mineral chemistry*

50
51 169 Fourteen samples were collected from the Longjingguan area, including six
52
53 170 meta-basites (samples 11LJG3-4-5-6-7-8) and eight meta-granitoids (samples 11LJG2,
54
55 171 1202LJG3, 1209LJG5, 1303LJG2, 1303LJG4, 1209LJG1, 1209LJG3 and 1209LJG4).
56
57 172 Their outcrops are concentrated within an area of few tens of square meters marked
58
59 173 by the black star in Figure 1. All the samples were collected as far as possible from
60
61

174 the contact with different lithologies, to avoid possible interaction between them.

175 The meta-basites occur as tectonic lenses within meta-granitoids (Fig. 2), with
176 the margins slightly deformed; the surface is locally characterized by few
177 light-coloured, weakly deformed spots of about 0.5 mm in size. The meta-basite
178 generally contains fine-grained symplectites mainly consisting of plagioclase and
179 amphibole. The symplectite composed of plagioclase and amphibole points to the
180 replaced former mineral, rather than derived from magma crystallization. Accessory
181 minerals are rutile, titanite, ilmenite and magnetite. A few amphibole porphyroblasts
182 occur in the meta-basites, and they contain inclusions of plagioclase, plagioclase +
183 rutile, rutile, rutile + ilmenite and rutile + titanite (Figs. 3a & b).

184 Electron microprobe analyses were carried out on representative minerals of three
185 samples 11LJG7, 1209LJG5 and 1209LJG1, which represent the meta-basites, low-Si
186 meta-granitoids and high-Si meta-granitoids, respectively. The results are listed in
187 Supplementary Table 1.

188 The meta-granitoids are subdivided into two types, named low-Si and high-Si
189 meta-granitoids, respectively, according to their bulk-rock SiO₂ content
190 (Supplementary Table 2). The low-Si meta-granitoid is mainly composed of
191 plagioclase (with K-feldspar exsolutions), quartz, and biotite, with minor amphibole
192 and apatite (Fig. 3c-d), while the high-Si meta-granitoid is dominated by quartz and
193 K-feldspar, with rare allanite, muscovite and amphibole (Figs. 3e-f). Minerals in the
194 meta-granitoids vary from few tens of microns to hundreds of microns in size,
195 significantly coarser than those in the matrix of the meta-basites. The structure varies
196 from gneissic, with a poorly developed foliation (Fig. 3c-d), to granoblastic (Figs.
197 3e-f).

198

199 2.2.1. 11LJG7

200 In this meta-basite sample, amphibole occurs as fine grains in the symplectitic
201 matrix or as porphyroblasts. Both porphyroblasts and the fine-grained amphibole in
202 the matrix are magnesiohornblende: the porphyroblasts have lower Mg[#] values
203 (72~73) and higher TiO₂ contents (0.26~0.35 wt%) than the fine grains in the matrix

204 (Mg[#]=79~81; TiO₂=0.02~0.13 wt%). Plagioclase is an oligoclase (Supplementary
205 Table 1). Two rutile inclusions within amphibole porphyroblast have Zr contents of
206 277 and 735 ppm, respectively. Rutile inclusions in Neoproterozoic metamorphic
207 zircon domains (see Section 4.2) have higher Zr contents, in the range 2107-2519 ppm
208 (Supplementary Table 3).

210 2.2.2. 1209LJG5

211 This low-Si meta-granitoid sample exhibits a weak foliation defined by biotite
212 and amphibole preferred orientation (Figs. 3c-d). Plagioclase is oligoclase (An₁₉₋₃₀)
213 and contains K-feldspar (Or₉₂₋₉₆) exsolutions. Amphibole is a ferro-edenite /
214 ferropargasite, with X_{Ca}=0.76–0.77 [X_{Ca}=Ca/(Ca+Na+K)] and X_{Fe}=0.66–0.68
215 [X_{Fe}=Fe/(Fe+Mg)]. Biotite has low Mg[#] (~36) and variable TiO₂ contents (3.68 to
216 4.12 wt%).

218 2.2.3. 1209LJG1

219 This high-Si meta-granitoid sample consists mainly of K-feldspar and quartz,
220 with minor allanite (Fig. 3e). The K-feldspar contains about 6% albite end-member
221 component.

223 2.3. Thermobarometry

224 Thermobarometric methods were applied on the meta-basite sample 11LJG7. The
225 main amphibole–plagioclase symplectitic assemblage gives a P-T range of
226 478-541 °C, 2.2-3.4 kbar (i.e. lower-T boundary of the amphibolite-facies) based on
227 the amphibole-plagioclase thermometer (Holland and Blundy, 1994) and the
228 Al^{Tot}-in-amphibole barometer (Schmidt, 1992).

229 Rutile inclusions within amphibole porphyroblast yield temperatures of
230 651-737 °C based on their Zr contents (Tomkins et al., 2007), with the pressure set to
231 ~12 kbar according to the coexistence of rutile, ilmenite and titanite (Bohlen and
232 Liotta, 1986; Angiboust and Harlov, 2017). Rutile inclusions in Neoproterozoic
233 metamorphic zircon domains (see Section 4.2) yield significantly higher temperatures

1 234 of about 850-870 °C. In the application of Zr-in-rutile thermometer, rutile
2 235 measurements with Si > 200 ppm should be excluded from further analysis if the Zr
3
4 236 concentration is substantially higher than that of other rutiles in the same sample
5
6 237 (Zack et al., 2004); accordingly, data of three analytical spots (No. 2, 3 and 4,
7
8 238 Supplementary Table 4) were excluded. In addition, the analytical spot No. 1
9
10 239 (Supplementary Table 4) was also excluded because of extremely low total contents.

11
12 240 Overall, thermobarometric results suggest that rutile inclusions within
13
14 241 Neoproterozoic metamorphic zircon domains preserve evidence of a HT,
15
16 242 granulite-facies metamorphic event (840-860°C, ~12 kbar), completely overprinted by
17
18 243 a later amphibolite-facies event (480-540 °C, 2.2-3.4 kbar), responsible for the
19
20 244 formation of the amphibole + plagioclase symplectites in the matrix. The
21
22 245 Neoproterozoic granulite-facies metamorphic event is also supported by the previous
23
24 246 investigations from the deeply subducted NDZ in Liu et al. (2007a). Rutile inclusions
25
26 247 within amphibole porphyroblasts were likely partially reequilibrated during the late
27
28 248 amphibolite-facies metamorphic event, due to the lack of protection by rigid
29
30 249 "container" such as zircon, thus indicating temperatures (652-737 °C) lower than
31
32 250 those preserved by rutiles included in zircons.
33
34
35
36
37

38 252 **3. Analytical methods**

39
40 253 Rock-crushing and powdering were performed at the Langfang Laboratory,
41
42 254 Hebei Bureau of Geological and Mineral Resources. Zircon grains were separated by
43
44 255 the procedures of crushing, heavy-liquid separation, magnetic separation. After that,
45
46 256 zircon grains were further selected by hand-picking under a binocular microscope,
47
48 257 and mounted in an epoxy mount, which was polished to section the crystals for
49
50 258 analyses, with a zircon U–Pb standard TEM (417 Ma) (Black et al., 2003) at Beijing
51
52 259 SHRIMP Center, Chinese Academy of Geological Sciences (CAGS).

53
54 260 Whole-rock major element composition was analyzed by wet chemical methods
55
56 261 at the Langfang Laboratory, Hebei Bureau of Geological and Mineral Resources.
57
58 262 Analytical uncertainties have a range from ±1 to ±5% for major elements. Trace
59
60
61
62
63
64
65

1 263 elements analysis was carried out at the CAS Key Laboratory of Crust-Mantle
2 264 Materials and Environments, University of Science and Technology of China (USTC)
3
4 265 in Hefei, by an Elan DRCII ICP-MS, with analytical uncertainties ranging from $\pm 5\%$
5
6 266 to $\pm 10\%$. Detailed analytical procedures and instrument parameters for trace element
7
8 267 analyses are documented in Hou and Wang (2007). Zircon SHRIMP U–Pb dating was
9
10 268 carried out at the Beijing SHRIMP Center, with transmitted and reflected light
11
12 269 micrographs and CL imaging as a guide to selection of U–Pb dating spot. The detailed
13
14 270 analytical method was described by Compston et al. (1992) and Williams (1998).
15
16 271 Common Pb corrections were made using measured ^{204}Pb , and the data were treated
17
18 272 following Compston et al. (1992) with the ISOPLOT program of Ludwig (2001).

21 273 Zircon trace elements analyses were performed by LA-ICP-MS at the CAS Key
22
23 274 Laboratory of Crust-Mantle Materials and Environments, USTC in Hefei and the
24
25 275 State Key Laboratory of Continental Dynamics, Northwest University in Xi'an. The
26
27 276 analyses were carried out with pulse rate of 10 Hz, beam energy of 10 J/cm^2 , and spot
28
29 277 diameter of $32 \mu\text{m}$. The detailed parameters of the instrument are similar to those
30
31 278 described by Yuan et al. (2004) and Liu et al. (2011a). Element contents of zircons
32
33 279 were calculated by using Pepita software with the zircon SiO_2 as internal standard and
34
35 280 the NIST610 as external standard. Precision and accuracy of analyses are 2–5% for
36
37 281 REE, Y, Rb, Sr, Nb, Ta, Hf, Th and U at the ppm concentration level, and from 8% to
38
39 282 10% for P, Ti and Pb. The detection limit for the different REE varies from 0.02 to
40
41 283 0.09 ppm.

44 284 In situ zircon Lu–Hf isotope analysis were conducted at the Institute of Geology
45
46 285 and Geophysics, the Chinese Academy of Sciences in Beijing, and the School of Earth
47
48 286 Sciences and Engineering, Nanjing University, each using a Neptune multi-collector
49
50 287 ICPMS, with a Geolas 193 nm laser ablation system. Instrumental parameters and
51
52 288 data acquisition followed those described by Wu et al. (2006a). The detailed processes
53
54 289 were shown in Liu et al. (2012). Initial Hf isotope ratios are denoted as $\epsilon_{\text{Hf}}(t)$ values
55
56 290 that are calculated with the reference to the chondritic reservoir (CHUR) at the time of
57
58 291 zircon crystallization. Parameters adopted in this study are: $1.865 \times 10^{-11} \text{ yr}^{-1}$ for the
59
60 292 decay constant of ^{176}Lu (Scherer et al., 2001), 0.282772 and 0.0332 for the $^{176}\text{Hf}/^{177}\text{Hf}$

1
2
3
4
5
6
7
8
9
10
11
12
13
14
15
16
17
18
19
20
21
22
23
24
25
26
27
28
29
30
31
32
33
34
35
36
37
38
39
40
41
42
43
44
45
46
47
48
49
50
51
52
53
54
55
56
57
58
59
60
61
62
63
64
65

293 and $^{176}\text{Lu}/^{177}\text{Hf}$ ratios of the chondrite (Blichert-Toft and Albarede, 1997). Single
294 stage model ages (T_{DMI}) were calculated referred to the depleted mantle with a
295 present day $^{176}\text{Hf}/^{177}\text{Hf}$ ratio of 0.28325, similar to that of the average MORB (Nowell
296 et al., 1998) and $^{176}\text{Lu}/^{177}\text{Hf}$ ratio of 0.0384 (Griffin et al., 2000).

297 Mineral inclusions in zircon were identified using Raman spectroscopy at the
298 CAS Key Laboratory of Crust–Mantle Materials and Environments, University of
299 Science and Technology of China in Hefei, and analyzed using the electron
300 microprobe (EMP) at the Institute of Mineral Resources, CAGS in Beijing. The
301 analytical conditions of the Raman and EMP were reported by Liu et al. (2009). The
302 compositions of the representative minerals in thin sections were detected by EMP at
303 the Department of Resource and Environment Engineering, Hefei University of
304 Technology in Hefei. The accelerating voltage and beam current were 15 kV and
305 15nA, respectively.

306 Rb-Sr, Sm-Nd, and Pb isotopic analyses were performed at the Laboratory for
307 Radiogenic Isotope Geochemistry, in USTC according to the methods of Chen et al.
308 (2000, 2007). Sm, Nd, Rb, and Sr concentrations were determined by isotopic dilution
309 using ^{149}Sm , ^{150}Nd , ^{84}Sr , and ^{85}Rb tracers. The isotopic abundance ratios were
310 determined on a Finnigan MAT 262. Sr and Nd isotopic ratios were corrected for mass
311 fractionation relative to $^{86}\text{Sr}/^{88}\text{Sr} = 0.1194$ and $^{146}\text{Nd}/^{144}\text{Nd} = 0.7219$, respectively.
312 NBS987 and La Jolla standard solutions analyzed along with samples yielded
313 0.710250 ± 12 (2σ) for $^{87}\text{Sr}/^{86}\text{Sr}$ and 0.511860 ± 12 (2σ) for $^{143}\text{Nd}/^{144}\text{Nd}$. Measured Pb
314 isotopic ratios were then corrected for instrumental mass fractionation using a value
315 of 0.11% per atomic mass unit inferred from analysis of the reference material
316 NBS981.

317 318 **4. Results**

319 *4.1. Major and trace elements*

320 Whole-rock major and trace elemental compositions of the studied meta-basites
321 and meta-granitoids are listed in Supplementary Table 2.

322

323 *4.1.1. Meta-basites*

324 The meta-basite samples 11LJG3-4-5-6-7-8 have uniform bulk-rock
325 compositions. The SiO₂ contents range from 45.72 to 51.81 wt%, Al₂O₃ from 12.46 to
326 14.30 wt%, and MgO from 4.37 to 13.29 wt%. They have high FeO^T (11.47–14.99
327 wt%) and Mg[#] values of 34–67. The TiO₂ contents are also relatively high (2.01–3.42
328 wt%). They are alkalic with Na₂O contents of 1.74–3.55 wt%, K₂O contents of
329 0.77–1.80 wt% and Na₂O/K₂O ratios of 1.25–4.14. Element pairs that have similar
330 bulk D values (solid/melt partition coefficient for modal melting), for example Y-Ho
331 and Eu-Sm, are correlated during magmatic processes (e.g., Workman and Hart, 2005).
332 In the Y vs. Ho and Eu vs. Sm plots (no attachment), all the studied meta-mafic rocks
333 fall along a linear trend, suggesting that they were derived from the same source.

334 In the TAS (Le Bas et al., 1986) and Zr/TiO₂ vs Nb/Y (Winchester and Floyd,
335 1977) diagrams (Fig. 4), the meta-mafic rocks plot very close to the boundary
336 between fields of alkaline and sub-alkaline series. The primitive mantle normalized
337 spider diagram (Fig. 5b) shows that they are enriched in incompatible elements
338 compared to MORB, and have negative anomalies of Sr, Nb and Ta, positive or
339 slightly negative Pb anomalies. They have uniform C1 chondrite normalized REE
340 patterns (Fig. 5a) characterized by enrichment in LREE, slight depletion in HREE and
341 weakly positive or negative Eu anomaly (Eu/Eu* = 0.80–1.06). Their (La/Yb)_N
342 (primitive mantle normalized) ratios range from 2.2 to 7.5 and (La/Sm)_N from 1.3 to
343 2.1. The UHP eclogites derived from basaltic protoliths have similar REE patterns and
344 related trace-element contents (Fig. 5c and d).

345
346 *4.1.2. Low-Si meta-granitoids*

347 The low-Si meta-granitoids (samples 11LJG2, 1209LJG5 and 1202LJG3) have
348 slightly inhomogeneous bulk compositions. The SiO₂ contents range from 60.45 to
349 61.50 wt%, Al₂O₃ from 14.18 to 14.96 wt%, TiO₂ from 1.16 to 1.38 wt% and MgO
350 from 1.60 to 1.86 wt%. They have high FeO^T (7.78–8.29 wt%) with Mg[#] values of
351 0.26–0.31. They have Na₂O ranging from 1.50 to 3.26 wt% and K₂O from 3.11 to

352 4.28 wt% with Na₂O/K₂O ratios of 0.35–1.05. In the TAS diagram, these rocks plot in
353 the field of andesite, close to the boundary with trachy-andesite; in the Zr/TiO₂ vs
354 Nb/Y diagram, they are distributed in the fields of dacite + rhyodacite and
355 trachyandesite. They exhibit significant depletion of HFSE including Nb, Ta, Ti and P,
356 as well as enrichment of Pb (Fig. 5b), which are typical features of crustal-sourced
357 rocks (Rudnick and Gao, 2003). They have identical C1 chondrite normalized REE
358 patterns (Fig. 5a) characterized by enrichment of LREE, weak depletion of HREE and
359 positive Eu anomalies (Eu/Eu* = 1.12–2.00). Their (La/Yb)_N ratios range from 9.59 to
360 17.49 and (La/Sm)_N from 2.77 to 4.02.

362 4.1.3. High-Si meta-granitoids

363 Compared to the meta-basites and low-Si meta-granitoids, the high-Si
364 meta-granitoids (samples 1303LJG2, 1303LJG4, 1209LJG1, 1209LJG3 and
365 1209LJG4) have more scattered bulk-rock compositions. The SiO₂ contents range
366 from 67.98 to 80.98 wt%, Al₂O₃ from 8.96 to 11.78 wt%, TiO₂ from 0.17 to 0.54 wt%
367 and MgO from 0.06 to 3.82 wt%. They have low FeO^T (2.09–4.30 wt%) contents with
368 varied Mg[#] values of 0.04–0.62. The Na₂O contents range from 1.12 to 2.99 wt% and
369 K₂O from 2.44 to 5.35 wt% with Na₂O/K₂O ratios of 0.29–0.98. In the TAS diagram,
370 four samples plot into the field of sub-alkaline rhyolite and one sample into that of
371 dacite; in the Zr/TiO₂ vs Nb/Y plot, the studied samples scatter among four categories:
372 comendite + pantellerite, rhyolite, rhyodacite + dacite and trachyandesite. They have
373 trace elements patterns comparable to those of the low-Si meta-granitoids (Fig. 5b),
374 and uniform C1 chondrite normalized REE patterns (Fig. 5a) characterized by
375 enrichment of LREE, slight depletion of HREE and strong negative Eu anomalies
376 (Eu/Eu* = 0.10–0.75). Their (La/Yb)_N ratios range from 10.29 to 49.87 and (La/Sm)_N
377 range from 3.64 to 5.41.

379 4.2. Zircon geochronology

380 4.2.1. Zircon morphology and mineral inclusions

381 Zircons from the meta-basites are anhedral to subhedral in shape with smooth

1 382 outlines, and their length-width ratios are generally smaller than 1.5. CL images show
2 383 that most of them have core, mantle and rim structures with clear boundaries between
3
4 384 them. The cores are grey colored with clear or weak oscillatory zoning while the
5
6 385 mantles are light colored and homogeneous (Fig. 6). Some zircon grains have a
7
8 386 mantle domain showing gradually darker luminance outwards. The rims are bright,
9
10 387 too thin to be analysed. According to the microstructures, the cores with oscillatory
11
12 388 zoning are interpreted to be of magmatic origin, while the homogeneous cores and
13
14 389 mantles are considered to be metamorphic zircon domains (e.g., Hanchar and Rudnick,
15
16 390 1995; Gebauer et al., 1997; Hermann et al., 2001). Most of the zircon cores exhibit
17
18 391 rounded shapes, suggesting that they were partially resorbed after crystallization,
19
20 392 maybe during the formation of the zircon mantles.

21
22
23 393 As opposed to the meta-basites, zircons from the meta-granitoids exhibit more
24
25 394 regular crystal shapes. Some of the zircons from the meta-granitoids are euhedral in
26
27 395 shape with clear oscillatory zones, indicative of magmatic origin. Other zircons show
28
29 396 core and mantle structures, wherein the cores are dark grey with clear oscillatory
30
31 397 zoning or no zoning, while the mantles are light grey with weak or no oscillatory
32
33 398 zonings. Similarly, the zircons in the meta-granitoids can also be divided into
34
35 399 magmatic (with oscillatory zoning) and metamorphic (no zoning) domains. Generally,
36
37 400 the metamorphic zircon domains from both the meta-basites and the meta-granitoids
38
39 401 are granular, platy and prismatic in shape with smooth boundaries, and some of them
40
41 402 retain plenty of mineral inclusions (Fig. 7), which are powerful tools to link zircon
42
43 403 growth to precise metamorphic events (e.g., Gebauer et al., 1997; Hermann et al.,
44
45 404 2001; Liu et al., 2007b, 2011a). The metamorphic zircons in the meta-basite sample
46
47 405 11LJG3 contain quartz, plagioclase, apatite, hornblende, K-feldspar, chlorite, epidote,
48
49 406 biotite, rutile, ilmenite and titanite, while those from the meta-granitoid sample
50
51 407 11LJG2 contain K-feldspar, muscovite, epidote and quartz. The compositions of
52
53 408 typical mineral inclusions in metamorphic zircons were detected by electron
54
55 409 microprobe, with the results listed in Supplementary Table 3. Biphase inclusions
56
57 410 composed of rutile + titanite or of titanite + ilmenite are recognized in a few
58
59 411 metamorphic zircons from sample 11LJG3.

1 412

2 413 *4.2.2. Zircon REE patterns*

3
4 414 Representative zircon REE contents of the meta-basites (samples 11LJG3 and
5
6 415 11LJG7) and the meta-granitoids (samples 11LJG2, 1202LJG3, 1303LJG2 and
7
8 416 1209LJG5) are listed in Supplementary Table 5 (all the analyzed results for zircon
9
10 417 rare earth elements in Supplementary Table 6). Zircon cores have almost identical
11
12 418 steep HREE patterns, positive Ce anomalies and negative Eu anomalies (Fig. 8),
13
14 419 typical of magmatic zircon (Hoskin and Ireland, 2000). On the contrary, the REE
15
16 420 patterns of metamorphic zircons are varied. In the meta-basites, most metamorphic
17
18 421 zircons (the cyan lines, Fig. 8a) exhibit higher REE contents than, but similar REE
19
20 422 patterns with, the magmatic zircons, except for one spot that show slightly positive Eu
21
22 423 anomaly; besides, a metamorphic zircon (the black line, Fig. 8a) has almost the same
23
24 424 La, Ce and HREE contents with the magmatic zircons, but it exhibits significantly
25
26 425 higher Pr, Nd, Sm and Eu. In the meta-granitoids, most metamorphic zircons exhibit
27
28 426 similar REE patterns with the magmatic cores, whereas some analyses exhibit higher
29
30 427 REE contents and/or higher LREE/HREE ratios than the magmatic zircons (Fig. 8b-d),
31
32 428 or exhibit no anomaly of Eu.

33
34
35 429
36
37 430 *4.2.3. Zircon SHRIMP U-Pb ages*

38
39 431 In-situ analyses have been performed on different zircon domains, with the
40
41 432 U-Th-Pb data listed in Supplementary Table 7 and U-Pb concordia diagram illustrated
42
43 433 in Figure 9.

44
45 434 Magmatic zircon cores from the meta-basite sample 11LJG3 yield a cluster of
46
47 435 concordant $^{206}\text{Pb}/^{238}\text{U}$ age averaging at 772 ± 4 Ma (MSWD=2.0, n=7; Fig. 9a), while
48
49 436 the metamorphic domains give a concordant $^{206}\text{Pb}/^{238}\text{U}$ age group of 768 ± 7 Ma
50
51 437 (MSWD=2.9, n=11; Fig. 9a). In another meta-basite sample 11LJG7, magmatic zircon
52
53 438 domains yield a cluster of concordant $^{206}\text{Pb}/^{238}\text{U}$ age of 772 ± 7 Ma (MSWD=2.5, n=5;
54
55 439 Fig. 9b), and the metamorphic domains give a concordant $^{206}\text{Pb}/^{238}\text{U}$ age group of 746
56
57 440 ± 4 Ma (MSWD=2.6, n=9; Fig. 9b). Summing up, the magmatic zircons yield a
58
59 441 cluster of concordant $^{206}\text{Pb}/^{238}\text{U}$ age at ~ 772 Ma (Ma domains), and the metamorphic

1 442 zircons yield two groups of concordant $^{206}\text{Pb}/^{238}\text{U}$ age at ~768 Ma (Me1 domains) and
2 443 ~746 Ma (Me2 domains), corresponding to magmatism, metamorphism and thermal
3
4 444 overprinting events, respectively.
5

6 445 Zircon cores in the low-Si meta-granitoids (samples 11LJG2, 1202LJG3,
7 446 1209LJG5) have a wide age spectrum spreading from ~800 Ma to ~2500 Ma.
8 447 Analytical spots on zircon cores in sample 11LJG2 are distributed along the concordia
9 448 curve or on a Pb loss line, yielding two upper intercept ages of 1940 ± 140 Ma
10 449 (MSWD=2.1; Fig. 9d) and 2529 ± 38 Ma (MSWD=3.1; Fig. 9d), respectively. Six
11 450 magmatic zircon spots give a concordant $^{206}\text{Pb}/^{238}\text{U}$ age cluster of 838 ± 18 Ma
12 451 (MSWD=0.73, n=6; Fig. 9e), while twelve metamorphic zircon analyses yield two
13 452 concordant $^{206}\text{Pb}/^{238}\text{U}$ age clusters averaging at 797 ± 7 Ma (MSWD=0.54, n=9; Fig.
14 453 10e) and 762 ± 22 Ma (MSWD=0.25, n=3; Fig. 9e), respectively. Zircons in sample
15 454 1209LJG5 plot along the concordia curve, or on a Pb loss line with an upper intercept
16 455 age of 1999 ± 57 Ma and a lower intercept age of 779 ± 49 Ma (MSWD=4.8; Fig. 9g).
17 456 Neoproterozoic magmatic zircons give a concordant $^{206}\text{Pb}/^{238}\text{U}$ age of 839 ± 7 Ma
18 457 (MSWD=0.99, n=6; Fig. 9h), and two analyses on metamorphic zircon yield
19 458 concordant $^{206}\text{Pb}/^{238}\text{U}$ ages of 785 ± 6 Ma and 744 ± 16 Ma, respectively. Three near
20 459 concordant $^{206}\text{Pb}/^{238}\text{U}$ age clusters were obtained from sample 1202LJG3: one age of
21 460 819 ± 12 Ma (MSWD=2.3, n=3; Fig. 9c) from magmatic zircon cores, and two ages
22 461 of 772 ± 7 Ma (MSWD=1.14, n=3; Fig. 9c) and 751 ± 6 Ma (MSWD=0.39, n=3; Fig.
23 462 9c) from metamorphic zircon domains.
24
25
26
27
28
29
30
31
32
33
34
35
36
37
38
39
40
41
42

43 463 Magmatic zircons from the high-Si meta-granitoid sample 1303LJG2 give an
44 464 average concordant $^{206}\text{Pb}/^{238}\text{U}$ age of 813 ± 5 Ma (MSWD=0.99, n=7; Fig. 9f), while
45 465 metamorphic zircons yield two concordant age clusters of 784 ± 7 Ma and 732 ± 6 Ma
46 466 (Fig. 9f). The zircon dating results indicate that the protoliths of the low-Si and
47 467 high-Si meta-granitoids were formed at about 819 ± 12 Ma and 813 ± 5 Ma,
48 468 respectively. The zircons yielding older ages are thus inherited from their source rocks,
49 469 with their original ages preserved or reset by Pb loss, corresponding to the apparent
50 470 concordant or discordant ages.
51
52
53
54
55
56
57
58
59
60
61
62
63
64
65

1 471

2
3 472 *4.3. Zircon Hf isotopes*

4
5 473 Zircon $\epsilon_{\text{Hf}}(t)$ values and T_{DM} ages of two meta-basites (samples 11LJG3 and
6
7 474 11LJG7), three low-Si meta-granitoids (samples 11LJG2, 1209LJG5 and 1202LJG3)
8
9 475 and one high-Si meta-granitoid (sample 1303LJG2) are listed in Supplementary Table
10
11 476 8.

12
13 477 The zircons in the meta-basites have $\epsilon_{\text{Hf}}(780 \text{ Ma})$ values from +2.6 to +7.9 (Fig.
14
15 478 10), and corresponded single stage model ages (T_{DM1}) of 1033 to 1248 Ma, slightly
16
17 479 older than their zircon U-Pb ages.

18
19 480 Six inherited zircon cores from low-Si meta-granitoids have $\epsilon_{\text{Hf}}(t)$ values of +7.1
20
21 481 to -6.6, with corresponding T_{DM1} ages of 2359 to 2702 Ma, and T_{DM2} ages of 2506 to
22
23 482 2823 Ma, respectively (Fig. 10). The Neoproterozoic zircon domains in the low-Si
24
25 483 meta-granitoids yield a relatively wide $\epsilon_{\text{Hf}}(800 \text{ Ma})$ spectrum of -3.2 to -12.0, with
26
27 484 T_{DM1} ages of 1513~1819 Ma and T_{DM2} ages of 1893~2446 Ma. Zircons from the
28
29 485 high-Si meta-granitoid have $\epsilon_{\text{Hf}}(800 \text{ Ma})$ values ranging from -7.5 to +1.4, with T_{DM1}
30
31 486 ages of 1313~1679 Ma, and T_{DM2} ages of 1618~2172 Ma. Neoproterozoic zircons
32
33 487 from low-Si and high-Si meta-granitoids have overlapped $\epsilon_{\text{Hf}}(t)$ values and T_{DM} ages,
34
35 488 but the high-Si rocks have slightly higher average $\epsilon_{\text{Hf}}(t)$ values and younger Hf model
36
37 489 ages.

38
39 490
40
41
42 491 *4.4. Sr-Nd-Pb isotope compositions*

43
44 492 The Rb-Sr, Sm-Nd and Pb contents and isotopic compositions of the
45
46 493 meta-basites are listed in Supplementary Tables 9 and 10, respectively. The
47
48 494 meta-basites have Rb and Sr contents of 16.0–62.9 and 87–320 ppm, and measured
49
50 495 $^{87}\text{Rb}/^{86}\text{Sr}$ and $^{87}\text{Sr}/^{86}\text{Sr}$ ratios of 0.1423–1.6997 and 0.705386–0.709376, Sm and Nd
51
52 496 contents of 4.15–9.64 and 13.1–35.9 ppm, and measured $^{147}\text{Sm}/^{144}\text{Nd}$ and $^{143}\text{Nd}/^{144}\text{Nd}$
53
54 497 ratios of 0.1515–0.1888 and 0.512511–0.512674. Sr and Nd isotopic compositions
55
56 498 were back calculated to $t=230 \text{ Ma}$, and thus the $(^{87}\text{Sr}/^{86}\text{Sr})_t$, $\epsilon_{\text{Nd}}(t)$ values and T_{DM2}
57
58 499 ages are 0.7023–0.7067, -1.8–+1.8 and 862–1156 Ma. The meta-basites have U, Th

1 500 and Pb contents of 0.34–0.70, 1.27–2.34 and 2.36–10.20 ppm, and measured
2 501 $^{206}\text{Pb}/^{204}\text{Pb}$, $^{207}\text{Pb}/^{204}\text{Pb}$ and $^{208}\text{Pb}/^{204}\text{Pb}$ ratios of 17.046–17.308, 15.403–15.467 and
3
4 502 38.119–38.344. Pb isotopic compositions were back calculated to $t=230$ Ma, and thus
5
6 503 the $(^{206}\text{Pb}/^{204}\text{Pb})_i$, $(^{207}\text{Pb}/^{204}\text{Pb})_i$ and $(^{208}\text{Pb}/^{204}\text{Pb})_i$ values are 16.84–17.11, 15.39–15.46
7
8 504 and 37.81–38.06, respectively. The Dabie orogen experienced two major geological
9
10 505 events: the Neoproterozoic rifting-related magmatism and the Triassic
11
12 506 subduction-related metamorphism. In deed, we also tried to calculate the Sr, Nd and
13
14 507 Pb isotope compositions back to $t=800$ Ma, but obtained much more scattered results,
15
16 508 indicating that the meta-basites experienced metamorphism at the Triassic, during
17
18 509 which their isotopes were reseted.
19
20

21 510

22 511 **5. Discussion**

23 512 *5.1. The relationship between the studied rocks and the UHP rocks in the CDZ*

24 513 *5.1.1. Low-grade meta-basites and meta-granitoids vs. \pm retrograded UHP eclogites* 25 514 *and granitic gneisses*

26 515 The CDZ contains a variety of coesite- and/or diamond-bearing rock types,
27 516 including eclogites and granitic gneisses; these rocks experienced Triassic UHP
28 517 metamorphism and post-peak amphibolite-facies retrogression, responsible for the
29 518 widespread development of amphibolite-facies assemblages in some eclogites in the
30 519 area (Wang et al., 1989; Cong et al., 1995; Zhang et al., 2003; Rolfo et al., 2004; Liu
31 520 et al., 2006b). In some strongly retrograded eclogites, most garnets and omphacites
32 521 are replaced by symplectites or pseudomorphs; even though, mineral inclusions (e.g.
33 522 coesite, diamond, omphacite and rutile) within relict garnet preserve the evidence of
34 523 peak metamorphism at UHP conditions. Even in the most retrograded eclogites that
35 524 do not contain garnet relics, the former occurrence of garnet is suggested by
36 525 pseudomorphs of Pl + Amp + Bt that exhibit isometric shape typical of garnet (e.g.,
37 526 Zhang et al., 2003). In contrast, no garnet and/or other microstructural evidence that
38 527 could be related to eclogite-facies metamorphism have been observed in the studied
39 528 meta-basites, thus suggesting that the studied rocks have not been involved in the
40
41
42
43
44
45
46
47
48
49
50
51
52
53
54
55
56
57
58
59
60
61
62
63
64
65

1 529 deep subduction of the SCB in the Triassic.

2 530 In addition to the main rock-forming minerals, inclusions in metamorphic zircon
3
4 531 can be also used to reveal the peak metamorphic conditions in strongly retrograded
5
6 532 metamorphic rocks (e.g., Xu et al., 1992b; Nasdala and Massonne, 2000; Bauer et al.,
7
8 533 2007; Liu et al., 2007b, 2011b). This is because zircon behaves as a rigid “container”
9
10 534 that can protect the inclusions from the retrogression occurring in the matrix. Mineral
11
12 535 inclusions related to UHP conditions (e.g. coesite, diamond, omphacite and rutile)
13
14 536 have been identified in Triassic metamorphic zircons from the retrograded eclogites in
15
16 537 the CDZ, thus confirming that they experienced UHP metamorphism, although the
17
18 538 matrix of the rocks is dominated by amphibolite-facies mineral assemblages (Liu et
19
20 539 al., 2001, 2006a). On the contrary, no Triassic metamorphic zircon and related
21
22 540 eclogite-facies mineral inclusions have been identified in the studied meta-basites (see
23
24 541 section 4.2.1).

25
26
27 542 Different from UHP eclogites, felsic gneisses that underwent deep subduction
28
29 543 and UHP metamorphism commonly do not preserve evidence of the peak
30
31 544 metamorphic mineral assemblage. Nevertheless, their metamorphic zircons can trap
32
33 545 and preserve peak metamorphic minerals. In the CDZ, UHP inclusions (e.g. coesite
34
35 546 and diamond) have been recognized in Triassic metamorphic zircons from the felsic
36
37 547 gneisses (Tabata et al., 1998; Liu et al., 2001). On the contrary, no Triassic ages have
38
39 548 been obtained from the metamorphic zircons in the studied meta-granitoids, and no
40
41 549 eclogite-facies mineral inclusions have been observed therein (see section 4.2.1).

42
43 550 The overall observations and data clearly indicate that the studied meta-basites
44
45 551 and meta-granitoids were not involved in the Triassic deep subduction and UHP
46
47 552 eclogite-facies metamorphism, but underwent lower-grade metamorphism, i.e., at
48
49 553 amphibolite-facies conditions as suggested by the mineral assemblages and estimated
50
51 554 temperatures of the meta-basites (see sections 2.2 and 2.3). The age of this low-grade
52
53 555 metamorphic event has not been directly constrained due to the lack of related
54
55 556 metamorphic zircon, which may be attributed to the relatively low temperatures (<541
56
57 557 °C, section 2.3). Nevertheless, similar low-grade rocks from the same region showing
58
59 558 identical Neoproterozoic protolith ages, yield Triassic whole-rock Rb-Sr isochronal
60

1 559 ages of 232 ± 8 Ma (Dong et al., 1997; Gao et al., 2006). We therefore suggest that
2 560 during the Triassic, the studied meta-basites and meta-granitoids underwent a shallow
3
4 561 subduction associated with amphibolite-facies metamorphism, nearly synchronous
5
6 562 with the deep subduction of the CDZ.
7

8 563

10 564 *5.1.2. The same source and crustal levels indicated by zircon Hf and bulk-rock*
11
12 565 *Sr-Nd-Pb isotopes*

14 566 *Zircon Hf isotopes*

16 567 Because Hf is more incompatible than Lu, the continental crust acquired a
17
18 568 Lu/Hf ratio much lower than that in the primitive mantle, when it differentiated from
19
20 569 the primitive mantle. As a result, the $^{176}\text{Hf}/^{177}\text{Hf}$ ratio in the continental crust increases
21
22 570 slower than in the depleted mantle and thus its $\epsilon_{\text{Hf}}(t)$ value becomes more and more
23
24 571 negative with time, whereas the depleted mantle develops more and more positive
25
26 572 $\epsilon_{\text{Hf}}(t)$ values (Rudnick and Gao, 2003; Kelemen et al., 2003; Salters and Stracke, 2004;
27
28 573 Palme and O'Neill, 2003). When a zircon crystallized from a crustal-derived melt, the
29
30 574 $^{176}\text{Hf}/^{177}\text{Hf}$ ratio in the melt was timely imprinted in the zircon, because Hf content in
31
32 575 zircon is several orders of magnitude higher than Lu content, and thus the change of
33
34 576 $^{176}\text{Hf}/^{177}\text{Hf}$ ratio in zircon with time is negligible; moreover, zircon $^{176}\text{Hf}/^{177}\text{Hf}$ ratio is
35
36 577 resistant to the influence of later processes such as weathering, fluid alteration and
37
38 578 metamorphic recrystallization (Patchett et al., 1984; Wu et al., 2006b; Zheng et al.,
39
40 579 2008; Hanyu et al., 2006; Carpentier et al., 2009; Hoffmann et al., 2011; Roux et al.,
41
42 580 2009; Yu et al., 2009; Chen et al., 2010; Tappe et al., 2011; Choi and Mukasa, 2012).
43
44 581 In this way, the $\epsilon_{\text{Hf}}(t)$ value of zircon reflects the mass source of the host rocks: given
45
46 582 the same zircon U-Pb age, the more negative zircon $\epsilon_{\text{Hf}}(t)$ value is, the higher
47
48 583 proportion of ancient continental crustal material the host rock contains. In principle,
49
50 584 the most positive $\epsilon_{\text{Hf}}(t)$ values correspond to the youngest single-stage Hf model ages
51
52 585 (T_{DM1}) that represent the maximum time of the emplacement of the mantle-derived
53
54 586 magma, while the most negative $\epsilon_{\text{Hf}}(t)$ values correspond to the oldest T_{DM1} ages that
55
56 587 represent the minimum time of the formation of the involved crust.
57

58 588 The UHP eclogites and gneisses in the CDZ exhibit varied zircon Hf isotope
59
60
61
62
63
64
65

1 589 compositions, indicating both source mixing and crustal contamination along an
2 590 active rifting zone, with varying degrees of mixing between different ages of crustal
3 591 materials at ~750 Ma. Therein, the youngest zircon T_{DM1} ages from the eclogites are
4 592 in agreement with the Neoproterozoic zircon U-Pb ages of ~750 Ma, while the oldest
5 593 zircon T_{DM2} ages from the gneisses are close to the Paleoproterozoic zircon U-Pb ages
6 594 of ~2.15 Ga, indicating growth and immediate reworking of juvenile crust at
7 595 Paleoproterozoic (~2.15 Ga) and Neoproterozoic (~750 Ma), respectively (e.g., Zheng
8 596 et al., 2006).

9 597 The studied meta-basites and meta-granitoids have varied zircon Hf isotope
10 598 compositions (Supplementary Table 8) which are in agreement with the UHP
11 599 eclogites and orthogneisses in the CDZ (e.g., Zheng et al., 2006) (Fig. 10), indicating
12 600 different degrees of mixing between Neoproterozoic depleted mantle materials and
13 601 Paleoproterozoic crustal components. The meta-basites have positive $\epsilon_{Hf}(t)$ values of
14 602 +2.6~+7.9 and young T_{DM1} ages of about 1.2~1.5 Ga, slightly older than their zircon
15 603 U-Pb ages, reflecting incongruent contamination of crustal materials during the
16 604 emplacement of their parental magmas. Inherited zircons from the low-Si
17 605 meta-granitoids exhibit overlapped T_{DM1} ages of 2359~2702 Ma and T_{DM2} ages of
18 606 2506~2823 Ma from late Archean to Paleoproterozoic, representing the time of the
19 607 formation of continental crust from the mantle. For the Neoproterozoic zircons with
20 608 negative $\epsilon_{Hf}(t)$ values, T_{DM2} can better reflect their origin than T_{DM1} . Neoproterozoic
21 609 zircons in the low-Si meta-granitoids exhibit negative $\epsilon_{Hf}(t)$ values of -3.2~-12.0 and
22 610 younger T_{DM2} ages of 1893~2446 resulting from mixing between depleted mantle
23 611 materials and late Archean continental crust at Neoproterozoic. Compared to the
24 612 low-Si meta-granitoids, the high-Si rocks do not contain ancient (late Archean)
25 613 inherited zircon, and have higher $\epsilon_{Hf}(t)$ values of -7.5~+1.4 and younger T_{DM2} ages of
26 614 1618~2172 Ma, indicating that they were mainly derived from remelting of younger
27 615 continental crust formed at early Paleoproterozoic. These clusters of T_{DM2} age of the
28 616 meta-granitoids are consistent with multiple episodes of crust growth of the South
29 617 China Block from the late Archean to Paleoproterozoic (Greentree et al., 2006; Zhang
30 618 et al., 2006a,b; Liu et al., 2008; Wang et al., 2010; Zhao and Cawood, 2012).

1 619 As a summary, the studied meta-basites and meta-granitoids derived from the
2 620 same sources as the UHP eclogites and felsic gneisses in the CDZ. Therein the
3
4 621 meta-basites were formed from depleted mantle upwelling and mafic magmatic
5
6 622 activities during the Neoproterozoic, with incongruent mixing with the Yangtze
7
8 623 crustal materials; the mafic magmatic activities remelted the basement of the South
9
10 624 China Block, which comprises the Archean and early Paleoproterozoic crustal rocks,
11
12 625 and generated the low-Si and high-Si meta-granitoids.
13
14
15 626

16 627 *Bulk-rock Sr-Nd-Pb isotopes*

17
18 628 Because Rb is more incompatible than Sr, and Nd is more incompatible than Sm,
19
20 629 melts will have higher Rb/Sr but lower Sm/Nd ratios than residues during partial
21
22 630 melting. Therefore, when the primitive mantle differentiated to form the crust and
23
24 631 depleted mantle, the crust acquired higher Rb/Sr and lower Sm/Nd ratios than the bulk
25
26 632 earth, while the depleted mantle acquired lower Rb/Sr and higher Sm/Nd ratios. Then
27
28 633 the $^{87}\text{Sr}/^{86}\text{Sr}$ of the crust will be more and more higher than the bulk earth, but the
29
30 634 $\epsilon_{\text{Nd}}(t)$ will be more and more negative with time; on the contrary, the $^{87}\text{Sr}/^{86}\text{Sr}$ and
31
32 635 $\epsilon_{\text{Nd}}(t)$ of the depleted mantle will evolve in the opposite direction. The meta-basites
33
34 636 have initial $^{87}\text{Sr}/^{86}\text{Sr}$ ratios of 0.7023–0.7067 (calculated to $t=230$ Ma), $\epsilon_{\text{Nd}}(230$ Ma)
35
36 637 values from -1.8 to +1.8 and T_{DM2} ages of 862–1156 Ma. In the $\epsilon_{\text{Nd}}(t)$ vs $(^{87}\text{Sr}/^{86}\text{Sr})_i$
37
38 638 diagram (Fig. 11), the meta-basites plot around the composition of the bulk silicate
39
40 639 earth and slightly toward lower continental crust, indicating that the meta-basites were
41
42 640 derived mainly from the mantle, with minor addition of lower continental crust. This
43
44 641 conclusion is also supported by their two-stage Nd model ages (T_{DM2}) of 862–1156
45
46 642 Ma, which are slightly older than their magmatic zircon U-Pb ages (~ 772 Ma).
47
48
49

50 643 U is more incompatible than Pb. This being the case, we would therefore predict
51
52 644 that continental crust should be more enriched in radiogenic Pb than the average of the
53
54 645 bulk-earth, while the depleted mantle should be depleted in radiogenic Pb. Upper
55
56 646 continental crustal rocks do have higher $^{206}\text{Pb}/^{204}\text{Pb}$ and $^{207}\text{Pb}/^{204}\text{Pb}$ ratios as expected, but
57
58 647 surprisingly, most mantle-derived rocks also exhibit higher Pb isotope ratios than the
59
60 648 average of the bulk-earth, whereas a majority of lower crustal rocks are relatively
61
62
63
64
65

1 649 depleted in radiogenic Pb. This phenomenon is known as the Pb paradox and it implies
2 650 that other processes apart from magmatism may have played key roles in the
3
4 651 differentiation of the U-Pb element pair.
5

6 652 In addition, Pb isotopes can be used to trace the crust affinity of given rocks from
7
8 653 upper or lower crust, i.e., upper crustal rocks commonly have higher radiogenic Pb
9
10 654 isotopes than lower crustal rocks (Zartman and Doe, 1981; Taylor and McLennan, 1985).
11
12 655 For example, Liu and Li (2008) concluded that the NDZ is of lower crustal origin, while
13
14 656 the CDZ and the SDZ are slices from middle to upper crust, according to their different
15
16 657 radiogenic Pb isotope compositions. As shown in Figure 12, the Pb isotope compositions
17
18 658 of the studied meta-basites fall into the range of the UHP meta-igneous rocks from the
19
20 659 CDZ, and are significantly higher than that of the UHP meta-igneous rocks from the NDZ.
21
22 660 This indicates that the studied meta-basites and the associated meta-granitoids were at
23
24 661 middle to upper crustal depths, consistent with the UHP meta-igneous rocks from the
25
26 662 CDZ.
27

28
29 663 Summing up, both zircon Hf and bulk-rock Sr-Nd-Pb isotopic data demonstrate
30
31 664 that the studied meta-basites and meta-granitoids are low-grade metamorphosed
32
33 665 counterparts of the UHP eclogites and orthogneisses in the CDZ; these rocks did not
34
35 666 experience deep subduction and UHP metamorphism during the Triassic, but were
36
37 667 detached from the subducting plate and exhumed from shallower depths, experiencing
38
39 668 amphibolite-facies metamorphic peak conditions.
40

41 669
42
43 670 *5.1.3. The studied rocks as the best candidates for elucidating the Neoproterozoic*
44
45 671 *evolution of the South China Block*
46

47 672 The UHP meta-igneous rocks in the CDZ consist mainly of granitic gneisses and
48
49 673 eclogites, which are generally considered to be transformed from bimodal igneous
50
51 674 rocks derived from rift magmatism in Neoproterozoic (e.g., Ames et al., 1996; Rowley
52
53 675 et al., 1997; Hacker et al., 1998). The studied meta-basites and meta-granitoids at
54
55 676 Longjinguan have consistent Neoproterozoic protolith ages and zircon Hf isotopic
56
57 677 compositions with those from the UHP meta-igneous rocks, most likely indicating that
58
59 678 they were derived from the same rifting events, during which depleted mantle
60
61

1 679 materials were added to the crust, and caused remelting of existing old crust and
2 680 generated bimodal magmas (Liu et al., 2007a). In addition, the bulk-rock Pb isotopic
3 681 compositions of the studied rocks fall into the range of the UHP meta-igneous rocks in
4 682 the CDZ (Fig.12), suggestive of upper crustal origin (Liu et al., 2017). In this regard,
5 683 the studied rocks are likely counterparts of the UHP rocks in the region, and both of
6 684 them were formed from partial melting of ancient crust in the Neoproterozoic.
7 685 Moreover, during the Triassic the studied rocks experienced lower-grade and
8 686 lower-pressure metamorphism with respect to their UHP counterpart. Therefore, we
9 687 suggest that the rocks could likely have better preserved their protolith compositions
10 688 than the UHP rocks, which often experienced interactions with melt and/or
11 689 supercritical fluids during UHP metamorphism (e.g., Zheng et al., 2011). In order to
12 690 test this hypothesis, the trace element patterns of the studied meta-basites are
13 691 compared to those of the UHP eclogites derived from basites (data from Tang et al.,
14 692 2007), as shown in Fig. 5: the studied meta-basites have identical REE and trace
15 693 element patterns, while the UHP eclogites exhibit similar REE patterns but
16 694 significantly varied large ion lithophile element (LILE) contents. This is consistent
17 695 with the fact that LILE have significantly higher mobilities than REE in hydrous
18 696 fluids during UHP metamorphism (Kessel et al., 2005; Hermann et al., 2006; Zheng et
19 697 al., 2011). As a conclusion, the rocks here have better preserved their protolith
20 698 compositions than their UHP counterparts, and thus they are more suitable for
21 699 elucidating the Neoproterozoic evolution in the area.

22 700

23 701 *5.2. Neoproterozoic magmatic and metamorphic events*

24 702 *5.2.1. Meta-basites*

25 703 Zircons in the meta-basites (samples 11LJG3 and 11LJG7) give a concordant
26 704 magmatic age cluster of ~772 Ma (Ma) and two concordant metamorphic age clusters
27 705 of ~768 Ma (Me1) and ~746 Ma (Me2) (see section 4.2.3). As mentioned above, the
28 706 magmatic zircons exhibit clear oscillatory zoning and REE patterns typical of
29 707 magmatic genesis, thus the age of ~772 Ma represents a magmatic event. As to the
30 708 metamorphic zircons, they formed during metamorphic events characterized by the

1 709 circulation of REE-enriched fluids controlled by fractures. In addition, most
2 710 metamorphic zircons exhibit slightly higher Nb + Ta, U and Th contents than the
3 711 magmatic zircons (Supplementary Table 5), thus suggesting that the metamorphic
4 712 fluids were also enriched in Nb+Ta, U and Th. These REE-, Nb+Ta-, U- and Th-
5 713 enriched fluids favoured the precipitation of minerals rich in these elements, such as
6 714 epidote, rutile, ilmenite and titanite (Figs. 7a-i), observed as inclusions in the
7 715 metamorphic zircons (e.g., sample 11LJG3; Me1 domains). Thermobarometric
8 716 estimates (see Section 2.3) based on rutile inclusions indicate that metamorphic zircon
9 717 domains Me1 grew at about 850-870 °C, 12 kbar. No rutile or other inclusions
10 718 suitable for thermometric estimates have been recognized in the Me2 domain of
11 719 zircons in sample 11LJG7, thus the temperatures of the late thermal overprinting at
12 720 ~746 Ma has not been estimated. Summing up, the meta-basites were formed at ca.
13 721 772 Ma (Me domains) and experienced subsequent granulite-facies (850-870 °C)
14 722 metamorphism at ca. 768 Ma (Me1 domains), followed by a thermal overprinting
15 723 event at ~746 Ma (Me2 domains). The almost overlapped magmatic and metamorphic
16 724 zircon ages (772 ± 4 and 768 ± 7 Ma, respectively) suggest that the Neoproterozoic
17 725 magmatism in this area occurred in pulse, and that the later magma underplating
18 726 warmed the already solidified rocks (e.g., Liu et al., 2007a; Liu et al., 2015) resulting
19 727 in granulite-facies metamorphism. The thermal overprinting age of ~746 Ma is
20 728 comparable with the emplacement age of some mafic rocks in the Dabie orogen, for
21 729 example the meta-basites in the BZ located in the northern part of the Dabie orogen
22 730 (Liu et al., 2017), indicating that a later magma emplacement at that time in the area
23 731 may have been the heat source of the thermal overprinting. Moreover, these ages are
24 732 in agreement with the time of Rodinia breakup indicated by large volumes of mafic
25 733 and felsic magmatism along the northern margin of the Yangtze Block (Li et al., 2002;
26 734 Li et al., 2003a,b,c; Zhou et al., 2002a,b, 2006a,b; Zhao and Zhou, 2007a,b, 2008),
27 735 suggesting that the studied rocks are generated from several episodes of magmatic
28 736 event related to the Rodinia breakup.

29 737

30 738 *5.2.2. Meta-granitoids*

1 739 Compared to the meta-basites, the low-Si meta-granitoids exhibit a more complex
2 740 zircon U-Pb age spectrum. Few inherited zircon cores preserve two groups of age at
3 741 ~2.0 and ~2.5 Ga, timely consistent with two episodes of Precambrian crustal growth
4 742 and immediate reworking event of the SCB (e.g., Zhang et al., 2006a,b,c; Liu et al.,
5 743 2008; Wang et al., 2010; Zhao and Cawood, 2012). Same for these inherited zircon
6 744 cores, the zircons in the studied rocks are distinguished into two types: magmatic
7 745 zircon domains yielding concordant ages of ca. 819 Ma (Ma domains) and
8 746 metamorphic zircon domains with concordant ages at ca. 784 (Me1 domains) and 746
9 747 Ma (Me2 domains). The latter are discriminated from the former by weaker or no
10 748 oscillatory zonings, lighter brightness in CL image and enrichment of mineral
11 749 inclusion. A typical zircon with magmatic zircon core and metamorphic mantle in
12 750 meta-granitoid sample 11LJG2 (Me1) is shown (Figs. 7j-l): the core is dark with
13 751 obvious oscillatory zoning, while the mantle is light and homogeneous in CL image;
14 752 the core is free of mineral inclusion, while the mantle contains K-feldspar +
15 753 muscovite inclusion; and there is a clear boundary between the core and the mantle.
16 754 Two analytical spots on metamorphic zircon domains exhibit significantly higher
17 755 LREE patterns than the magmatic zircons (Figs. 8b,c), therein a spot also exhibit
18 756 higher REE contents than the magmatic zircons. Moreover, muscovite + K-feldspar
19 757 inclusion is identified in metamorphic zircon (Fig. 7k), indicating that the
20 758 metamorphic zircons were formed in the presence of LREE-enriched fluid, in
21 759 agreement with the metamorphic zircons in the meta-basites. Therefore, the low-Si
22 760 meta-granitoids experienced two episodes of metamorphism at ~784 Ma and ~746 Ma,
23 761 respectively. It is worth noting that, the ~784 Ma metamorphic zircon ages are
24 762 comparable with the forming (i.e. magmatic) ages of the meta-basites (~772 Ma)
25 763 within error, suggesting that the emplacement of the basic magmas may be the heat
26 764 source for the metamorphism of the low-Si meta-granitoids. The thermal overprinting
27 765 of ~746 Ma is timely in agreement with the ca. 750 Ma forming age of the
28 766 meta-granitoids and meta-basites in the BZ (Jiang et al., 2005; Wu et al., 2007; Liu et
29 767 al., 2010, 2017), indicating that the low-Si meta-granitoids and the meta-basites in the
30 768 region experienced a coeval thermal event as a consequence of the emplacement of

1 769 the meta-basites within the BZ.

2 770 The high-Si meta-granitoids exhibit nearly the same Neoproterozoic magmatic
3
4 771 and metamorphic zircon ages with the low-Si type, indicating that they were
5
6 772 generated from the same or adjacent magmatic events and then jointly experienced the
7
8 773 same metamorphic processes during the Neoproterozoic. However, the two types of
9
10 774 meta-granitoids are likely derived from different sources: (i) the low-Si type contains
11
12 775 inherited zircons with two age clusters at ~2.5 Ga and ~2.0 Ga, suggesting that its
13
14 776 source could be a late Archean basement that experienced metamorphic reworking
15
16 777 during the Paleoproterozoic, whereas (ii) the high-Si type does not contain ancient
17
18 778 inherited zircon, and the oldest zircon Hf model age (T_{DM2}) is 2172 Ma, suggesting
19
20 779 that a derivation from the juvenile crust formed during the Paleoproterozoic. This
21
22 780 hypothesis can well explain the compositional gap, especially the different Si contents,
23
24 781 between the two types of meta-granitoids (see section 4.1), and also the slightly higher
25
26 782 zircon $\varepsilon_{Hf}(t)$ values and younger Hf model ages of the high-Si meta-granitoids (see
27
28 783 section 4.3).

29
30 784 The meta-basites and meta-granitoids with similar mid- to late-Neoproterozoic
31
32 785 ages have been reported from other localities within the Dabie orogen, for example,
33
34 786 Ganghe within the CDZ (Dong et al., 1997), Yuexi within the NDZ (Gao et al., 2006),
35
36 787 and Huwan, Sujiahe and Luzhenguan within the BZ (Jiang et al., 2005; Wu et al.,
37
38 788 2007; Liu et al., 2010, 2017). In addition, extensive mid- to late-Neoproterozoic mafic
39
40 789 dyke swarms and granitic bodies (Zhao and Zhou, 2009; Hong et al., 2009; Xue et al.,
41
42 790 2011; Wang et al., 2013) are exposed in Suizhou-Zaoyang of the Hubei province,
43
44 791 along the northern margin of the SCB. Moreover, the forming ages of these rocks are
45
46 792 clearly comparable with the protolith ages of the UHP eclogites and orthogneisses
47
48 793 (Rowley et al., 1997; Hacker et al., 1998; Liu et al., 2007a,b, 2011a; and references
49
50 794 therein) in the Dabie orogen. In this regard, these rocks, including those from
51
52 795 Longjingguan in this study, should be counterparts of the UHP meta-igneous rocks in
53
54 796 the Dabie orogen, implying that the protoliths of the latter could have been formed
55
56 797 during the same Neoproterozoic magmatic events, and could have experienced the
57
58 798 same Neoproterozoic metamorphism.

1 799

2 800 *5.3. Petrogenesis and tectonic setting*

3 801 *5.3.1. Meta-basites*

4 802 Mantle-normalized trace element patterns are frequently used to infer
5 803 petrogenesis and tectonic settings of igneous rocks, because the same rock type
6 804 formed in different tectonic settings can display significantly different trace element
7 805 patterns. For example, the basites of mid-ocean ridges (MORB) are formed from the
8 806 depleted mantle within a narrow depth interval, and thus have a uniform chemical
9 807 composition, while the island-arc basalts (IAB) and within-plate basalts (WPB)
10 808 exhibit large variation in trace element contents and patterns, and generally
11 809 enrichment in LILE and LREE compared to MORB, depending on addition
12 810 component of crustal materials. The strong negative Sr anomalies, together with
13 811 slightly positive or negative anomalies of HFSE elements of the studied meta-basites
14 812 (Fig. 5b) indicate that they are unlikely IAB or post-collision basic rocks (PCB),
15 813 which commonly exhibit positive Sr anomalies and strong depletion of the HFSE.
16 814 WPB fits better with the studied meta-basites, with respect to the mantle-normalized
17 815 trace element pattern (e.g., Velikoslavinsky and Krylov, 2014 and references therein),
18 816 thus the meta-basites were most likely formed in a within-plate environment. To
19 817 reinforce the hypothesis, the discrimination diagrams proposed by Velikoslavinsky
20 818 and Krylov (2014) were applied (Fig. 13). Nearly all major elements as well as many
21 819 trace elements are involved in the discriminant functions of these diagrams; hence
22 820 they include comprehensive information of the geochemical characteristics of basalts.
23 821 In this way, the average weighted uncertainty of IAB, MORB, and WPB identification
24 822 is substantially small as compared with previously elaborated plots. All of the studied
25 823 meta-basites plot into the category of WPB in the $DF_1(x)$ range (Fig. 13a) and most of
26 824 them fall into continental WPB field with only a small percentage of OIB in the $DF_3(x)$
27 825 range (Fig. 13b). In addition, the $DF_5(x)$ values of the meta-basites are coincident with
28 826 most WPB but only few post-collision basic rocks (PCB) (Fig. 13c). As a
29 827 consequence, the studied meta-basites are most likely continental WPB not related to
30 828 post-collision processes, but rather involved in mantle plume or continental rifting.

1 829 This conclusion is highly in agreement with the zircon Hf isotopic features of the
2 830 meta-basites (see section 5.1), which demonstrate mixing between the depleted mantle
3
4 831 and the crust.
5

6 832

8 833 *5.3.2. Meta-granitoids*

9
10 834 Various binary discrimination diagrams were applied to constrain the tectonic
11 835 setting of the meta-granitoids in Longjingguan. The diagrams employing Ga/Al
12
13 836 (Whalen et al., 1987) show that the meta-granitoids have similar geochemical features
14
15 837 with A-type granites (Fig. 14). A-type granite was firstly proposed to be related to
16
17 838 anorogenic environments (Chappell and White, 1974), but afterwards more and more
18
19 839 studies suggest that A-type granite may form under different environments (Whalen et
20
21 840 al., 1987; Eby, 1990; Wu et al., 2002; Bonin, 2007). Nevertheless, it is widely
22
23 841 accepted that high melting temperatures (>830 °C) are required to generate A-type
24
25 842 granite magmas (Clemens et al., 1986), probably through the emplacement of
26
27 843 mantle-derived mafic magmas into the lower crust. In this study, the meta-granitoids
28
29 844 are spatially and temporally associated with meta-basites, indicating that they were
30
31 845 formed under a geodynamic setting characterized by asthenosphere upwelling and
32
33 846 basic magmatism, which can provide sufficient heat to generate high-T granitoids.
34
35 847 Zircon Hf isotopic compositions of the meta-granitoids (see section 5.1) also suggest
36
37 848 addition of the depleted mantle materials into the felsic magmas.
38
39

40
41 849 Trace elements and REE patterns are frequently used in identifying petrogenesis
42
43 850 and tectonic setting of granitoids. The significant depletion of HREE, Nb, Ta, and Ti
44
45 851 of the studied meta-granitoids (Fig. 5b) is in agreement with adakite and arc-related
46
47 852 ADR (andesite, dacite and rhyolite) (see Castillo, 2006 for an overview). Adakite and
48
49 853 arc-related ADR are generally associated to slab subducting and mantle convecting,
50
51 854 consistent with the aforementioned high temperature characteristics of the studied
52
53 855 meta-granitoids. However, the high Sr, low Yb and high Sr/Y characteristics of
54
55 856 adakite are in contrast with the studied meta-granitoids, which exhibit low Sr (13-275
56
57 857 ppm), high Y (19-46 ppm) and low Sr/Y (0.34-10.39). In the Sr/Y vs Y diagram (Fig.
58
59 858 15), which is usually used to discriminate adakites and TTGs from typical arc
60
61
62
63
64
65

1 859 calc-alkaline rocks (Drummond and Defant, 1990), all the studied meta-granitoids
2 860 plot into the field of typical arc rocks. Therefore, based on the geochemical
3 861 characteristics, zircon U-Pb ages and Hf isotopic compositions described above, the
4 862 studied meta-granitoids most likely formed under magmatic arc setting, in agreement
5 863 with the previous investigations on the Neoproterozoic igneous rocks in the periphery
6 864 of the SCB (Zheng et al., 2007; Zhao et al., 2018 and references therein); and the
7 865 low-Si and high-Si types are mainly derived from partial melting of late-Archean and
8 866 Paleoproterozoic continental crustal materials, respectively, with various degrees of
9 867 addition of mantle materials.

10 868 In summary, the meta-granitoids were formed at ca. 819 Ma by partial melting of
11 869 ancient continental crustal materials in an arc setting, whereas the meta-basites were
12 870 derived mainly from the depleted mantle at ca. 772 Ma in a rifting setting. Thus, the
13 871 studied rocks witness the transition from a convergent to an extensional tectonic
14 872 setting, and provide new constraints for the beginning of the Neoproterozoic rifting in
15 873 northern SCB, which can further help to better understand the breakup of the
16 874 supercontinent Rodinia.

17 875

18 876 **6. Conclusions**

19 877 (1) The meta-basites and meta-granitoids in Longjingguan are relatively low-grade
20 878 metamorphosed counterparts of the UHP eclogites and orthogneisses within the
21 879 CDZ; they were detached from the subducted crust of the SCB and exhumed from
22 880 shallow depths during subduction, and subsequently thrust over the CDZ during
23 881 collisional orogenesis.

24 882 (2) The precursors of the studied meta-granitoids and meta-basites were formed at ca.
25 883 819 Ma and 772–784 Ma, respectively. They jointly experienced a granulite-facies
26 884 metamorphism at ca. 768 Ma and a thermal overprinting at ca. 746 Ma resulted
27 885 from underplating of mafic magmas, strongly pointing to multiple episodes of
28 886 continental rifting during the Neoproterozoic.

29 887 (3) The meta-granitoids are derived mainly from partial melting of ancient continental

1 888 crustal materials of the SCB in an arc setting. The low-Si meta-granitoids were
2 889 derived from the late Archean basement rocks that underwent Paleoproterozoic
3
4 890 metamorphic reworking, while the high-Si meta-granitoids mainly come from the
5
6 891 Paleoproterozoic juvenile crust. The meta-basites were derived from the depleted
7
8 892 mantle in a rifting environment. The studied rocks thus witness the transition from
9
10 893 a convergent to an extensional tectonic setting, and provide new time constraints
11
12 894 for the beginning of the Neoproterozoic rifting in northern SCB, which can further
13
14 895 help to better understand the breakup of the supercontinent Rodinia.
15
16
17 896

18 19 897 **Acknowledgements**

20
21
22 898 This study is financially supported by the National Basic Research Program of
23
24 899 China (2015CB856104) and the National Natural Science Foundation of China
25
26 900 (41273036 and 41773020). We thank B. Song and Q. Yang for their help in SHRIMP
27
28 901 U-Pb dating, P. Sun for Hf-isotope and Z.H. Hou and X.M. Liu for trace-element
29
30 902 analysis on zircon, F.-K. Chen for Sr-Nd-Pb isotope and Raman analysis, and Z.-Y.
31
32 903 Chen and Y.H. Shi for electron microprobe analysis. Many suggestions and
33
34 904 constructive comments by Yunpeng Dong and three anonymous reviewers have
35
36 905 greatly improved the paper.
37
38 906

References

- Ames, L., Zhou, G.Z., Xiong, B.C., 1996. Geochronology and isotopic character of ultrahigh-pressure metamorphism with implications for the collision of the Sino-Korean and Yangtze cratons, central China. *Tectonics* 15, 472–489.
- Angiboust, S., Harlov, D., 2017. Ilmenite breakdown and rutile-titanite stability in metagranitoids: Natural observations and experimental results. *American Mineralogist* 102, 1696–1708.
- Bauer, C., Rubatto, D., Krenn, K., Proyer, A., Hoinkes, G., 2007. A zircon study from the rhodope metamorphic complex, n-greece: time record of a multistage evolution. *Lithos* 99(3), 207–228.
- Black, L.P., Kamo, S.L., Allen, C.M., Aleinikoff, J.N., 2003. TEMORA 1: a new zircon standard for phanerozoic U–Pb geochronology. *Chemical Geology* 200, 155–170.
- Blichert-Toft, J., Albarede, F., 1997. The Lu–Hf isotope geochemistry of chondrites and the evolution of the mantle–crust system. *Earth and Planetary Science Letters* 148, 243–258.
- Bohlen, S.R., Liotta, J.J., 1986. A Barometer for Garnet Amphibolites and Garnet Granulites. *Journal of Petrology* 27, 1025–1034.
- Bonin, B., 2007. A-type granites and related rocks: evolution of a concept, problems and prospects. *Lithos* 97(1–2), 1–29.
- Carpentier, M., Chauvel, C., Maury, R., Mattielli, N., 2009. The “zircon effect” as recorded by the chemical and Hf isotopic compositions of the Lesser Antilles forearc sediments. *Earth and Planetary Science Letters* 287, 86–99.
- Castillo, P.R., 2006. An overview of adakite petrogenesis. *Chinese Science Bulletin* 51(3), 257–268.
- Chappell, B.W., White, A.J.R., 1974. Two contrasting granite types. *Pacific Geology* 8, 173–174.
- Chemenda, A.I., Mattauer, M., Bokun, A.N., 1996. Continental subduction and a mechanism for exhumation of high-pressure metamorphic rocks: new modelling,

- 1 936 field data from Oman. *Earth and Planetary Science Letters* 143, 173–182.
- 2 937 Chen, F., Hegner, E., Todt, W., 2000. Zircon ages and Nd isotopic and chemical
3 compositions of orthogneisses from the Black Forest, Germany: evidence for a
4 938 Cambrian magmatic arc. *International Journal of Earth Sciences* 88, 791– 802.
- 5
6 939
7
8 940 Chen, F.K., Guo, J.H., Jiang, L.L., Siebel, W., Cong, B., Satir, M., 2003. Provenance
9 of the Beihuaiyang lower-grade metamorphic zone of the Dabie
10 941 ultrahigh-pressure collisional orogen, China: evidence from zircon ages. *Journal*
11 942 *of Asian Earth Science* 22(4), 343–352.
- 12
13 943
14
15 944 Chen, F., Li, X.H., Wang, X.L., Li, Q.L., Siebel, W., 2007. Zircon age and Nd-Hf
16 isotopic composition of the Yunnan Tethyan belt, southwestern China.
17 945 *International Journal of Earth Science* 96, 1179–1194.
- 18
19 946
20
21 947 Chen, R.X., Zheng, Y.F., Xie, L., 2010. Metamorphic growth and recrystallization of
22 zircon: distinction by simultaneous in-situ analyses of trace elements, U–Th–Pb
23 948 and Lu–Hf isotopes in zircons from eclogite-facies rocks in the Sulu orogen.
24 *Lithos* 114, 132–154.
- 25
26 949
27
28 950
29
30 951 Choi, S.H., Mukasa, S.B., 2012. Lu–Hf and Sm–Nd isotope systematic of Korean
31 spinel peridotites: a case for metasomatically induced Nd–Hf decoupling. *Lithos*
32 952 154, 263–276.
- 33
34 953
35
36 954 Chopin, C., 1984. Coesite and pure pyrope in high grade blueschists of the western
37 Alps: a first record and some consequences. *Contributions to Mineralogy and*
38 955 *Petrology* 86, 107–118.
- 39
40 956
41
42 957 Clemens, J.D., Holloway, J.R., White, A.J.R., 1986. Origin of an A-type granite:
43 experimental constraints. *American Mineralogist* 71, 317–324.
- 44
45 958
46
47 959 Compston, W., Williams, I.S., Kirschvink, J.L., 1992. Zircon U–Pb ages for the Early
48 Cambrian time-scale. *Journal of the Geological Society* 149, 171–184.
- 49
50 960
51
52 961 Cong, B., Zhai, M., Carswell, D.A., Wilson, R.N., Wang, Q., Zhao, Z., Windly, B.F.,
53 1995. Petrogenesis of ultrahigh-pressure rocks and their country rocks at
54 962 Shuanghe in Dabieshan, central China. *European Journal of Mineralogy* 7, 119–
55 138.
- 56
57 963
58
59 964
60
61 965 Dong, S.W., Wang, X.F., Huang, D.Z., 1997. Discovery of low grade metamorphic

- 1 966 volcanic rock sheets within UHP in Dabie Mts. and its implications. Chinese
2 Science Bulletin 42, 1199–1203.
3
4 968 Drummond, M.S., Defant, M.J., 1990. A model for trondhjemite–tonalite–dacite
5 genesis and crustal growth via slab melting: Archaean to modern comparisons.
6
7 969 Journal of Geophysical Research 95, 21503–21521.
8
9 970
10 971 Eby, G.N., 1990. The A-type granitoids: a review of their occurrence and chemical
11 characteristics and speculations on their petrogenesis. Lithos 26, 115–134.
12
13 972
14 973 Ernst, W.G., Maruyama, S., Wallis, S., 1997. Buoyancy-driven, rapid exhumation of
15 ultrahigh-pressure metamorphosed continental crust. Proceedings of the National
16 Academy of Science, USA 94, 9532–9537.
17
18 974
19 975
20 976 Gao, T.S., Tang, J.F., Sang, H.Q., Hu, S.L., Qian, C.C., 2006. Whole-rock Ar-Ar
21 dating for low-grade metavolcanics within the Dabie orogen and its geological
22 implications. Chinese Science Bulletin 51, 1197–1202.
23
24 977
25 978
26 979 Gebauer, D., Schertl, H.P., Brix, M., Schreyer, W., 1997. 35 Ma old ultrahigh-pressure
27 metamorphism and evidence for very rapid exhumation in the Dora Maira Massif,
28 Western Alps. Lithos 41, 5–24.
29
30 980
31 981
32 982 Greentree, M.R., Li, Z.X., Li, X.H., Wu, H., 2006. Late mesoproterozoic to earliest
33 neoproterozoic basin record of the sibao orogenesis in western south china and
34 relationship to the assembly of rodinia. Precambrian Research 151(1–2), 79–100.
35
36 983
37 984
38 985 Griffin, W.L., Pearson, N.J., Belousova, E., Jackson, S.E., van Achterbergh, E.,
39 O’Reilly, S.Y., Shee, S.R., 2000. The Hf isotope composition of cratonic mantle:
40 LAM-MC-ICPMS analysis of zircon megacrysts in kimberlites. Geochimica et
41 Cosmochimica Acta 64, 133–147.
42
43 986
44 987
45 988
46 989 Groppo, C., Rolfo, F., Liu, Y.C., Deng, L.P., Wang, A.D., 2015. P-T evolution of
47 elusive UHP eclogites from the Luotian dome (north Dabie zone, China): how
48 far can the thermodynamic modeling lead us? Lithos 226, 183–200.
49
50 990
51 991
52 992 Hacker, B.R., Ratschbacher, L., Webb, L., Ireland, T., Walker, D., Dong, S.W., 1998.
53 U/Pb zircon ages constrain the architecture of the ultrahigh-pressure
54 Qinling–Dabie orogen, China. Earth and Planetary Science Letters 161,
55 215–230.
56
57 993
58 994
59 995
60
61
62
63
64
65

- 1 996 Hacker, B.R., Ratschbacher, L., Webb, L., McWilliams, M.O., Ireland, T., Calvert, A.,
2 997 Dong, S.W., Wenk, H.R., Chateigner, D., 2000. Exhumation of ultrahigh-pressure
3 998 continental crust in east central China: Late Triassic-Early Jurassic tectonic
4 999 unroofing. *Journal of Geophysical Research* 105 (B6), 13339–13364.
5
6
7
8 1000 Hanchar, J.M., Rudnick, R.L., 1995. Revealing hidden structures: the application of
9 1001 cathodoluminescence and back-scattered electron imaging to dating zircons from
10 1002 lower crustal xenoliths. *Lithos* 36, 289–303.
11
12
13 1003 Hanyu, T., Tatsumi, Y., Nakai, S., Chang, Q., Miyazaki, T., Sato, K., Tani, K., Shi-bata,
14 1004 T., Yoshida, T., 2006. Contribution of slab melting and slab dehydration to
15 1005 magmatism in the NE Japan arc for the last 25 Myr: Constraints from
16 1006 geochemistry. *Geochemistry Geophysics Geosystems* 7, Q08002.
17
18
19 1007 Hermann, J., Rubatto, D., Korsakov, A., Shatsky, V.S., 2001. Multiple zircon growth
20 1008 during fast exhumation of diamondiferous, deeply subducted continental crust
21 1009 (Kokchetav massif, Kazakhstan). *Contributions to Mineralogy and Petrology* 141,
22 1010 66–82.
23
24
25 1011 Hermann, J., Spandlera, C., Hacka, A., Korsakovb, A.V., 2006. Aqueous fluids and
26 1012 hydrous melts in high-pressure and ultra-high pressure rocks: Implications for
27 1013 element transfer in subduction zones. *Lithos* 92, 399–417.
28
29
30 1014 Hoffmann, J.E., Münker, C., Polat, A., Rosing, M.T., Schulz, T., 2011. The origin of
31 1015 decoupled Hf–Nd isotope compositions in Eoarchean rocks from southern West
32 1016 Greenland. *Geochimica et Cosmochimica Acta* 75, 6610–6628.
33
34
35 1017 Holland, T., Blundy, J., 1994. Non-ideal interactions in calcic amphiboles and their
36 1018 bearing on amphibole-plagioclase thermometry. *Contributions to Mineralogy and*
37 1019 *Petrology* 116, 433–447.
38
39
40 1020 Hong, J.A., Ma, B., Huang, Q., 2009. The Dafushan meta-basic/ultrameta-basic
41 1021 complex and genesis of the related rutile ore deposit at Zaoyang, Hubei (in
42 1022 Chinese with English abstract). *Chinese Journal of Geology* 44, 231–244.
43
44
45 1023 Hoskin, P.W., Ireland, T.R., 2000. Rare earth element chemistry of zircon and its use
46 1024 as a provenance indicator. *Geology* 28(7), 627–630.
47
48
49 1025 Hou, Z.H., Wang, C.X., 2007. Determination of 35 trace elements in geological
50
51
52
53
54
55
56
57
58
59
60
61
62
63
64
65

- 1 1026 samples by inductively coupled plasma mass spectrometry (in Chinese with
2 English abstract). *Journal of University of Science and Technology of China* 37,
3 1027
4 940–944.
5 1028
- 6 1029 Jiang, L., Siebel, W., Chen, F., Liu, Y.C., Chu, D., 2005. U-Pb zircon ages for the
7 Luzhengan Complex in northern part of the eastern Dabie orogen. *Science*
8 1030
9 China (Series D) 48, 1357–1367.
10 1031
- 11 1032 Kelemen, P.B., Hanghoj, K., Greene, A.R., 2003. One view of the geochemistry of
12 subducted-related magmatic arcs, with an emphasis on primitive andesites and
13 1033
14 lower crust. *Treatise of Geochemistry* 3, 593–659.
15 1034
- 16 1035 Kessel, R., Schmidt, M.W., Ulmer, P., Pettke, T., 2005. Trace element signature of
17 subduction-zone fluids, melts and supercritical liquids at 120–180 km depth.
18 1036
19 Nature 437, 724–727.
20 1037
- 21 1038 Le Bas, M.J., Le Maitre, R.W., Streckeisen, A., Zanettin, B., 1986. A chemical
22 classification of volcanic rocks based on the total alkali-silica diagram. *Journal*
23 1039
24 of Petrology 27(3), 745–750.
25 1040
- 26 1041 Lee, C.A., Luffi, P., Plank, T., Dalton, H., Leeman, W.P., 2009. Constraints on the
27 depths and temperatures of basic magma generation on Earth and other terrestrial
28 1042
29 planets using new thermobarometers for mafic magmas. *Earth and Planetary*
30 1043
31 Science Letters 279, 20–33.
32 1044
- 33 1045 Li, S.G., Xiao, Y.L., Liou, D.L., Ge, N.J., Zhang, Z.Q., Sun, S.S., Cong, B.L., Zhang,
34 R.Y., Hart, S.R., Wang, S.S., 1993. Collision of the North China and Yangtze
35 1046
36 blocks and formation of coesite bearing eclogites: timing and processes.
37 1047
38 Chemical Geology 109, 89–111.
39 1048
- 40 1049 Li, S.G., Jagoutz, E., Chen, Y.Z., Li, Q.L., 2000. Sm–Nd and Rb–Sr isotope
41 1050
42 chronology of ultrahigh-pressure metamorphic rocks and their country rocks at
43 1051
44 Shuanghe in the Dabie Mountains, central China. *Geochimica et Cosmochimica*
45 1052
46 Acta 64, 1077–1093.
47 1053
- 48 1053 Li, S.Z., Kusky, T.M., Zhao, G.C., Liu, X.C., Zhang, G.W., Kopp, H., Wang, L., 2010.
49 1054
50 Two-stage Triassic exhumation of HP–UHP terranes in the western Dabie orogen
51 1055
52 of China: constraints from structural geology. *Tectonophysics* 490, 267–293.
53
54
55
56
57
58
59
60
61
62
63
64
65

- 1 1056 Li, X.H., Li, Z.X., Ge, W.C., Zhou, H.W., Li, W.X., Liu, Y., Wingate, M.T.D., 2003a.
2
3 1057 Neoproterozoic granitoids in South China: crustal melting above a mantle plume
4
5 1058 at ca 825 Ma? *Precambrian Research* 122, 45–83.
- 6 1059 Li, X.H., Li, Z.X., Zhou, H., Liu, Y., Liang, X., Li, W., 2003b. SHRIMP U–Pb zircon
7
8 1060 age, geochemistry and Nd isotope of the Guandaoshan pluton in SW Sichuan:
9
10 1061 petrogenesis and tectonic significance. *Science China (Series D)* 46, 73–83.
- 11 1062 Li, X.P., Zheng, Y., Wu, Y., Chen, F., Gong, B., Li, Y.L., 2004. Low-T eclogite in the
12
13 1063 Dabie terrane of China: petrological and isotopic constrains on fluid activity and
14
15 1064 radiometric dating. *Contributions to Mineralogy and Petrology* 148, 443–470.
- 16 1065 Li, Z.X., Li, X.H., Kinny, P.D., Wang, J., Zhang, S., Zhou, H., 2003c. Geochronology
17
18 1066 of Neoproterozoic syn-rift magmatism in the Yangtze Craton, South China and
19
20 1067 correlations with other continents: evidence for a mantle superplume that broke
21
22 1068 up Rodinia. *Precambrian Research* 122, 85–109.
- 23 1069 Li, S.G., Huang, F., Zhou, H.Y., Li, H.M., 2003d. U-Pb isotopic compositions of the
24
25 1070 ultrahigh pressure metamorphic (UHPM) rocks from Shuanghe and gneisses
26
27 1071 from Northern Dabie zone in the Dabie Mountains, central China: Constraint on
28
29 1072 the exhumation mechanism of UHPM rocks. *Science China (Series D)* 46(3),
30
31 1073 200–209.
- 32 1074 Li, Y., Liu, Y.C., Yang, Y., Deng, L.P., 2017. New U-Pb geochronological constraints
33
34 1075 on formation and evolution of the Susong complex zone in the Dabie orogen.
35
36 1076 *Acta Geologica Sinica* 91, 1915–1918.
- 37 1077 Liu, F., Gerdes, A., Xue, H., Liang, F., 2006a. SHRIMP U-Pb zircon dating from
38
39 1078 eclogite lenses in marble, Dabie-Sulu UHP terrane: restriction on the prograde,
40
41 1079 UHP and retrograde metamorphic ages. *Acta Petrologica Sinica* 22, 1761–1778.
- 42 1080 Liu, J., Ye, K., Maruyama, S., Cong, B., Fan, H., 2001. Mineral inclusions in zircon
43
44 1081 from gneisses in the ultrahigh-pressure zone of the Dabie Mountains, China.
45
46 1082 *Journal of Geology* 109, 523–535.
- 47 1083 Liu, X.C., Jahn, B.-M., Liu, D., Dong, S., Li, S., 2004. SHRIMP U-Pb zircon dating
48
49 1084 of a metagabbro and eclogites from western Dabieshan (Hong'an Block), China,
50
51 1085 and its tectonic implications. *Tectonophysics* 394, 171–192.

- 1 1086 Liu, X.M, Gao, S., Diwu, C.R, Ling, W.L., 2008. Precambrian crustal growth of
2 Yangtze Craton as revealed by detrital zircon studies. *American Journal of*
3 *Science* 308(4), 421–468.
4
5 1088
6 1089 Liu, Y.C., Deng, L.P., Gu, X.F., Groppo, C., Franco, R., 2015. Application of
7 Ti-in-zircon and Zr-in-rutile thermometers to constrain high-temperature
8 metamorphism in eclogites from the Dabie orogen, central China. *Gondwana*
9 *Research* 27, 410–423.
10
11 1091
12 1092
13 1093 Liu, Y.C., Gu, X.F., Li, S.G., Hou, Z.F., Song, B., 2011a. Multistage metamorphic
14 events in granulitized eclogites from the North Dabie complex zone, central
15 China: evidence from zircon U-Pb age, trace element and mineral inclusion.
16 *Lithos* 122, 107–121.
17
18 1094
19 1095
20 1096
21 1097 Liu, Y.C., Gu, X.F., Rolfo, F., Chen, Z.Y., 2011b. Ultrahigh-pressure metamorphism
22 and multistage exhumation of eclogite from the Luotian dome, North Dabie
23 Complex Zone (central China): Evidence from mineral inclusions and
24 decompression texture. *Journal of Asian Earth Science* 42, 607–617.
25
26 1098
27 1099
28 1100
29 1101 Liu, Y.C., Li, S.G., 2005. Lower crustal rocks from the Dabie Mountains and their
30 subduction. *Acta Petrologica Sinica* 21, 1059–1066.
31
32 1102
33 1103 Liu, Y.C., Li, S.G., 2008. Detachment within subducted continental crust and
34 multi-plate successive exhumation of ultrahigh-pressure metamorphic rocks:
35 Evidence from the Dabie-Sulu orogenic belt. *Chinese Science Bulletin* 53,
36 3105–3119.
37
38 1104
39 1105
40 1106
41 1107 Liu, Y.C., Li, S.G., Gu, X.F., Hou, Z.H., 2006b. Zircon SHRIMP U-Pb dating for
42 olivine gabbro at Wangmuguan in the Beihuaiyang zone and its geological
43 significance. *Chinese Science Bulletin* 51, 2500–2506.
44
45 1108
46 1109
47 1110 Liu, Y.C., Li, S.G., Gu, X.F., Xu, S.T., Chen, G.B., 2007a. Ultrahigh-pressure eclogite
48 transformed from mafic granulite in the Dabie orogen, east-central China.
49 *Journal of Metamorphic Geology* 25, 975–989.
50
51 1111
52 1112
53 1113 Liu, Y.C., Li S.G., Xu, S.T., 2007b. Zircon SHRIMP U-Pb dating for gneiss in
54 northern Dabie high T/P metamorphic zone, central China: Implication for
55 decoupling within subducted continental crust. *Lithos* 96, 170–185.
56
57 1114
58 1115
59
60
61
62
63
64
65

- 1 1116 Liu, Y.C., Li, S.G., Xu, S.T., John, B., Zheng, Y.F., Zhang, Z.Q., Jiang, L.L., Chen,
2 G.B., Wu, W.P., 2005. Geochemistry and geochronology of eclogites from the
3 northern Dabie Mountains, central China. *Journal of Asian Earth Science* 25,
4 431–443.
5
6 1119
7
8 1120 Liu, Y.C., Liu, L.X., Gu, X.F., Li, S.G., Liu, J., Song, B., 2010. Occurrence of
9 Neoproterozoic low-grade metagranite in the western Beihuaiyang zone, the
10 Dabie orogen. *Chinese Science Bulletin* 55, 3490–3498.
11
12 1122
13
14 1123 Liu, Y.C., Liu, L.X., Li, Y., Gu, X.F., Song, B., 2017. Zircon U-Pb geochronology and
15 petrogenesis of metabasites from the western Beihuaiyang zone in the Hong’an
16 orogen, central China: Implications for detachment within subducting continental
17 crust at shallow depths. *Journal of Asian Earth Science* 145, 74–90.
18
19 1125
20
21 1126
22
23 1127 Liu, Y.C., Wang, A.D., Rolfo, F., Groppo, C., Gu, X.F., Song, B., 2009.
24 Geochronological and petrological constraints on Palaeoproterozoic granulite
25 facies metamorphism in southeastern margin of the North China Craton. *Journal*
26 *of Metamorphic Geology* 27, 125–138.
27
28 1129
29
30 1130
31
32 1131 Liu, Y.S., Gao, S., Yuan, H.L., Zhou, L., Liu, X.M., Wang, X.C., Hu, Z.C., Wang, L.S.,
33 2004. U–Pb zircon ages and Nd, Sr, and Pb isotopes of lower crustal xenoliths
34 from North China Craton: insights on evolution of lower continental crust.
35 *Chemical Geology* 211, 87–109.
36
37 1134
38
39 1135 Ludwig, K.R., 2001. Users Manual for Isoplot/Ex (rev. 2.49): A Geochronological
40 Toolkit for Microsoft Excel. Berkeley Geochronology Center, Special
41 Publication No. 1a, 55 p.
42
43 1137
44
45 1138 Maruyama, S., Liou, J.G., Terabayashi, M., 1996. Blueschists and eclogites of the
46 world, and their exhumation. *International Geology Review* 38, 485–594.
47
48 1139
49
50 1140 Nasdala, L., Massonne, H.J., 2000. Microdiamonds from the Saxonian Erzgebirge,
51 Germany: in situ micro-Raman characterisation. *European Journal of Mineralogy*
52 12, 495–498.
53
54 1142
55
56 1143 Nowell, G.M., Kempton, P.D., Noble, S.R., Fitton, J.G., Saunders, A.D., Mahoney, J.J.,
57 Taylor, R.N., 1998. High precision Hf isotope measurements of MORB and OIB
58 by thermal ionisation mass spectrometry: insights into the depleted mantle.
59
60 1145
61
62
63
64
65

- 1 1146 Chemical Geology 149, 211–233.
- 2 1147 Okay, A.I., Xu, S.T., Sengör, A.M.C., 1989. Coesite from the Dabie Shan eclogites,
3
4 1148 central China. *European Journal of Mineralogy* 1, 595–598.
- 5
6 1149 Okay, A.I., Sengör, A.M.C., 1992. Evidence for intracontinental thrust-related
7
8 1150 exhumation of the ultra-high-pressure rocks in China. *Geology* 20, 411–414.
- 9
10 1151 Okay, A.I., Sengör, A.M.C., Satir, M., 1993. Tectonics of an ultrahigh-pressure
11
12 1152 metamorphic terrane: the Dabie Shan/Tongbai orogen, China. *Tectonics* 12,
13
14 1153 1320–1334.
- 15
16 1154 Palme, H., O'Neill, H.St.C., 2003. Cosmochemical constraints of mantle composition.
17
18 1155 *Treatise of Geochemistry* 2, 1–38.
- 19
20 1156 Patchett, P.J., White, W.M., Feldmann, H., Kienlinczuk, S., Hofmann, A.W., 1984.
21
22 1157 Hafnium/rare earth element fractionation in the sedimentary system and crustal
23
24 1158 recycling into the Earth's mantle. *Earth and Planetary Science Letters* 1984,
25
26 1159 365–378.
- 27
28 1160 Rolfo, F., Compagnoni, R., Xu, S., Jiang, L., 2000. First report of felsic whiteschist in
29
30 1161 the ultrahigh-pressure metamorphic belt of Dabie Shan, China. *European Journal*
31
32 1162 *of Mineralogy* 12, 883–898.
- 33
34 1163 Rolfo, F., Compagnoni, R., Wu, W.P., Xu, S.T., 2004. A coherent lithostratigraphic
35
36 1164 unit in the coesite–eclogite complex of Dabie Shan, China: geologic and
37
38 1165 petrologic evidence. *Lithos* 73, 71–94.
- 39
40 1166 Roux, V.L., Bodinier, J.L., Alard, O., O'Reilly, S.Y., Griffin, W.L., 2009. Isotopic
41
42 1167 decoupling during porous melt flow: a case-study in the Lherzperidotite. *Earth*
43
44 1168 *and Planetary Science Letters* 279, 76–85.
- 45
46 1169 Rowley, D.B., Xue, F., Tucker, R.D., Peng, Z.X., Baker, J., Davis, A., 1997. Ages of
47
48 1170 ultrahigh pressure metamorphism and protolith orthogneisses from the eastern
49
50 1171 Dabie Shan: U/Pb zircon geochronology. *Earth and Planetary Science Letters*
51
52 1172 151, 191–203.
- 53
54 1173 Rudnick, R.L., Gao, S., 2003. Composition of the continental crust. *Treatise on*
55
56 1174 *Geochemistry* 3, 1–64.
- 57
58 1175 Salters, V.J.M., Stracke, A., 2004. Composition of the depleted mantle. *Geochemistry*
59
60
61
62
63
64
65

1 1176 Geophysics Geosystems 5, Q05004.

2 1177 Scherer, E., Munker, C., Mezger, K., 2001. Calibration of the lutetium–hafnium clock.

3 1178 Science 293, 683–687.

4 1179 Schertl, H.P., Okay, A.I., 1994. A coesite inclusion in dolomite in Dabie Shan, China;

5 1180 petrological and rheological significance. European Journal of Mineralogy 6,

6 1181 995–1000.

7 1182 Schmidt, M.W., 1992. Amphibole composition in tonalite as a function of pressure: an

8 1183 experimental calibration of the Al-in-hornblende barometer. Contributions to

9 1184 Mineralogy and Petrology 110, 304–310.

10 1185 Smith, D.C., 1984. Coesite in clinopyroxene in the Caledonides and its implications

11 1186 for geodynamics. Nature 310, 641–644.

12 1187 Sobolev, N.V., Shatsky, V.S., 1990. Diamond inclusions in garnets from metamorphic

13 1188 rocks: a new environment for diamond formation. Nature 343, 742–746.

14 1189 Su, W., Xu, S., Jiang, L., Liu, Y.C., 1996. Coesite from quartz jadeitite in the Dabie

15 1190 Mountains, Eastern China. Mineralogical Magazine 60, 659–662.

16 1191 Sun, S.S., McDonough, W.F., 1989. Chemical and isotopic systematics of oceanic

17 1192 basalts: implications for mantle composition and processes. In: Saunders, A.D.,

18 1193 Norry, M.J. (Eds.), Magmatism in the ocean basins. Geological Society, London,

19 1194 Special Publications 42, pp. 313–345.

20 1195 Tabata, H., Yamauchi, K., Maruyama, S., Liou, J.G., 1998. Tracing the Extent of a

21 1196 UHP Metamorphic Terrane: Mineral-Inclusion Study of Zircons in Gneisses from

22 1197 the Dabie Shan. In: Hacker, B.R., Liou, J.G. (Eds), When Continents Collide:

23 1198 Geodynamics and Geochemistry of Ultrahigh-Pressure Rocks. Springer

24 1199 Netherlands 10, pp. 261–273.

25 1200 Tang, H.F., Liu, C.Q., Nakai, S., Orihashi, Y., 2007. Geochemistry of eclogites from

26 1201 the Dabie–Sulu terrane, eastern china: new insights into protoliths and trace

27 1202 element behaviour during UHP metamorphism. Lithos 95, 441–457.

28 1203 Tang, J., Zheng, Y.F., Wu, Y. B., Gong, B., 2006. Zircon SHRIMP U–Pb dating, C and

29 1204 O isotopes for impure marbles from the Jiaobei terrane in the Sulu orogen:

30 1205 Implication for tectonic affinity. Precambrian Research 144, 1–18.

- 1 1206 Tappe, S., Pearson, D.G., Nowell, G., Nielsen, T., Milstead, P., Muehlenbachs, K.,
2 1207 2011. A fresh isotopic look at Greenland kimberlites: cratonic mantle lithosphere
3
4 1208 imprint on deep source signal. *Earth and Planetary Science Letters* 305, 235–248.
5
6 1209 Taylor, S.R., McLennan, S.M., 1985. *The Continental Crust: Its Composition and*
7
8 1210 *Evolution*. Blackwell Scientific Publications, Oxford.
9
10 1211 Tomkins, H.S., Powell, R., Ellis, D.J., 2007. The pressure dependence of the
11
12 1212 zirconium-in-rutile thermometer. *Journal of Metamorphic Geology* 25, 703–713.
13
14 1213 Tsai, C.H., Liou, J.G., 2000. Eclogite-facies relics and inferred ultrahigh-pressure
15
16 1214 metamorphism in the North Dabie Complex, central-eastern China. *American*
17
18 1215 *Mineralogist* 85, 1–8.
19
20 1216 Velikoslavinsky, S.D., Krylov, D.P. 2014. Geochemical discrimination of basalts
21
22 1217 formed in major geodynamic settings. *Geotectonics* 48(6), 427–439.
23
24 1218 Wang, L.J., Griffin, W.L., Yu, J.H., O'Reilly, S.Y., 2010. Precambrian crustal
25
26 1219 evolution of the Yangtze Block tracked by detrital zircons from Neoproterozoic
27
28 1220 sedimentary rocks. *Precambrian Research* 177(1), 131–144.
29
30 1221 Wang, M.X., Wang, C.Y., Zhao, J.H., 2013. Zircon U/Pb dating and Hf-O isotopes of
31
32 1222 the Zhouan ultramafic intrusion in the northern margin of the Yangtze Block, SW
33
34 1223 China: Constraints on the nature of mantle source and timing of the
35
36 1224 supercontinent Rodinia breakup. *Chinese Science Bulletin* 58(7), 777–787.
37
38 1225 Wang, X., Liou, J.G., Mao, H.K., 1989. Coesite-bearing eclogites from the Dabie
39
40 1226 Mountains in central China. *Geology* 17, 1085–1088.
41
42 1227 Whalen, J.B., Currie, K.L., Chappell, B.W., 1987. A-type granites: geochemical
43
44 1228 characteristics, discrimination and petrogenesis. *Contributions to Mineralogy and*
45
46 1229 *Petrology* 95, 407–419.
47
48 1230 Whitney, J.A., Stormer, J.C., 1977. Two-feldspar geothermometry, geobarometry in
49
50 1231 mesozonal granitic intrusions: three examples from the Piedmont of Georgia.
51
52 1232 *Contributions to Mineralogy and Petrology* 63(1), 51–64.
53
54 1233 Williams, I.S., 1998. U–Th–Pb geochronology by ion microprobe. Applications of
55
56 1234 Microanalytical Techniques to Understanding Mineralizing Processes. In:
57
58 1235 McKibben, M.A., Shanks III, W.C., Ridley, W.I. (Eds.), *Reviews in Economic*
59
60
61
62
63
64
65

- 1 1236 Geology 7, pp. 1–35.
- 2 1237 Winchester, J.A., Floyd, P.A., 1977. Geochemical discrimination of different magma
3 series and their differentiation products using immobile elements. Chemical
4 1238 Geology 20, 325–343.
- 5
6 1239
7
8 1240 Workman, R.K., Hart, S.R., 2005. Major and trace element composition of the
9 depleted MORB mantle (DMM). Earth and Planetary Science Letters 231,
10 1241 53–72.
- 11
12 1242
13
14 1243 Wu, F.Y., Sun, D.Y., Li, H., Jahn, B.M., Wilde, S., 2002. A-type granites in
15 northeastern china: age and geochemical constraints on their petrogenesis.
16 1244 Chemical Geology 187, 143–173.
- 17
18 1245
19
20 1246 Wu, Y.B., Zheng, Y.F., Zhao, Z.F., Gong, B., Liu, X.M., Wu, F.Y., 2006a. U–Pb, Hf
21 and O isotope evidence for two episodes of fluid-assisted zircon growth in
22 marble-hosted eclogites from the Dabie orogen. Geochimica et Cosmochimica
23 1247 Acta 70, 3743–3761.
- 24
25 1248
26
27 1249
28
29 1250 Wu, R.X., Zheng, Y.F., Wu, Y.B., Zhao, Z.F., Zhang, S.B., Liu, X.M., Wu, F.Y., 2006b.
30 Reworking of juvenile crust: element and isotope evidence from Neoproterozoic
31 granodiorite in South China. Precambrian Research 146, 179–212.
- 32
33 1252
34
35 1253 Wu, Y.B., Zheng, Y.F., Tang, J., Gong, B., Zhao, Z.F., Liu, X., 2007. Zircon U–Pb
36 dating of water–rock interaction during Neoproterozoic rift magmatism in South
37 1254 China. Chemical Geology 246, 65–86.
- 38
39 1255
40
41 1256 Xiao, Y., Hoefs, J., van den Kerkhof, A.M., Li, S.G., 2001. Geochemical constraints of
42 the eclogite and granulite facies metamorphism as recognized in the Raobazhai
43 1257 complex from North DabieShan, China. Journal of Metamorphic Geology 19,
44 1258 3–19.
- 45
46 1259
47
48 1260 Xu, S.T., Jiang, L.L., Liu, Y.C., Zhang, Y., 1992a. Tectonic Framework and Evolution
49 of the Dabie Mountains in Anhui, Eastern China. Acta Geologica Sinica 5,
50 1261 221–238.
- 51
52 1262
53
54 1263 Xu, S.T., Okay, A.I., Ji, S.Y., Sengör, A.M.C., Su, W., Liu, Y.C., Jiang, L.L., 1992b.
55 Diamond from the Dabie Shan metamorphic rocks and its implication for
56 1264 tectonic setting. Science 256, 80–82.
- 57
58 1265
59
60
61
62
63
64
65

- 1 1266 Xu, S.T., Liu, Y.C., Su, W., Wang, R.C., Jiang, L.L., Wu, W.P., 2000. Discovery of the
2 eclogite and its petrography in the Northern Dabie Mountains. Chinese Science
3 Bulletin 45, 273–278.
4
5 1268
6 1269 Xu, S.T., Liu, Y.C., Chen, G.B., Compagnoni, R., Rolfo, F., He, M.C., Liu, H.F., 2003.
7
8 1270 New finding of micro-diamonds in eclogites from Dabie-Sulu region in
9
10 1271 central-eastern China. Chinese Science Bulletin 48, 988–994.
11
12 1272 Xu, S.T., Liu, Y.C., Chen, G.B., Ji, S.Y., Ni, P., Xiao, W.S., 2005. Microdiamonds,
13
14 1273 their classification and tectonic implications for the host eclogites from the Dabie
15
16 1274 and Su-Lu regions in central eastern China. Mineralogical Magazine 69,
17
18 1275 509–520.
19
20 1276 Xue, H.M., Ma, F., Song, Y.Q., 2011. Geochemistry and SHRIMP zircon U-Pb data of
21
22 1277 Neoproterozoic meta-magmatic rocks in the Suizhou-Zaoyang area, northern
23
24 1278 margin of the Yangtze Craton, Central China. Acta Petrologica Sinica 27,
25
26 1279 1116–1130.
27
28 1280 Yu, S.Y., Xu, Y.G., Huang, X.L., Ma, J.L., Ge, W.C., Zhang, H.H., Qin, X.F., 2009.
29
30 1281 Hf–Nd isotopic decoupling in continental mantle lithosphere beneath Northeast
31
32 1282 China: effects of pervasive mantle metasomatism. Journal of Asian Earth Science
33
34 1283 35, 554–570.
35
36 1284 Yuan, H.L., Gao, S., Liu, X.M., Gunther, D., Wu, F.Y., 2004. Accurate U–Pb age and
37
38 1285 trace element determinations of zircon by laser ablation-inductively coupled
39
40 1286 plasma mass spectrometry. Geostandards and Geoanalytical Research 28,
41
42 1287 353–370.
43
44 1288 Zack, T., Moraes, R., Kronz, A., 2004. Temperature dependence of Zr in rutile:
45
46 1289 empirical calibration of a rutile thermometer. Contributions to Mineralogy and
47
48 1290 Petrology, 148, 471–488.
49
50 1291 Zartman, R.E., 1981. Plumbotectonics—the model. Tectonophysics 75, 135–162.
51
52 1292 Zhang, H.F., Gao, S., Zhang, Z.Q., Zhang, B.R., Zhang, L., Hu, S.H., 2002.
53
54 1293 Geochemical and Sr-Nd-Pb isotopic compositions of Cretaceous granitoids:
55
56 1294 constraints on tectonic framework and crustal structure of the Dabieshan
57
58 1295 ultrahigh-pressure metamorphic belt, China. Chemical Geology 186, 281–299.
59
60
61
62
63
64
65

- 1 1296 Zhang, R.Y., Liou, J.G., Zheng, Y.F., Fu, B., 2003. Transition of UHP eclogites to
2 1297 gneissic rocks of low-amphibolite facies during exhumation: evidence from the
3 1298 Dabie terrane, central China. *Lithos*, 70, 269–291.
- 4 1299 Zhang, S.B., Zheng, Y.F., Wu, Y.B., Zhao, Z.F., Gao, S., Wu, F.Y., 2006a. Zircon
5 1300 isotope evidence for ≥ 3.5 Ga continental crust in the Yangtze craton of China.
6 1301 *Precambrian Research* 146, 16–34.
- 7 1302 Zhang, S.B., Zheng, Y.F., Wu, Y.B., Zhao, Z.F., Gao, S., Wu, F.Y., 2006b. Zircon
8 1303 U–Pb age and Hf–O isotope evidence for Paleoproterozoic metamorphic event in
9 1304 South China. *Precambrian Research* 151, 265–288.
- 10 1305 Zhang, S.B., Zheng, Y.F., Wu, Y.B., Zhao, Z.F., Gao, S., Wu, F.Y., 2006c. Zircon
11 1306 U–Pb age and Hf isotope evidence for 3.8 Ga crustal remnant and episodic
12 1307 reworking of Archean crust in South China. *Earth and Planetary Science Letters*
13 1308 252, 56–71.
- 14 1309 Zhao, G.C., Cawood, P.A., 2012. Precambrian geology of China. *Precambrian*
15 1310 *Research* 222–223, 13–54.
- 16 1311 Zhao, J.H., Zhou, M.F., 2009. Secular evolution of the Neoproterozoic lithospheric
17 1312 mantle underneath the northern margin of the Yangtze Block, South China.
18 1313 *Lithos* 107, 152–168.
- 19 1314 Zhao, J.H., Li, Q.W., Liu, H., Wang, W., 2018. Neoproterozoic magmatism in the
20 1315 western and northern margins of the Yangtze Block (South China) controlled by
21 1316 slab subduction and subduction-transform-edge-propagator. *Earth-Science*
22 1317 *Reviews* 187, 1–18.
- 23 1318 Zheng, Y.F., Zhou, J.B., Wu, Y.B., Xie, Z., 2005. Low-grade metamorphic rocks in the
24 1319 Dabie-Sulu orogenic belt: a passive-margin accretionary wedge deformed during
25 1320 continent subduction. *International Geology Review* 47, 851–871.
- 26 1321 Zheng, Y.F., Zhao, Z.F., Wu, Y.B., Zhang, S.B., Liu, X.M., Wu, F.Y., 2006. Zircon
27 1322 U–Pb age, Hf and O isotope constraints on protolith origin of ultrahigh-pressure
28 1323 eclogite and gneiss in the Dabie orogen. *Chemical Geology* 231, 135–158.
- 29 1324 Zheng, Y.F., Zhang, S.B., Zhao, Z.F., Wu, Y.B., Li, X.H., Li, Z.X., Wu, F.Y., 2007.
30 1325 Contrasting zircon Hf and O isotopes in the two episodes of Neoproterozoic

1 1326 granitoids in South China: implications for growth and reworking of continental
2 1327 crust. *Lithos* 96, 127–150.

3
4 1328 Zheng, Y.F., Wu, R.X., Wu, Y.B., Zhang, S.B., Yuan, H.L., Wu, F.Y., 2008. Rift
5
6 1329 melting of juvenile arc-derived crust: geochemical evidence from
7
8 1330 Neoproterozoic volcanic and granitic rocks in the Jiangnan Orogen, South China.
9
10 1331 *Precambrian Research* 163, 351–383.

11
12 1332 Zheng, Y.F., Xia, Q.X., Chen, R.X., Gao, X.Y., 2011. Partial melting, fluid
13
14 1333 supercriticality and element mobility in ultrahigh-pressure metamorphic rocks
15
16 1334 during continental collision. *Earth Science Reviews* 107, 342–374.

17
18 1335 Zhou, M.F., Kennedy, A.K., Sun, M., Malpas, J., Leshner, C.M., 2002a. Neoproterozoic
19
20 1336 arc-related mafic intrusions in the northern margin of South China: implications
21
22 1337 for accretion of Rodinia. *The Journal of Geology* 110, 611–618.

23
24 1338 Zhou, M.F., Yan, D.P., Kennedy, A.K., Li, Y.Q., Ding, J., 2002b. SHRIMP zircon
25
26 1339 geochronological and geochemical evidence for Neo-proterozoic arc-related
27
28 1340 magmatism along the western margin of the Yangtze Block, South China. *Earth
29
30 1341 and Planetary Science Letters* 196, 51–67.

31
32 1342 Zhou, M.F., Ma, Y.X., Yan, D.P., Xia, X.P., Zhao, J.H., Sun, M., 2006a. The Yanbian
33
34 1343 Terrane (Southern Sichuan Province, SW China): a Neoproterozoic arc
35
36 1344 assemblage in the western margin of the Yangtze Block. *Precambrian Research*
37
38 1345 144, 19–38.

39
40 1346 Zhou, M.F., Yan, D.P., Wang, C.L., Qi, L., Kennedy, A., 2006b. Subduction related
41
42 1347 origin of the 750 Ma Xuelongbao adakitic complex (Sichuan Province, China):
43
44 1348 implications for the tectonic setting of the giant Neoproterozoic magmatic event
45
46 1349 in South China. *Earth and Planetary Science Letters* 248, 286–300.

47
48 1350 Zindler, A., Hart, S., 1986. Chemical geodynamics. *Annual Review of Earth and
49
50 1351 Planetary Science* 14, 493–571.

51
52 1352

53
54
55
56
57
58
59
60
61
62
63
64
65

Figure captions

1 1353

2
3 1354 **Figure 1** Schematic geological map of the Dabie orogen. The inset shows its location
4
5 1355 within the Triassic Qinling–Dabie–Sulu collision orogen in central China (modified
6
7 1356 from Liu et al., 2007a). Sample locality is marked by a red star. BZ = Beihuaiyang
8
9 1357 zone, NDZ = North Dabie high-T/UHP complex zone, CDZ = Central Dabie
10
11 1358 mid-T/UHP metamorphic zone, SDZ = South Dabie low-T eclogite zone, SZ =
12
13 1359 Susong complex zone, HMZ = Huwan mélangé zone, HZ = Hong'an low-T eclogite
14
15 1360 zone, DC = amphibolite-facies Dabie complex, XMF = Xiaotian-Mozitan fault, WSF
16
17 1361 = Wuhe-Shuihou fault, HMF = Hualiangting-Mituo fault, TSF = Taihu-Shanlong fault,
18
19 1362 TLF = Tan-Lu fault.

21 1363

22
23 1364 **Figure 2** Field photograph showing meta-basite lens tectonically enclosed within
24
25 1365 meta-granitoid.

26 1366

27
28
29 1367 **Figure 3** Photomicrographs of plane- and corresponding cross-polarized images for
30
31 1368 the meta-basite sample 11LJG7 (a & b), low-Si meta-granitoid sample 1209LJG5 (c
32
33 1369 & d), high-Si meta-granitoid sample 1209LJG1 (e & f). Pl: plagioclase; Rt: rutile;
34
35 1370 Amp: amphibole; Bt: biotite; Qz: quartz; Ap: apatite; Kfs: K-feldspar; Aln: allanite.

36 1371

37
38
39 1372 **Figure 4** TAS (total alkalis versus silica) diagram (Le Bas et al., 1986) (a) and
40
41 1373 Zr/TiO₂ vs Nb/Y (Winchester and Floyd, 1977) (b) plots for the studied rocks in
42
43 1374 Longjingguan. Green circles: meta-basites; red circles: low-Si granitoids; blue circles:
44
45 1375 high-Si granitoids; Pc: microbasalt; B: basalt; O1: basaltic andesite; O2: andesite; O3:
46
47 1376 dacite; R: rhyolite; S1: trachybasalt; S2: basaltic trachyandesite; S3: trachyandesite; T:
48
49 1377 trachyte; U1: basanite; U2: phonotephrite; U3: tephriphonolite; Ph: phonolite; F:
50
51 1378 foidite. Symbols used for different types of samples are the same as in the following
52
53 1379 figures.

54 1380

55
56
57 1381 **Figure 5** Chondrite-normalized REE patterns (a) and primitive mantle-normalized

1 1382 trace element patterns (b) for the studied rocks in Longjingguan and for the UHP
2 1383 eclogites (c & d) in the CDZ. Normalized values and the data of the N-MORB and
3
4 1384 E-MORB are from Sun and McDonough (1989), the elemental data of the UHP
5
6 1385 eclogites are from Tang et al. (2007).
7

8 1386
9
10 1387 **Figure 6** Representative CL images of zircons from the meta-basites (samples
11
12 1388 11LJG3 and 11LJG7), low-Si meta-granitoids (samples 11LJG2, 1209LJG5 and
13
14 1389 1202LJG3) and high-Si meta-granitoid (sample 1303LJG2) in Longjingguan. The red
15
16 1390 circles locate the SHRIMP analysis spots, and the red numbers are the corresponding
17
18 1391 $^{206}\text{Pb}/^{238}\text{U}$ ages.
19

20 1392
21
22 1393 **Figure 7** Mineral inclusions within metamorphic zircon domains from samples
23
24 1394 11LJG3 (a-i) and 11LJG2 (j-l). Hbl, hornblende; Rt, rutile; Qz, quartz; Ap, apatite;
25
26 1395 Kfs, K-feldspar; Mus, muscovite; Ep, epidote; Ttn, titanite; Ilm, ilmenite.
27

28 1396
29
30 1397 **Figure 8** Zircon rare earth element (REE) patterns for the meta-basites (samples
31
32 1398 11LJG3 and 11LJG7) and meta-granitoids (samples 1209LJG5, 11LJG2, 1303LJG2
33
34 1399 and 1202LJG3) in Longjingguan. Normalized values are from Sun and McDonough
35
36 1400 (1989).
37

38 1401
39
40 1402 **Figure 9** SHRIMP zircon U-Pb ages for the meta-basites (a & b), low-Si
41
42 1403 meta-granitoids (c, d, e, g & h) and high-Si meta-granitoid (f) in Longjingguan. (e)
43
44 1404 and (h) correspond to the dashed squares in (d) and (g), respectively.
45

46 1405
47
48 1406 **Figure 10** Zircon $\varepsilon_{\text{Hf}}(t)$ vs U-Pb age of the studied meta-basites and meta-granitoids,
49
50 1407 as well as the UHP eclogites and gneisses (data from Zheng et al., 2006) from the
51
52 1408 CDZ. The evolution trendlines of the depleted mantle (DMM) and chondrite are from
53
54 1409 Griffin et al. (2000).
55

56 1410
57
58 1411
59
60

1 1412 **Figure 11** Plot of Nd vs Sr isotopes for the meta-basites (samples 11LJG3 to 11LJG8)
2 1413 from Longjingguan. MORB: mid-ocean ridge basalt; UCC: upper continental crust;
3
4 1414 LCC: lower continental crust.
5

6 1415
7
8 1416 **Figure 12** ($^{207}\text{Pb}/^{204}\text{Pb}$)_i vs ($^{206}\text{Pb}/^{204}\text{Pb}$)_i and ($^{208}\text{Pb}/^{204}\text{Pb}$)_i vs ($^{206}\text{Pb}/^{204}\text{Pb}$)_i plots for
9 1417 the meta-basites (samples 11LJG3 to 11LJG8) from Longjingguan. The initial Pb
10 1418 isotopes data of the meta-basites are calibrated with $t=230$ Ma, the blue-green and
11 1419 grey areas in the diagrams represent the UHP orthogneiss and eclogites in the North
12 1420 Dabie (NDZ) and Central Dabie (CDZ) terranes, respectively (data from Zhang et al.,
13 1421 2002; Li et al., 2003d). The initial Pb isotope data of MORB, EMI and EMII are from
14 1422 Zindler and Hart. (1986), and that of lower crust (LC) is from Liu et al. (2004).
15 1423 ($^{207}\text{Pb}/^{204}\text{Pb}$)_{NHRL} = $0.1084 \times (^{206}\text{Pb}/^{204}\text{Pb})_i + 13.401$; ($^{208}\text{Pb}/^{204}\text{Pb}$)_{NHRL} = $1.209 \times (^{206}\text{Pb}/$
16 1424 $^{204}\text{Pb})_i + 15.627$.
17
18
19
20
21
22
23
24
25
26

27 1425
28
29 1426 **Figure 13** Tectonic discrimination diagrams (Velikoslavinsky and Krylov, 2014) for
30 1427 the meta-basites in Longjingguan. Values of the discriminant functions $DF_1(x)$, $DF_2(x)$,
31 1428 $DF_3(x)$ and $DF_5(x)$ have been calculated from formula: $D(x) = \sum a_i \cdot x_i + \text{constant}$,
32 1429 where a_i is coefficient at corresponding variable; x_i is value of variable (oxide content,
33 1430 wt %; trace element content, ppm). In the $DF_1(x) - DF_2(x)$ diagram (a), the
34 1431 meta-basites (green circles) plot in the field of WPB. In the $DF_3(x) - \text{frequency} (\%)$ (b)
35 1432 and $DF_5(x) - \text{frequency} (\%)$ (c) diagrams, the rocks (the red rectangles with dashed
36 1433 oblique lines) have function values coincident with the majority population of WPB.
37
38
39
40
41
42
43
44
45

46 1434
47
48 1435 **Figure 14** Plots employing Ga/Al (Whalen et al., 1987) for the meta-granitoids in
49 1436 Longjingguan. I & S: I-type and S-type granite; A: A-type granite.
50
51

52 1437
53
54 1438 **Figure 15** (Sr/Y) vs. Y diagram discriminating adakite and TTG from typical arc
55 1439 calc-alkaline rocks (Drummond and Defant, 1990).
56
57

58 1440
59
60
61
62
63
64
65

Figure 1
[Click here to download high resolution image](#)

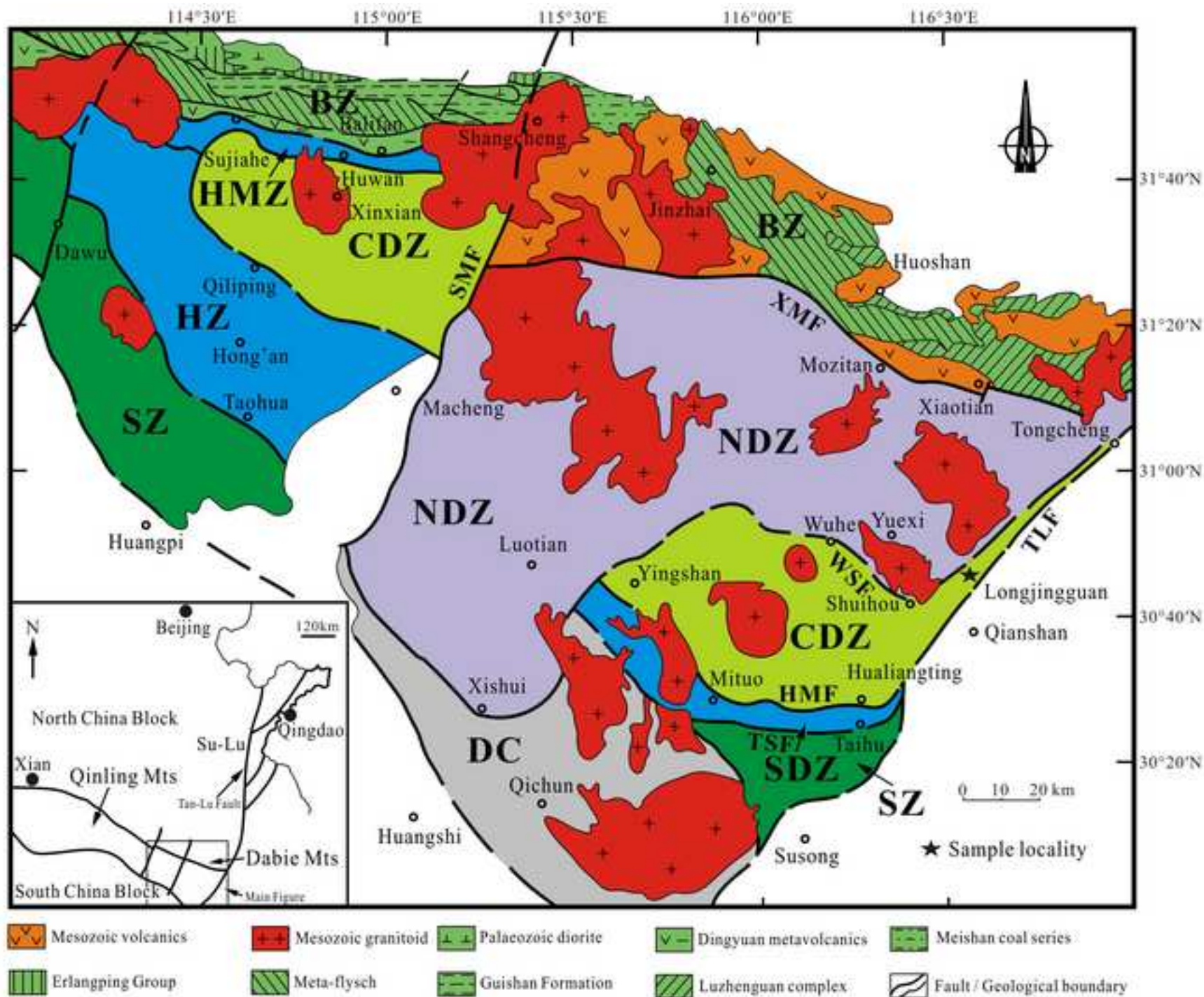


Figure 2

[Click here to download high resolution image](#)

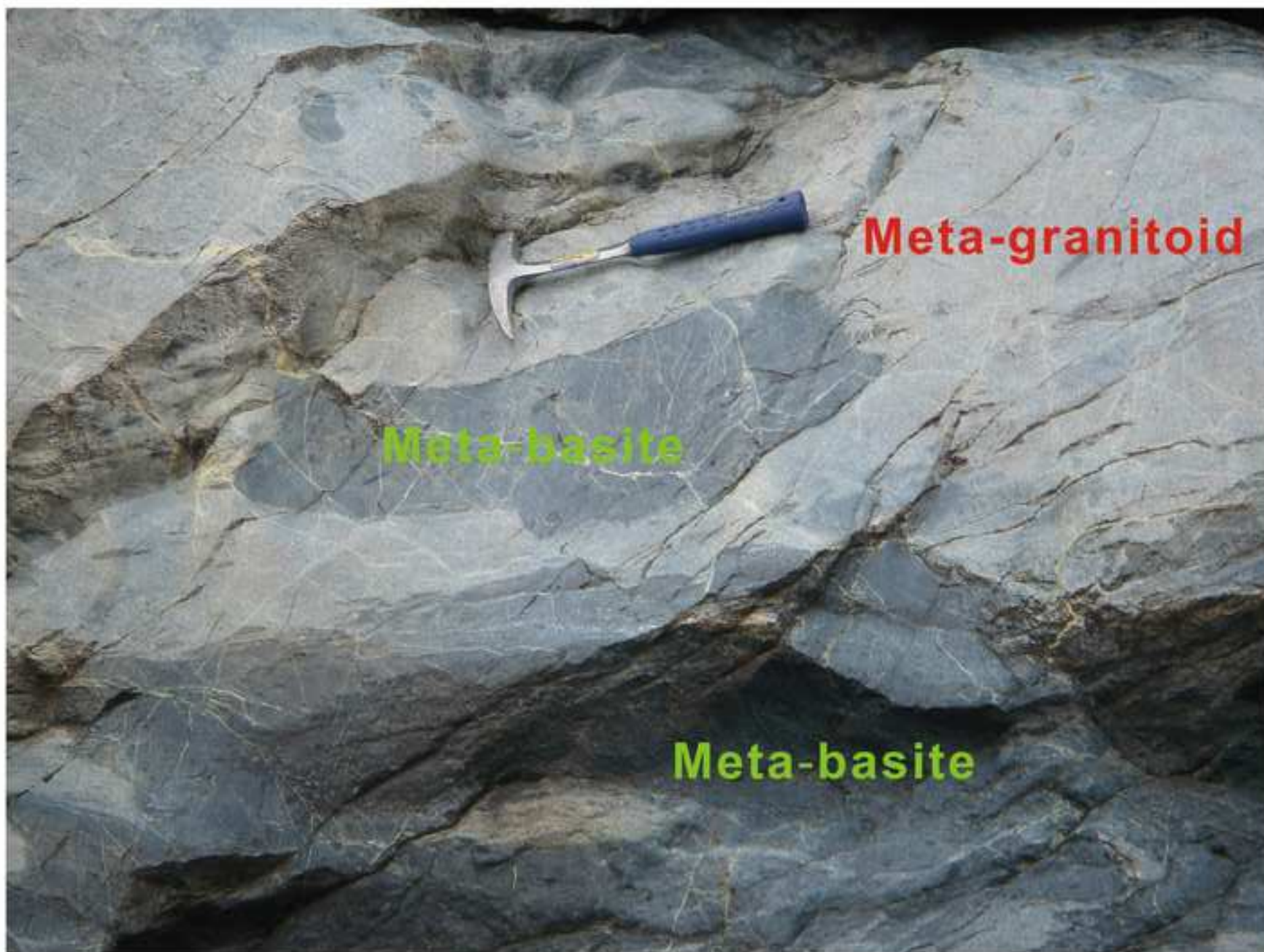


Figure 3
[Click here to download high resolution image](#)

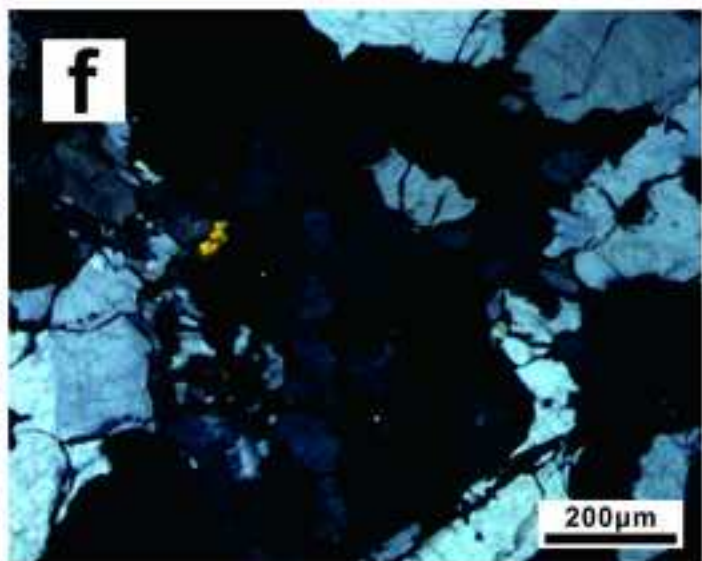
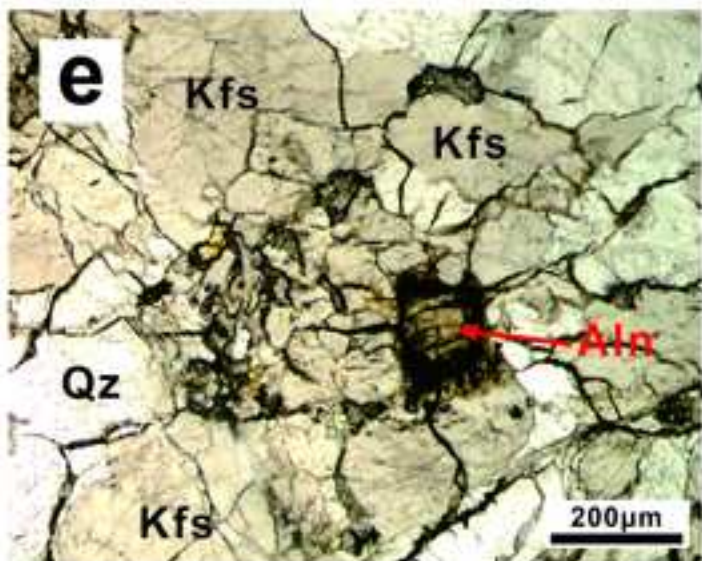
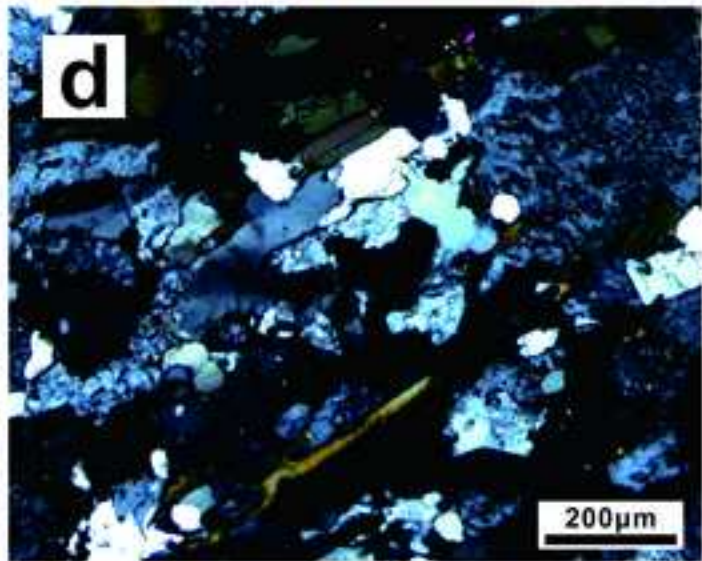
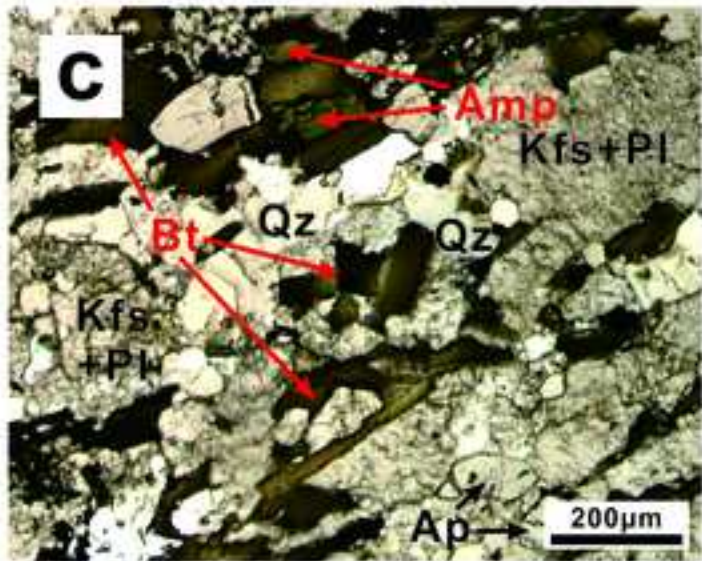
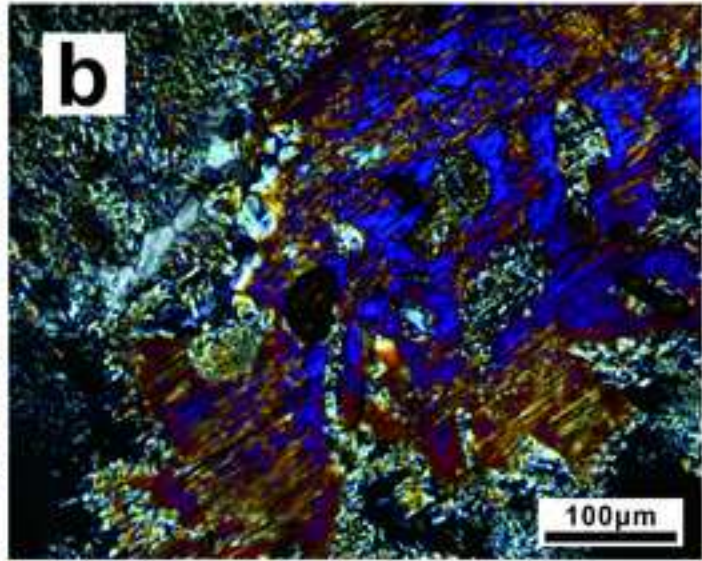
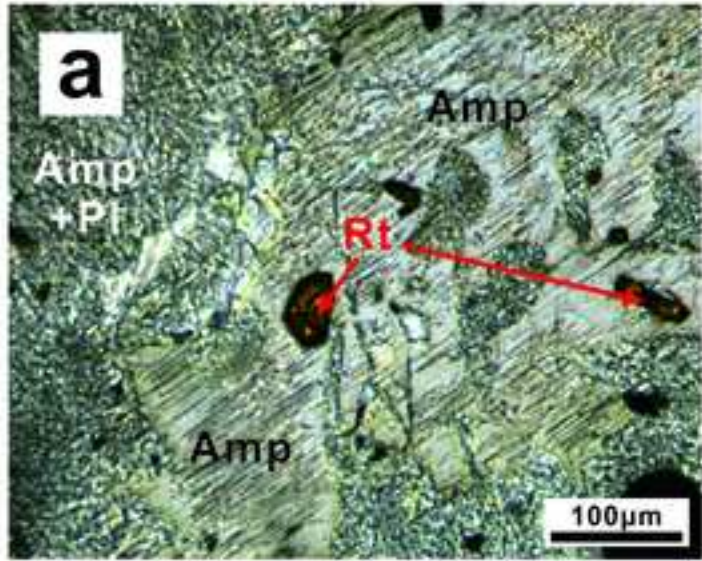


Figure 4
[Click here to download high resolution image](#)

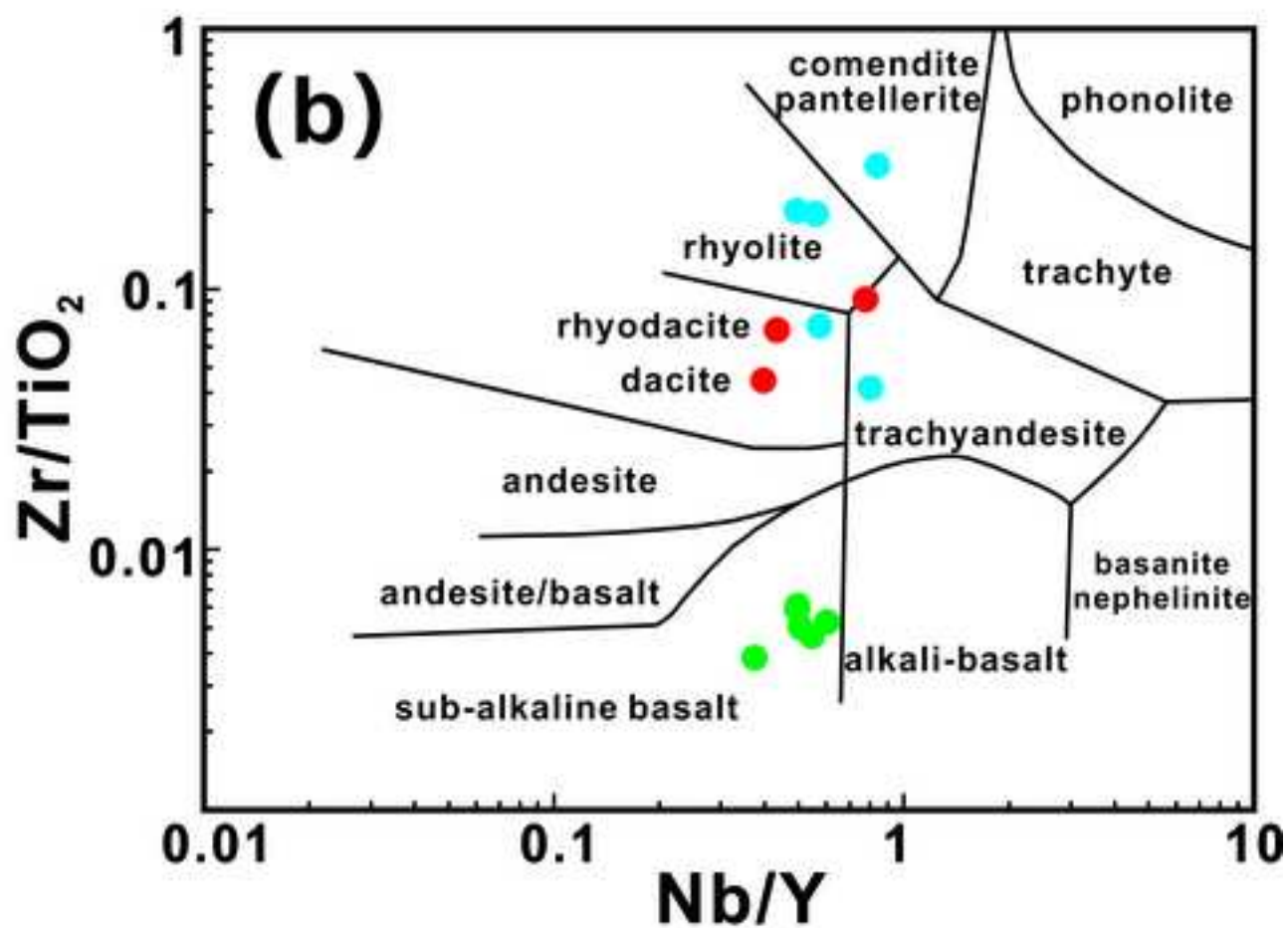
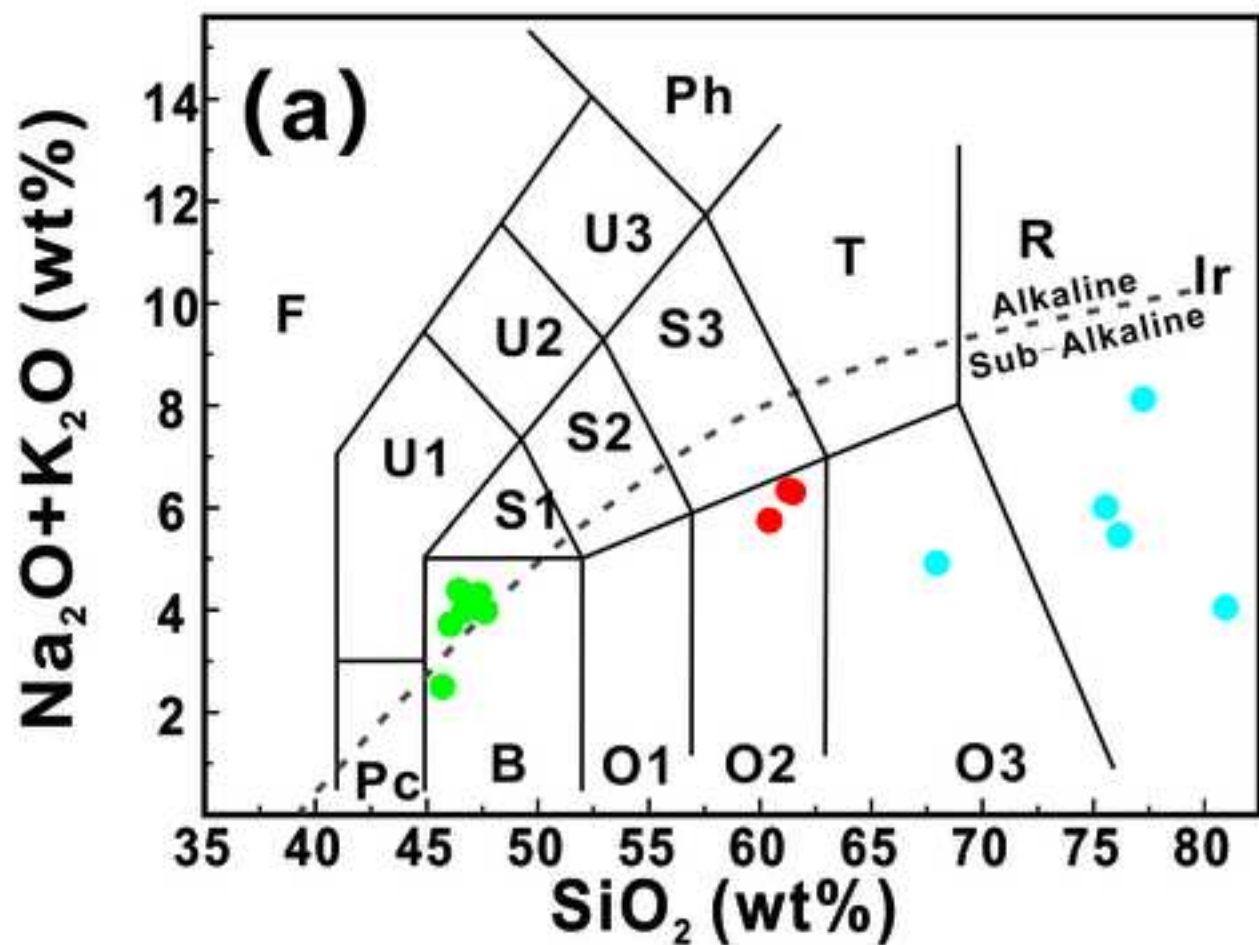


Figure 5
[Click here to download high resolution image](#)

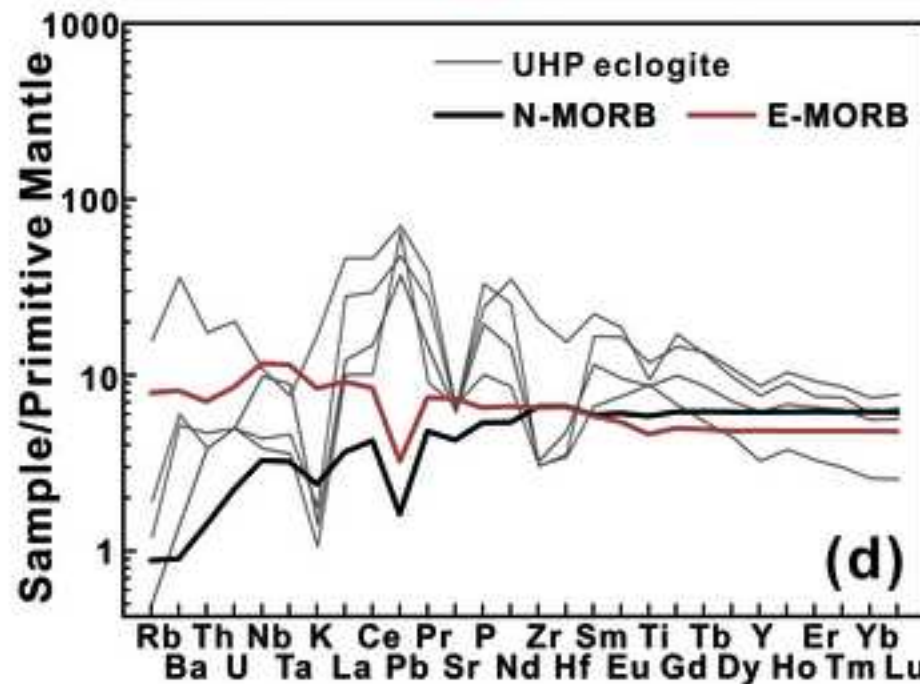
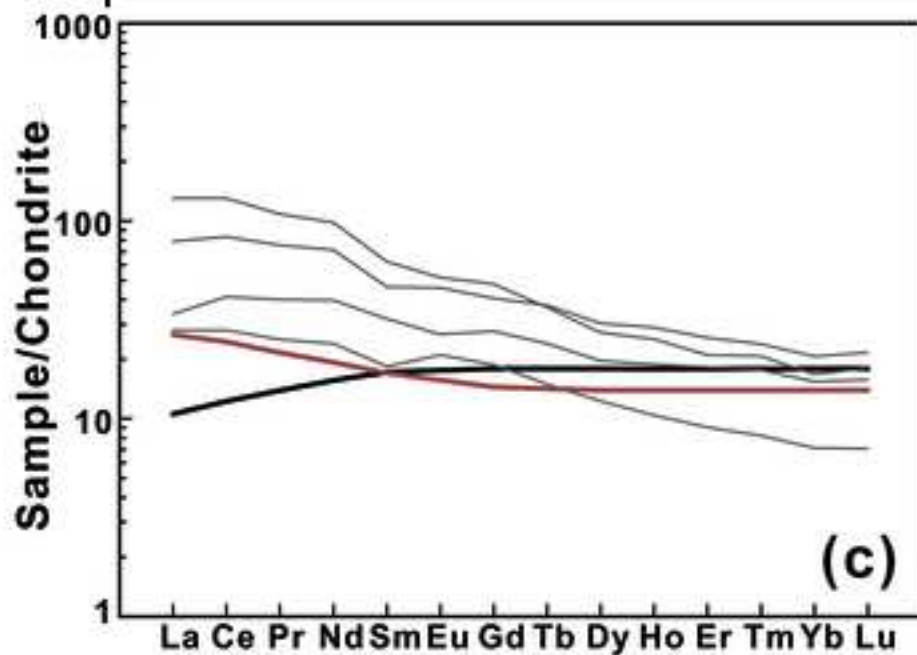
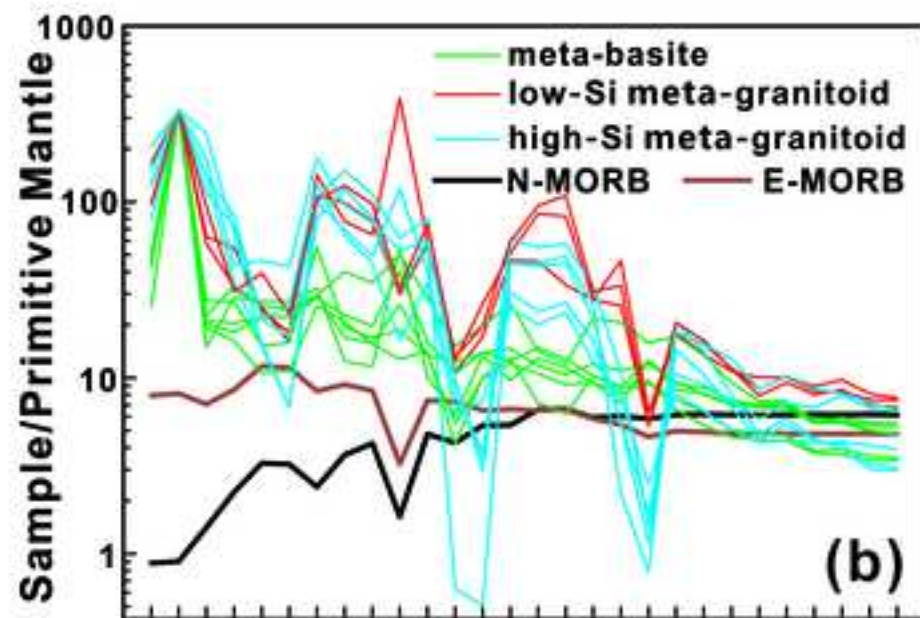
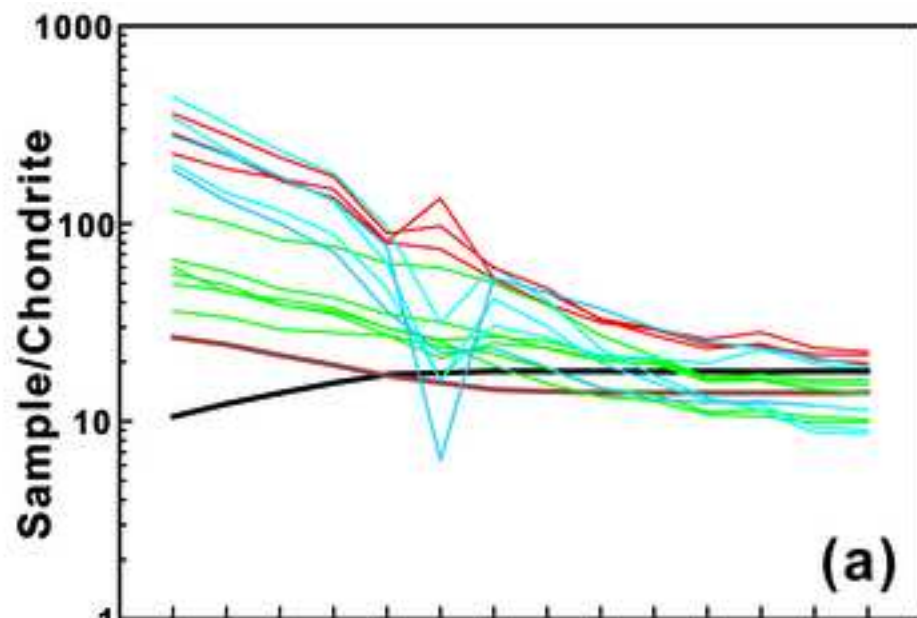


Figure 6
[Click here to download high resolution image](#)

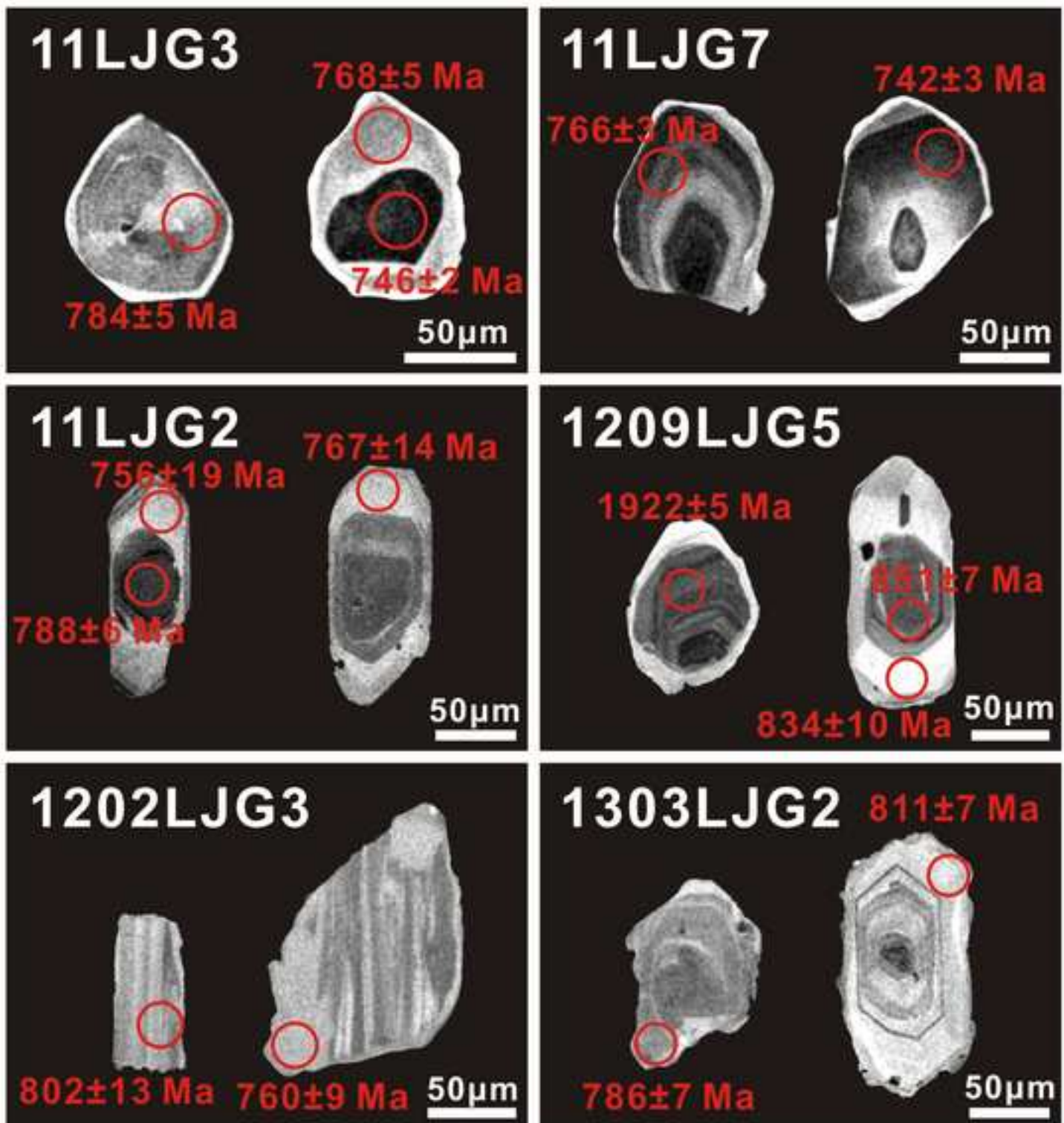


Figure 7
[Click here to download high resolution image](#)

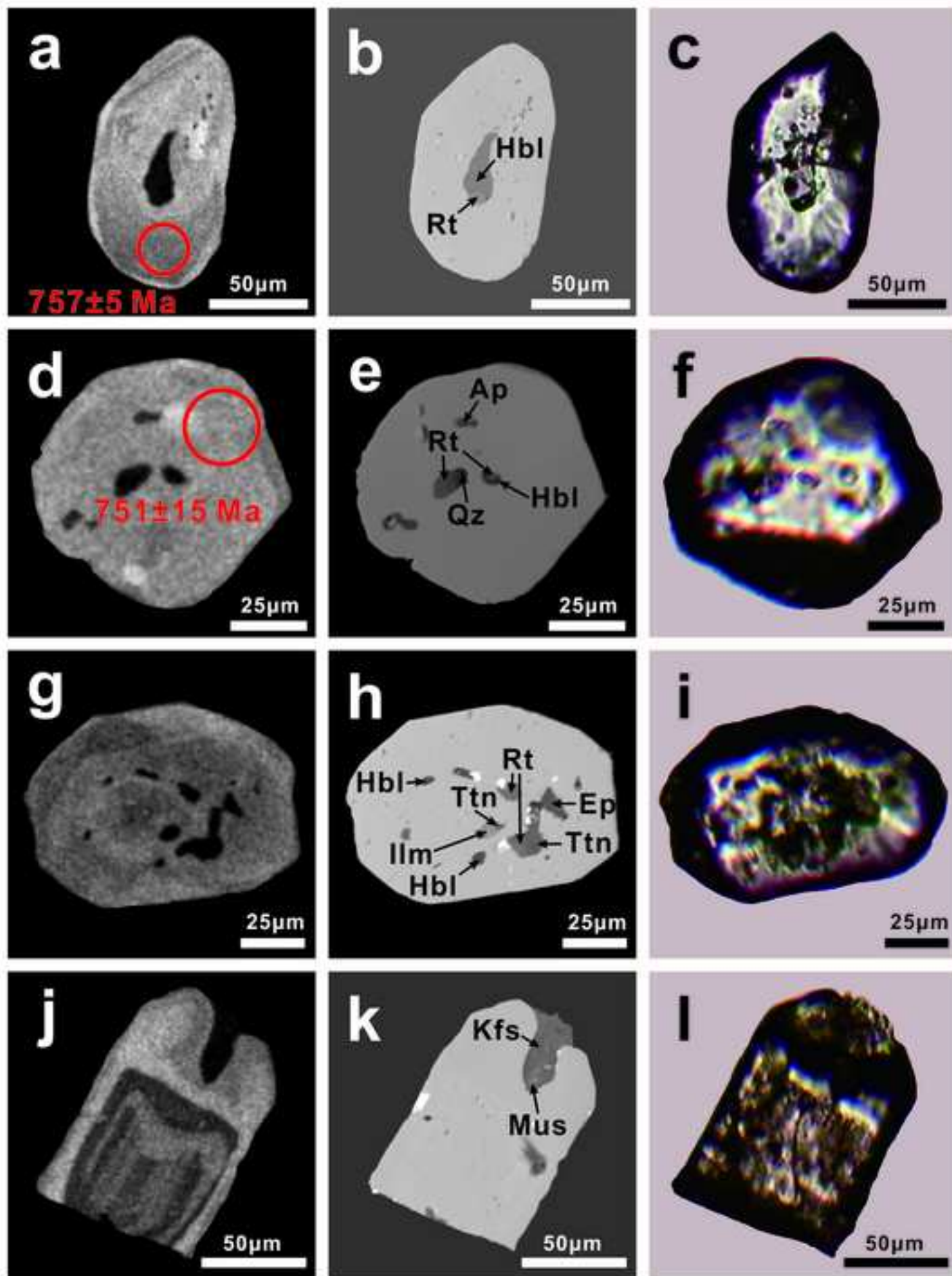


Figure 8
[Click here to download high resolution image](#)

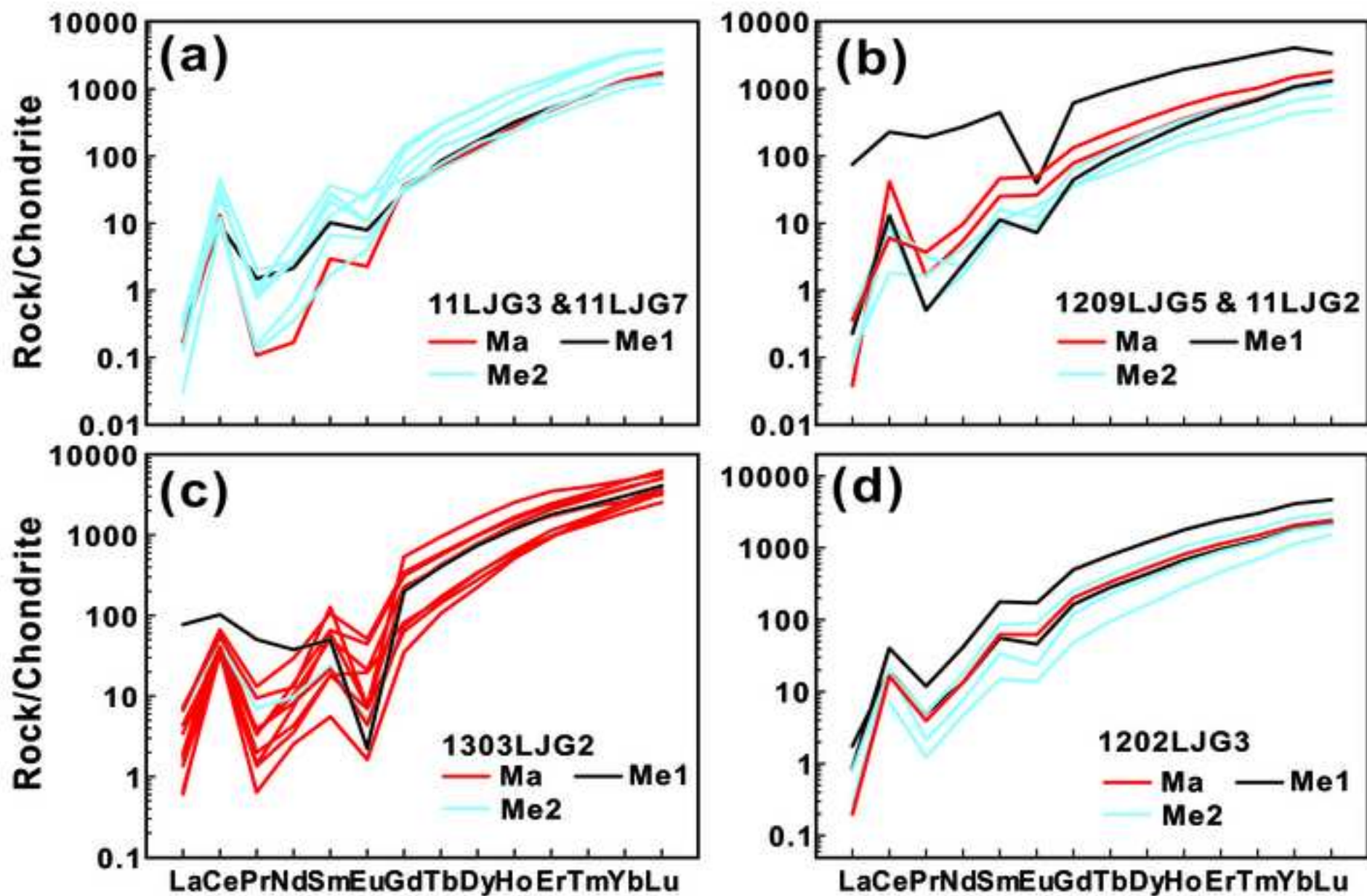


Figure 9
[Click here to download high resolution image](#)

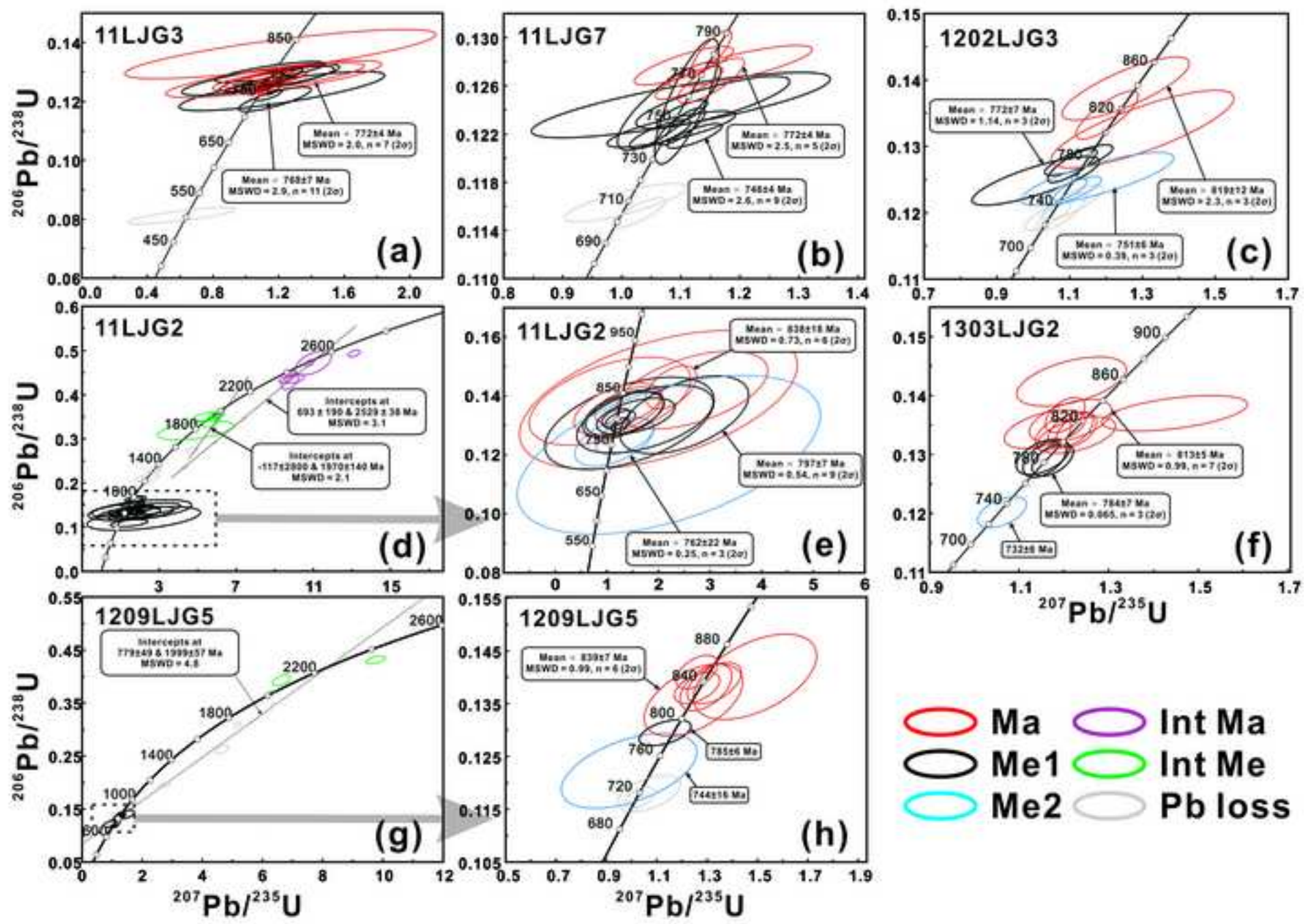


Figure 10
[Click here to download high resolution image](#)

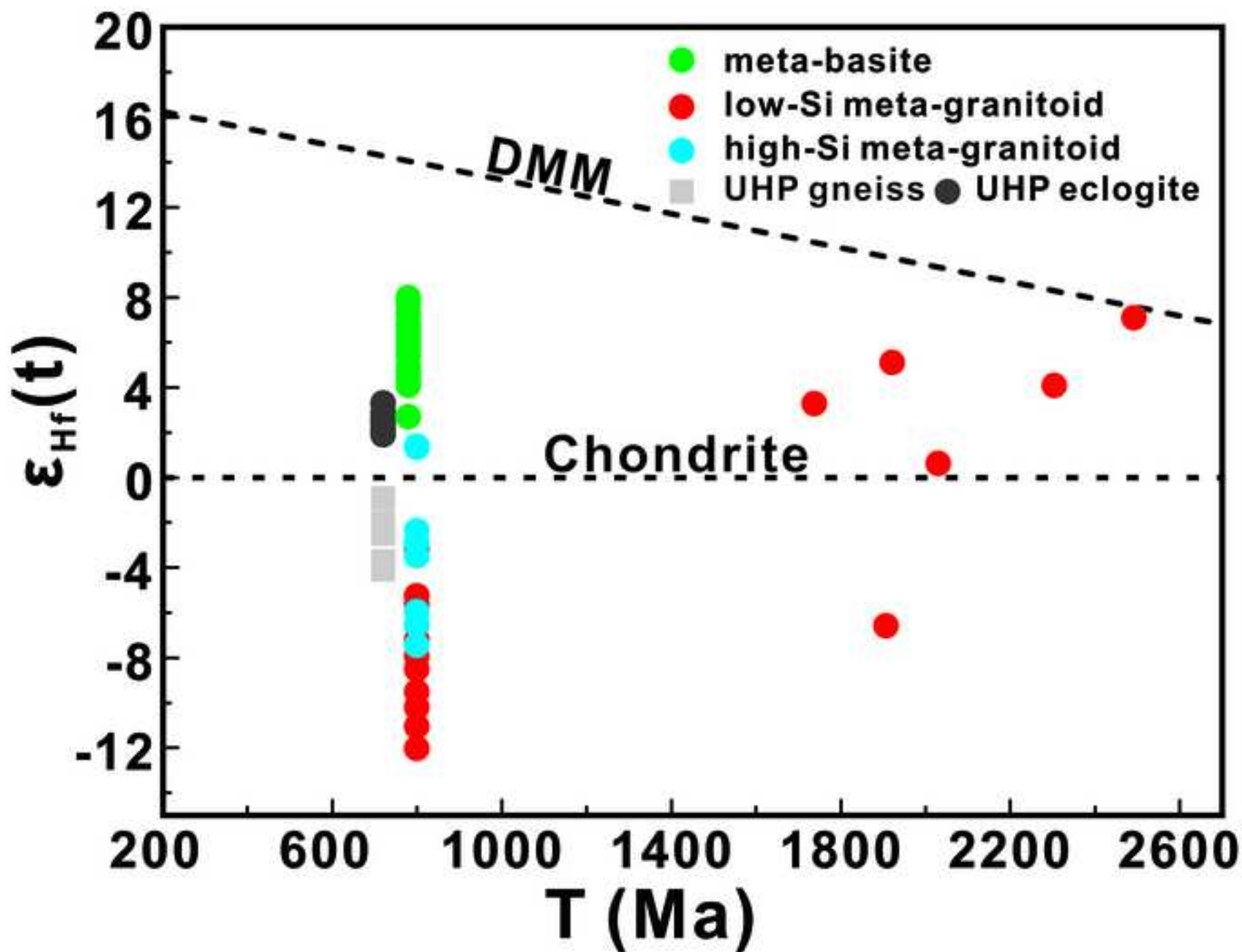


Figure 11
[Click here to download high resolution image](#)

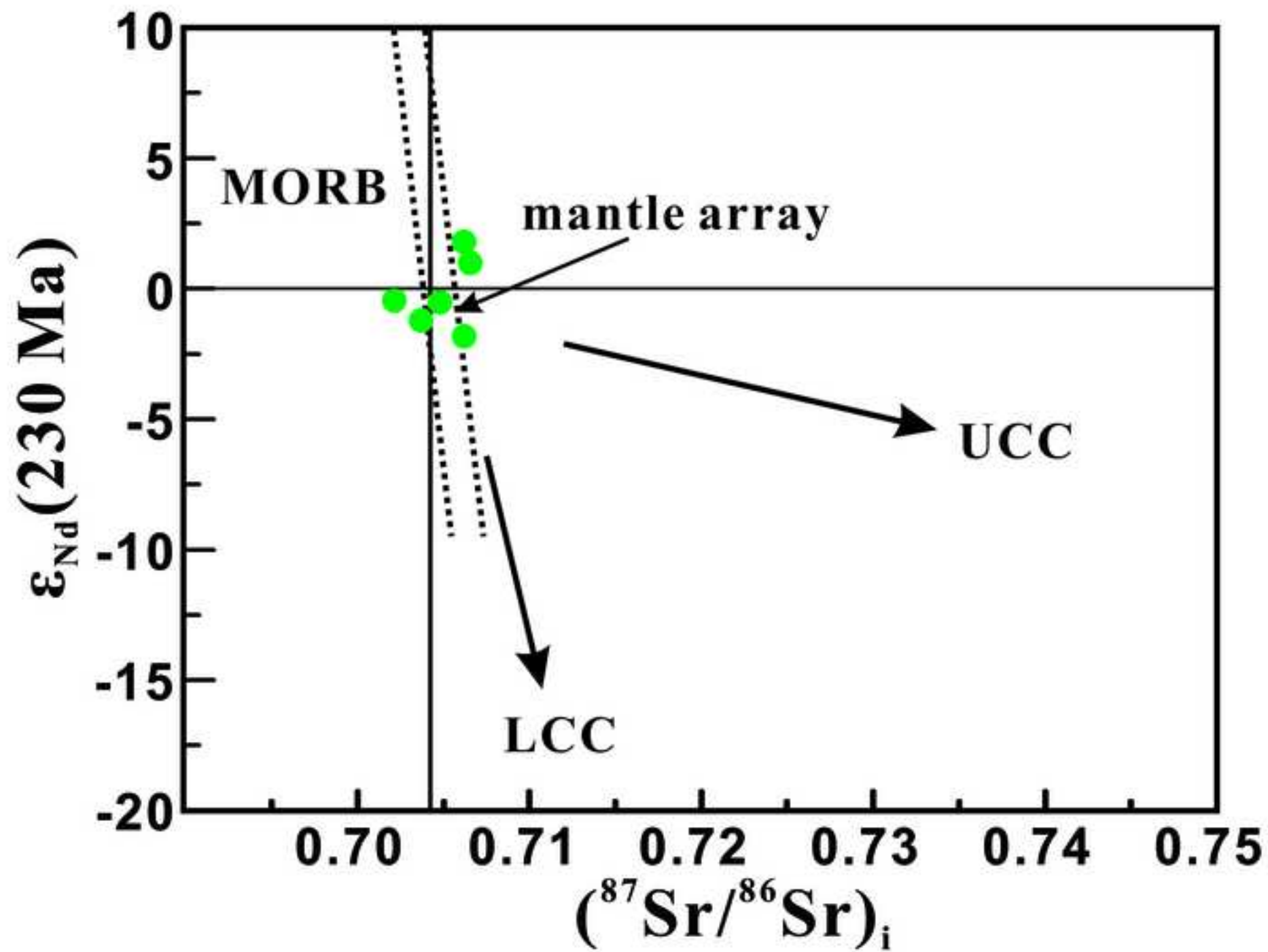


Figure 12
[Click here to download high resolution image](#)

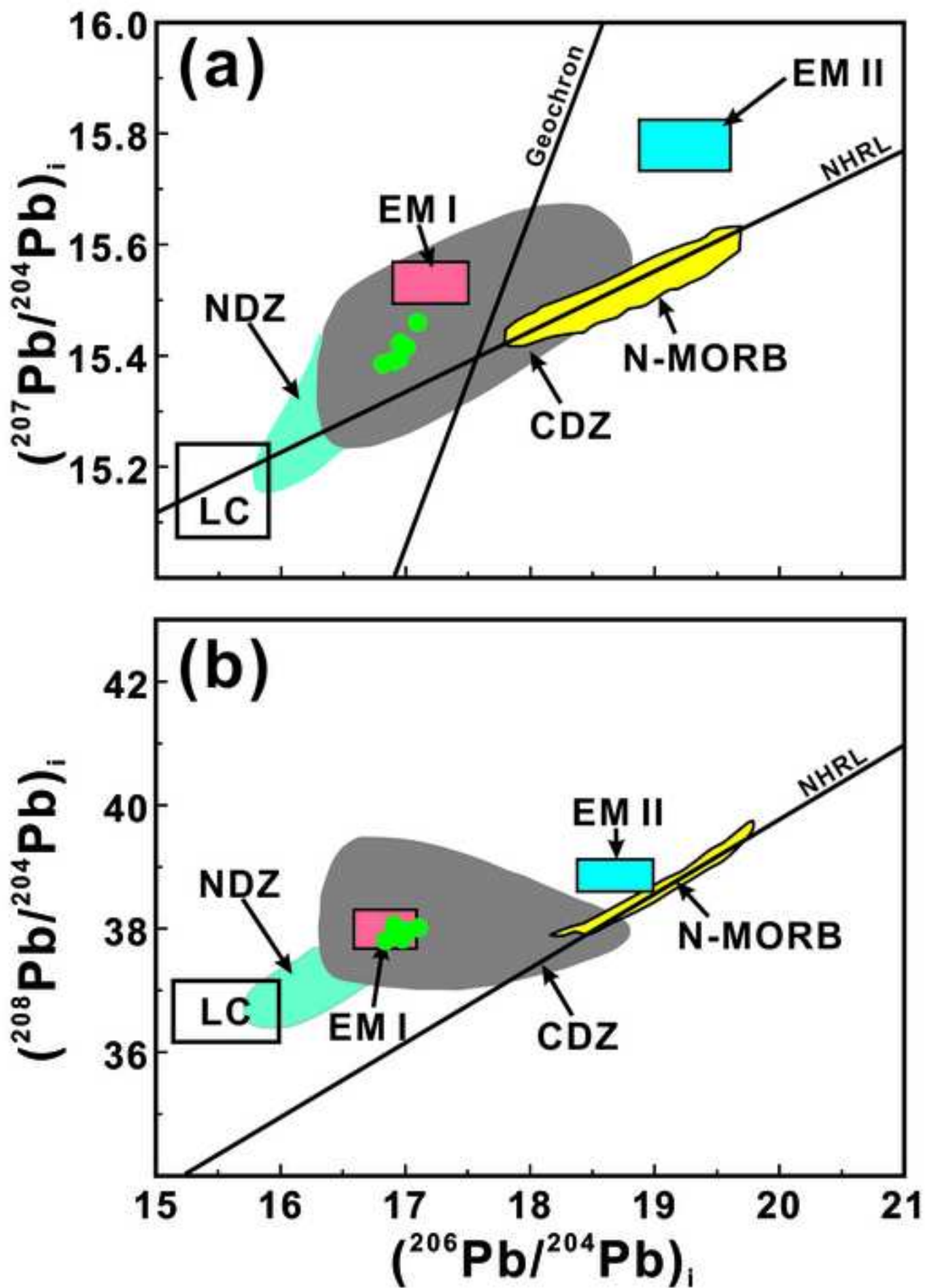


Figure 13
[Click here to download high resolution image](#)

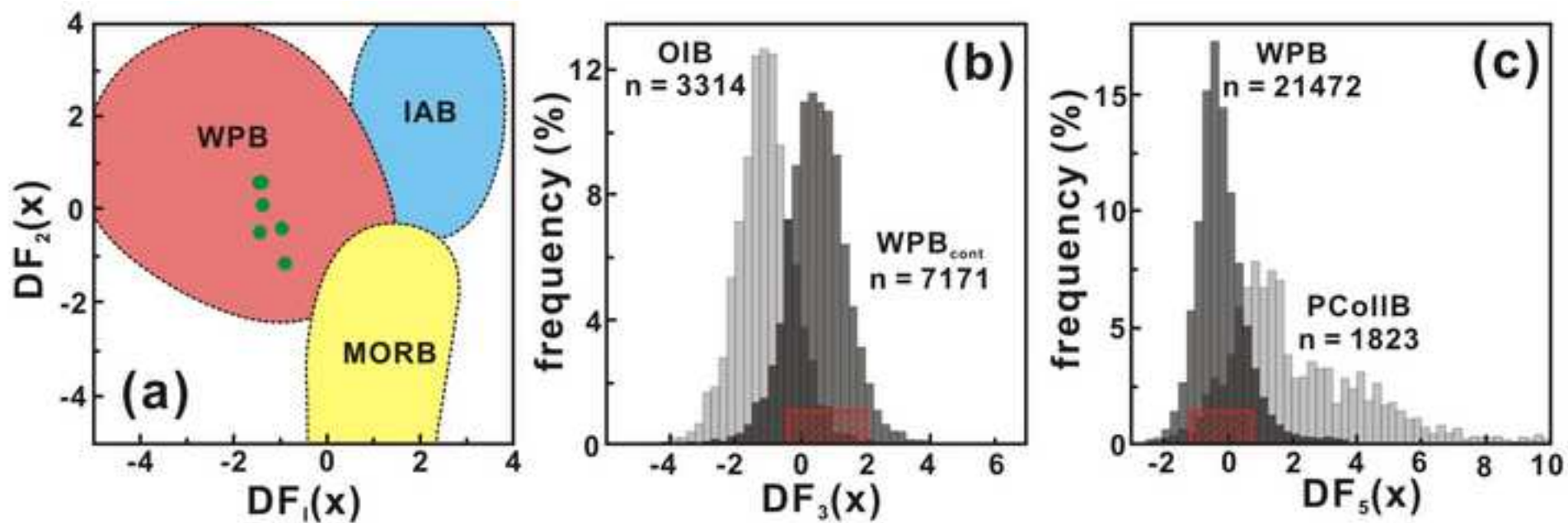


Figure 14

[Click here to download high resolution image](#)

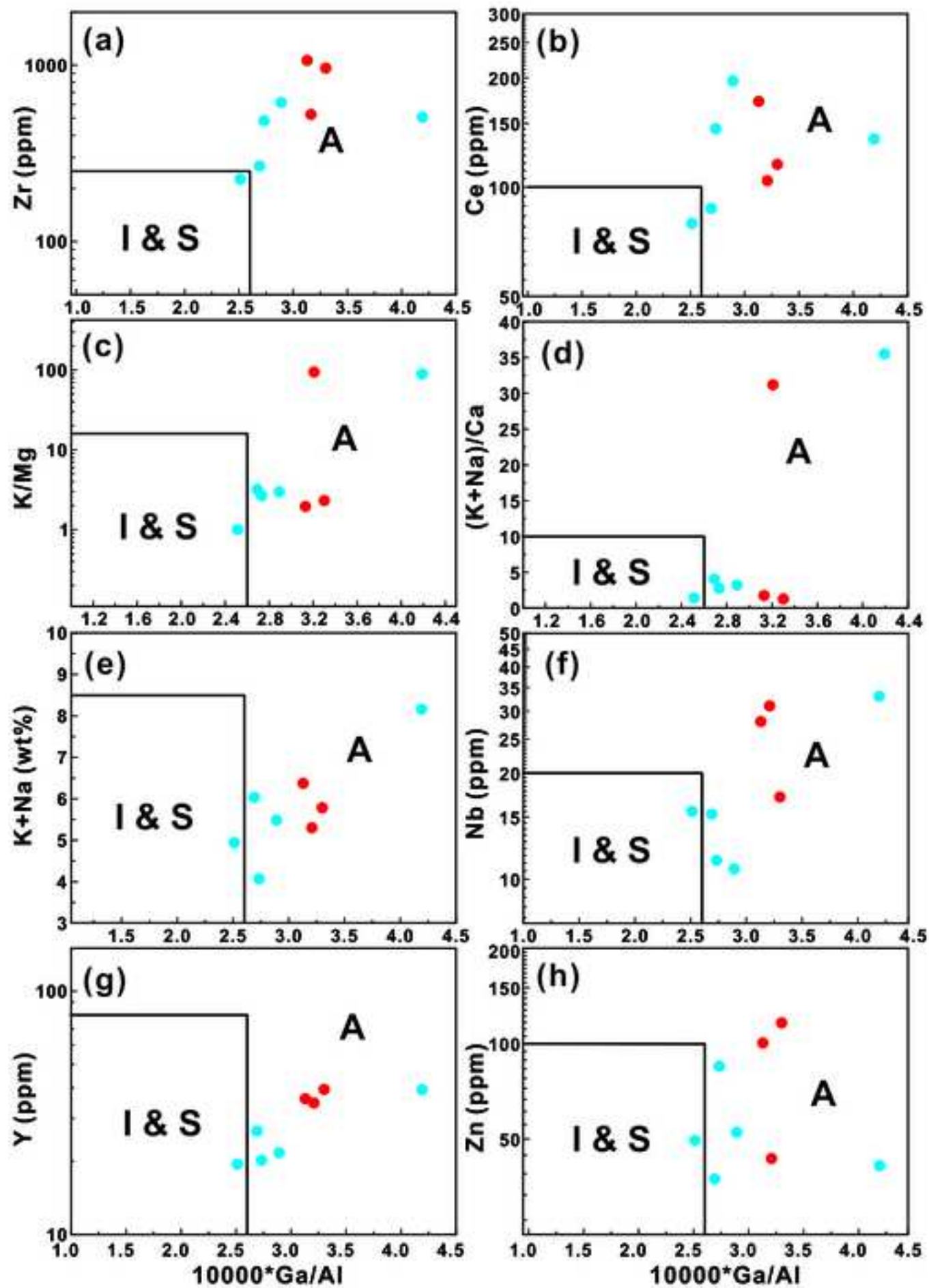
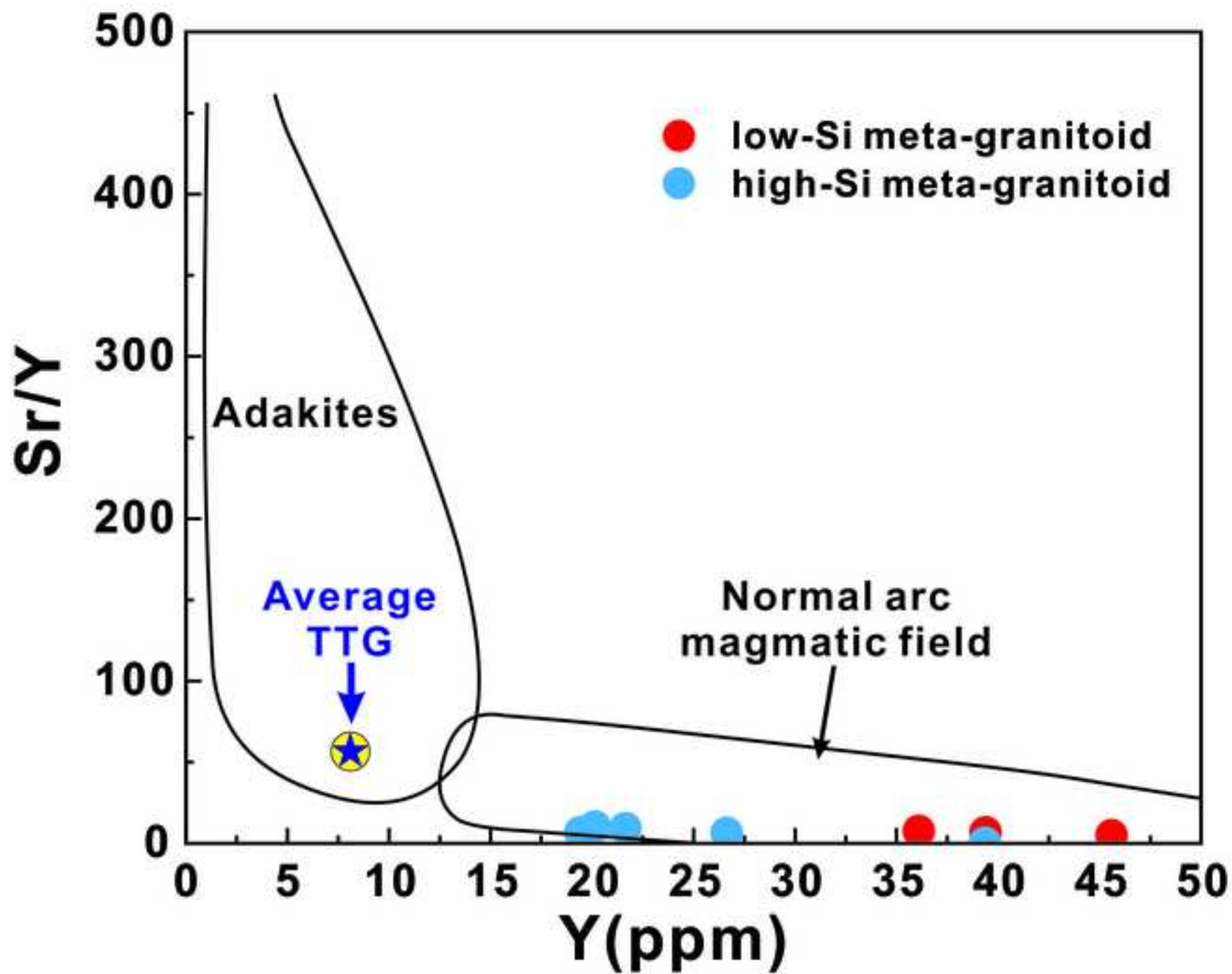


Figure 15
[Click here to download high resolution image](#)



Supplementary Table 1. Electron microprobe analyses of representative minerals from the **meta-basites and meta-granitoids** in Longjingguan (wt%).

Sample	11LJG7						1209LJG1		1209LJG5			
Mineral	Pl(int)	Pl(ic)	Amp(int)	Amp(porp)	Ru	Ru	Kfs	Aln	Kfs	Pl	Amp	Bt
SiO ₂	64.66	66.87	51.87	49.27	0.08	0.04	65.52	34.10	65.90	61.52	40.97	34.86
Al ₂ O ₃	21.11	19.91	5.93	7.94	0.03	0.04	17.63	20.62	17.74	23.59	9.93	14.38
FeO	0.59	0.12	7.63	10.67	0.54	0.39	--	8.64	0.10	0.07	22.65	23.76
MgO	0.33	--	17.94	15.30	0.00	0.04	--	0.32	--	--	6.56	7.41
MnO	0.03	--	0.11	0.27	0.13	0.20	0.03	0.05	--	--	2.99	1.93
CaO	2.94	1.92	11.96	11.82	0.09	0.16	--	14.39	0.02	6.14	11.30	0.03
Na ₂ O	9.66	10.52	0.76	0.96	0.05	--	0.65	0.19	0.86	7.89	1.03	0.06
K ₂ O	0.05	0.10	0.21	0.23	--	--	15.75	0.06	15.15	0.14	1.28	9.64
TiO ₂	0.02	--	0.13	0.35	97.93	98.10	--	--	0.03	--	0.89	4.12
Cr ₂ O ₃	0.05	0.01	0.09	0.11	0.30	0.21	0.06	--	0.02	0.00	0.08	0.01
NiO	0.02	--	--	--	0.03	0.04	--	0.01	--	0.03	--	--
Cl	--	--	0.02	0.02	--	--	--	--	--	--	0.22	0.22
ZrO ₂	--	--	--	--	0.04	0.10	--	--	--	--	--	--
Ce ₂ O ₃	--	--	--	--	--	--	--	4.57	--	--	--	--
Total	99.47	99.44	96.64	96.94	99.31	99.21	99.63	82.94	99.81	99.37	97.84	96.36

int: intergrowth; ic: inclusion; porp: porphyroblast; --: not detected.

Supplementary Table 2

Supplementary Table 2. Major and trace elements compositions of the **meta-basites and meta-granitoids** from Longjingguan.

Lithology	Meta-basite						Low-Si meta-granitoid			High-Si meta-granitoid				
Sample	11LJG3	11LJG4	11LJG5	11LJG6	11LJG7	11LJG8	11LJG2	1209LJG5	1202LJG3	1209LJG1	1303LJG4	1209LJG3	1303LJG2	1209LJG4
Major elements (wt%)														
SiO ₂	46.72	47.64	47.38	46.08	45.72	46.48	61.50	61.30	60.45	75.57	67.98	76.20	77.26	80.98
Al ₂ O ₃	13.32	13.55	14.30	12.83	12.46	13.72	14.76	14.96	14.18	11.24	11.78	10.48	10.90	8.96
TiO ₂	3.42	2.74	2.73	2.01	2.10	2.61	1.16	1.17	1.38	0.37	0.54	0.31	0.17	0.25
Fe ₂ O ₃	4.86	3.87	5.94	3.91	3.47	7.56	3.06	3.60	1.60	1.15	0.84	1.32	1.83	0.46
FeO	8.24	8.50	7.07	8.12	8.86	8.19	5.03	4.78	6.85	1.56	3.54	1.84	1.08	1.68
CaO	10.85	9.14	9.35	8.14	8.34	10.50	3.52	3.63	4.53	1.49	3.50	1.71	0.23	1.47
MgO	6.43	7.73	5.92	11.41	13.29	4.37	1.93	1.60	1.86	0.95	3.82	1.08	0.06	0.92
K ₂ O	0.89	0.97	0.89	1.66	0.77	0.86	3.28	3.11	4.28	3.05	3.82	3.20	5.35	2.44
Na ₂ O	3.12	3.02	3.44	2.08	1.74	3.55	3.05	3.26	1.50	2.99	1.12	2.29	2.81	1.63
MnO	0.18	0.18	0.17	0.19	0.19	0.19	0.15	0.21	0.45	0.06	0.06	0.03	0.05	0.02
P ₂ O ₅	0.43	0.29	0.30	0.22	0.22	0.30	0.37	0.43	0.57	0.08	0.16	0.08	0.01	0.06
H ₂ O	1.13	1.75	1.83	2.66	2.39	1.12	1.17	1.24	1.56	0.92	1.99	1.18	0.06	0.97
LOI	1.63	2.31	2.14	3.25	3.22	1.53	1.48	1.51	1.79	1.22	2.85	1.29	0.17	1.04
Total	100.08	99.95	99.62	99.89	100.38	99.86	99.30	99.56	99.45	99.72	100.01	99.81	99.92	99.89
Trace elements (ppm)														
Li	6.61	15.00	13.00	45.20	38.80	17.30	27.80	26.88	39.41	18.62	47.53	14.95	1.39	12.93
Be	1.39	1.48	1.00	1.97	0.52	2.21	1.63	1.62	1.67	2.01	1.88	0.75	2.37	0.95
Sc	30.40	37.00	28.30	26.20	23.10	27.90	18.80	28.04	40.21	6.14	9.75	4.51	1.20	3.63
V	326.00	352.00	289.00	213.00	155.00	279.00	86.80	61.20	65.20	52.80	68.10	43.60	9.30	24.20
Cr	172.00	142.00	126.00	292.00	282.00	113.00	31.30	20.00	13.90	29.20	42.70	19.10	2.10	20.90
Co	41.90	54.70	46.30	58.70	44.60	54.60	13.10	16.40	12.40	6.00	13.30	11.10	0.20	5.20
Ni	113.00	95.60	104.00	317.00	228.00	115.00	49.40	12.20	7.70	15.00	35.30	18.80	0.60	7.10
Cu	15.00	60.90	289.00	28.10	8.40	12.40	24.00	80.60	30.10	12.00	26.90	5.00	3.50	3.20
Zn	143.00	146.00	145.00	164.00	113.00	120.00	108.00	100.40	116.20	37.40	49.50	52.50	41.20	84.80
Ga	24.30	19.00	22.70	17.70	14.10	20.40	24.90	24.79	24.78	16.01	15.67	16.04	24.19	12.96
Rb	16.00	29.60	27.00	62.90	32.90	27.70	63.00	61.50	105.40	78.60	131.40	80.90	96.20	50.40
Sr	320.00	129.00	261.00	116.00	87.30	225.00	227.00	275.50	266.70	169.80	134.00	201.00	13.40	209.30
Y	33.50	32.20	31.80	21.80	20.20	30.80	45.60	36.10	39.39	26.64	19.43	21.65	39.36	20.15
Zr	159.00	144.00	166.00	118.00	80.50	131.00	518.00	1064.00	960.40	267.40	225.50	614.00	506.60	483.90
Nb	18.30	19.40	15.80	10.80	7.57	15.60	18.10	28.02	17.11	15.29	15.58	10.69	33.03	11.30
Cs	0.20	0.46	0.34	1.06	0.58	0.25	1.44	1.35	4.52	0.79	2.38	0.59	0.83	0.61
Ba	189.00	215.00	221.00	411.00	126.00	135.00	2324.00	2298.00	4001.00	945.70	979.50	802.80	78.30	503.30
La	27.50	8.55	11.70	13.30	14.30	15.60	67.70	85.09	53.34	47.47	44.30	103.60	65.94	80.87
Ce	61.60	20.60	27.90	29.90	27.50	35.00	138.00	172.30	115.60	87.41	79.41	196.30	135.80	144.80
Pr	7.88	2.78	3.68	3.72	3.93	4.43	15.70	20.52	16.11	11.08	9.49	22.39	16.42	16.40
Nd	35.90	13.10	16.80	16.30	17.50	19.80	63.20	80.66	69.52	41.33	33.80	83.58	61.52	60.76
Sm	9.64	4.15	4.54	4.17	4.53	5.32	12.30	13.67	12.44	7.17	5.55	14.73	11.68	9.65
Eu	3.47	1.21	1.50	1.38	1.47	1.84	4.31	5.62	7.78	0.95	1.29	1.82	0.37	0.93

Gd	10.30	5.10	5.49	4.50	3.93	5.64	10.80	12.26	10.87	6.27	4.80	12.44	10.91	8.55
Tb	1.45	0.88	0.95	0.69	0.58	0.87	1.47	1.76	1.68	0.99	0.70	1.53	1.67	1.13
Dy	6.91	5.32	5.50	3.74	3.39	5.13	8.02	8.25	8.37	5.46	3.75	5.91	9.44	4.99
Ho	1.21	1.16	1.14	0.77	0.72	1.10	1.65	1.54	1.67	1.18	0.73	0.97	1.68	0.89
Er	2.77	2.77	2.70	1.85	1.79	2.64	4.05	3.86	4.30	3.25	2.05	2.18	4.17	2.11
Tm	0.42	0.44	0.41	0.29	0.27	0.41	0.61	0.63	0.72	0.59	0.32	0.29	0.60	0.31
Yb	2.63	2.74	2.49	1.78	1.68	2.46	3.72	3.49	3.99	3.31	2.04	1.49	3.58	1.59
Lu	0.39	0.41	0.35	0.26	0.25	0.35	0.55	0.50	0.57	0.46	0.29	0.22	0.48	0.23
Hf	3.72	3.54	3.97	2.83	1.93	3.23	10.40	33.54	25.66	8.29	7.23	17.92	15.15	13.91
Ta	1.02	1.12	0.91	0.65	0.45	0.91	0.65	0.95	0.74	0.70	1.04	0.28	1.75	0.28
Pb	9.34	10.20	4.83	3.45	2.36	7.48	5.51	6.00	72.30	22.10	3.00	11.50	9.90	5.90
Th	1.91	1.27	1.73	2.34	1.65	1.80	4.95	7.98	5.39	9.59	11.73	20.91	14.98	11.95
U	0.70	0.60	0.38	0.57	0.34	0.43	0.69	0.65	1.15	1.53	1.76	1.40	0.91	0.73

wt%: weight percentage; ppm: part per million; --: not detected.

Supplementary Table 3

Supplementary Table 3. Electron microprobe analyses of typical mineral inclusions within zircon from the **meta-basites** and meta-granitoids from Longjingguan (wt%).

Sample	11LJG3								11LJG2				11LJG3			
Mineral	Ep	Ap	Hbl	Kfs	Bi	Ttn	Ilm	Pl	Ep	Bi	Kfs	Mus	Rt	Rt	Rt	
SiO ₂	40.86	0.15	44.01	63.57	57.18	30.55	0.20	63.52	37.62	34.03	60.31	46.31	SiO ₂	0.11	0.16	0.15
TiO ₂	0.68	0.00	0.82	0.00	0.68	36.88	49.40	0.03	0.23	3.17	0.00	0.16	Al ₂ O ₃	0.01	0.02	0.02
Al ₂ O ₃	24.72	0.00	9.07	17.71	24.22	0.98	0.00	22.98	15.66	14.15	23.63	30.51	MgO	0.00	0.00	0.00
FeO ^T	8.39	0.00	18.10	0.00	2.27	0.52	44.40	0.07	22.90	25.14	0.54	7.05	TiO ₂	99.53	99.69	99.83
MnO	0.05	0.00	0.21	0.02	0.00	0.02	1.79	0.00	0.51	0.48	0.08	0.09	FeO ^T	0.34	0.48	0.35
MgO	1.07	0.00	10.31	0.01	2.25	0.00	0.65	0.00	3.76	8.55	0.05	0.89	Cr ₂ O ₃	0.06	0.02	0.11
Na ₂ O	0.06	0.01	1.26	0.31	0.09	0.00	0.00	7.97	1.14	0.00	0.48	0.10	Nb ₂ O ₅	0.14	0.09	0.07
CaO	17.25	54.03	11.66	0.07	0.15	27.90	0.00	4.23	11.15	0.52	0.01	0.01	V ₂ O ₃	0.54	0.56	0.51
K ₂ O	2.48	0.01	0.96	17.42	8.77	0.00	0.00	0.25	2.38	6.97	15.65	10.66	MnO	0.01	0.01	0.01
P ₂ O ₅	0.02	40.59	0.00	0.02	0.14	0.01	0.01	0.00	0.00	0.00	0.00	0.00	ZrO ₂	0.30	0.29	0.35
Cr ₂ O ₃	0.01	0.02	0.10	0.00	0.00	0.06	0.09	0.00	0.04	0.02	0.00	0.01	F	--	--	--
NiO	0.00	0.00	0.01	0.01	0.02	0.02	0.06	0.00	0.00	0.02	0.01	0.00	Cl	--	--	--
F	0.07	4.18	0.06	--	--	--	--	--	--	--	--	--	Total	101.04	101.32	101.40
Cl	0.00	0.25	0.15	--	--	--	--	--	--	--	--	--	Zr(ppm)	2197	2107	2519
Total	95.62	97.42	96.65	99.14	95.76	96.94	96.60	99.05	95.38	93.05	100.75	95.79	T(°C)	843	839	860

The temperatures of sample 11LJG3 were estimated according to the Zr-in-rutile thermometer (Tomkins et al., 2007; P=10 kbar). --: not detected.

Supplementary Table 4. Electron microprobe analytical results of the rutile inclusions in zircon from the sample 11LJG3

Spot No.	1	2	3	4	5	6	7
SiO ₂	0.18	0.29	1.80	0.75	0.11	0.16	0.15
Al ₂ O ₃	0.03	0.02	0.28	0.01	0.01	0.02	0.02
MgO	0.01	0.00	0.02	0.00	0.00	0.00	0.00
TiO ₂	86.96	84.77	95.46	99.47	99.53	99.69	99.83
FeO	0.19	0.31	0.35	0.36	0.34	0.48	0.35
Cr ₂ O ₃	0.11	0.04	0.05	0.07	0.06	0.02	0.11
Nb ₂ O ₅	0.06	0.14	0.06	0.15	0.14	0.09	0.07
V ₂ O ₃	0.56	0.57	0.48	0.55	0.54	0.56	0.51
MnO	0.00	0.00	0.00	0.00	0.01	0.01	0.01
ZrO ₂	0.26	0.66	0.57	0.73	0.30	0.29	0.35
Total	88.39	86.80	99.08	102.09	101.04	101.32	101.40
Zr(ppm)	2196	5595	4235	5307	2197	2107	2519
T(°C)	843	966	926	958	843	839	860

Supplementary Table 5

 Supplementary Table 5. LA-ICPMS trace element analysis for zircons in the **meta-basites and meta-granitoids** from Longjingguan (ppm).

Spot No.	11LJG2_5.1	11LJG2_16.1	11LJG2_2.1	11LJG2_20.1	11LJG2_41.1	11LJG3_5.2	11LJG3_12.1	11LJG3_12.2	1209LJG5_9.1	1209LJG5_4.1	1202LJG3_4.1
Age(Ma)	2385	1938	845	797	730	771	768	746	845	785	750.4
Nb	2.87	3.57	1.6	1.43	1.67	3.07	1.05	2.11	0.53	2.71	0.96
La	1.57	0.04	0.01	0.00	0.03	0.00	0.00	0.03	0.09	0.05	0.19
Ce	17.26	12.02	25.39	3.25	1.11	16.30	9.15	18.82	3.70	7.88	12.33
Pr	0.99	0.08	0.15	0.07	0.16	0.00	0.08	0.07	0.35	0.05	0.20
Nd	6.59	0.77	2.54	0.65	1.99	0.35	0.00	1.29	4.54	1.13	3.54
Sm	3.57	1.26	3.86	1.23	1.64	0.44	0.45	1.98	7.04	1.72	5.17
Eu	0.73	0.11	1.52	0.75	1.05	0.64	0.05	1.67	2.87	0.42	1.37
Gd	11.49	12.25	16.06	7.98	7.34	12.88	4.70	9.17	27.31	9.12	24.75
Tb	3.63	4.25	4.98	2.85	2.06	5.67	2.36	5.10	8.40	3.49	8.57
Dy	42.67	51.37	55.84	32.45	23.00	64.94	23.88	56.85	92.57	42.06	93.47
Ho	15.94	18.12	20.47	12.99	8.53	27.62	11.10	23.59	31.97	16.69	34.53
Er	71.57	75.47	85.50	52.47	33.25	130.13	49.13	122.95	133.76	79.02	146.95
Tm	17.38	16.30	18.21	11.96	7.31	32.18	12.89	28.91	26.26	17.37	30.25
Yb	169.57	142.90	180.62	116.04	74.14	340.23	135.43	311.40	254.93	183.06	299.98
Lu	25.21	21.77	34.26	18.28	12.41	54.98	23.71	62.04	45.84	33.54	52.71
Hf	8290	8531	7250	5229	4281	8091	7839	8882	6063	8163	7269
Ta	0.88	1.16	0.27	0.20	0.09	0.70	0.41	0.73	0.22	0.96	0.54
Th	105.63	62.35	71.78	15.49	4.99	450.74	192.76	698.54	28.37	57.38	111.16
U	256.61	94.95	42.44	22.84	8.33	507.06	295.99	927.89	31.14	120.39	290.04
ΣREE	388.17	356.71	449.41	260.97	174.02	686.36	272.93	643.87	639.63	395.6	714.01

Supplementary Table 6

Supplementary Table 6. LA-ICPMS rare earth element analysis for zircons in the meta-basites and meta-granitoids from Longjingguan.

Spot No.	Age(Ma)	La	Ce	Pr	Nd	Sm	Eu	Gd	Tb	Dy	Ho	Er	Tm	Yb	Lu
11LJG2															
1.1	2492	0.00	4.77	0.04	1.29	3.26	1.19	14.34	5.38	61.10	22.22	91.62	21.86	207.84	35.66
2.1	8834	0.01	25.39	0.15	2.54	3.86	1.52	16.06	4.98	55.84	20.47	85.50	18.21	180.62	34.26
4.1	2304	0.06	7.30	0.00	0.10	0.83	0.45	3.75	1.32	17.59	6.55	31.57	8.88	99.09	16.57
5.1	2385	1.57	17.26	0.99	6.59	3.57	0.73	11.49	3.63	42.67	15.94	71.57	17.38	169.57	25.21
6.1	1786	0.00	2.48	0.05	1.08	2.13	1.16	12.87	3.74	42.35	14.39	55.60	11.92	107.63	16.10
7.1	1237	0.00	8.09	0.07	1.97	4.20	1.46	19.55	7.31	84.47	30.87	123.43	26.36	239.12	37.55
9.1	798	17.82	139.16	17.98	127.83	68.17	2.30	127.06	35.71	348.52	110.48	408.51	81.89	696.48	85.67
10.1	1325	0.01	34.35	0.08	1.75	5.93	0.80	36.79	15.99	215.02	82.14	337.69	71.47	612.21	76.61
11.1	1366	0.03	8.00	0.19	6.42	8.55	3.64	25.86	10.13	107.59	32.20	129.81	28.88	235.54	39.16
12.1	2492	3.79	26.83	2.76	16.93	9.70	2.22	28.90	9.63	91.03	30.40	126.42	27.96	269.74	35.52
13.1	810	0.00	32.70	0.20	4.27	6.42	1.33	38.66	14.40	174.13	63.68	253.10	54.57	489.55	69.90
15.1	2327	1.36	43.20	1.57	16.92	17.56	4.83	45.07	12.42	110.37	31.55	110.28	20.84	186.31	26.49
16.1	1938	0.04	12.02	0.08	0.77	1.26	0.11	12.25	4.25	51.37	18.12	75.47	16.30	142.90	21.77
18.1	837	0.00	3.32	0.22	2.84	5.07	3.35	20.59	7.74	74.48	27.76	109.03	21.62	214.26	39.59
19.1	1907	0.04	38.80	0.04	1.26	1.38	0.70	9.29	3.46	46.62	19.78	104.10	26.88	301.12	55.16
20.1	792	0.00	3.25	0.07	0.65	1.23	0.75	7.98	2.85	32.45	12.99	52.47	11.96	116.04	18.28
24.1	1936	0.04	27.21	0.10	2.04	4.32	0.52	13.83	5.09	53.37	17.44	68.95	14.38	136.53	18.00
24.2	1566	0.04	16.17	0.09	0.70	2.02	0.19	7.00	2.95	37.69	14.55	58.57	14.43	138.73	20.76
26.1	1325	0.03	29.14	0.09	2.39	4.59	0.11	26.17	9.88	123.99	46.50	194.82	42.32	394.55	58.12
27.1	1952	0.00	23.92	0.01	0.56	2.68	0.11	11.75	4.36	49.63	17.52	72.21	16.11	149.99	22.53
28.1	808	0.00	2.74	0.00	0.03	1.67	1.36	7.99	2.36	32.56	11.09	48.25	11.57	106.90	17.17
29.1	1645	0.10	4.66	0.07	0.30	0.25	0.11	3.37	1.58	21.89	9.63	47.03	13.14	145.33	26.07

32.1	826	0.00	5.62	0.06	0.90	1.71	0.33	7.24	3.35	34.93	13.83	63.25	14.07	125.54	23.69
32.2	803	0.00	7.01	0.01	0.68	2.50	0.77	17.98	6.89	83.06	30.97	121.93	26.03	225.50	35.89
40.1	2332	0.02	9.50	0.00	0.25	0.95	0.20	8.36	3.50	45.85	17.52	77.66	18.85	190.92	31.05
41.1	730	0.03	1.11	0.16	1.99	1.64	1.05	7.34	2.06	23.00	8.53	33.25	7.31	74.14	12.41
<hr/>															
11LJG3															
1.1	778	0.09	6.75	0.00	0.13	0.39	0.09	5.76	2.23	26.12	11.81	53.73	12.38	128.72	25.52
5.1	783	0.00	7.24	0.00	0.00	0.47	0.17	4.95	1.94	28.85	11.71	61.68	16.48	173.34	37.48
5.2	771	0.00	16.30	0.00	0.35	0.44	0.64	12.88	5.67	64.94	27.62	130.13	32.18	340.23	54.98
6.1	774	0.00	12.89	0.00	0.00	2.07	0.42	8.46	2.28	42.05	18.31	104.26	27.15	290.78	63.06
6.2	774	0.00	8.25	0.01	0.94	0.68	0.14	5.31	2.27	26.47	9.62	45.12	13.16	128.84	22.32
7.1	773	0.00	1.56	0.00	0.06	0.26	0.09	1.71	0.48	6.97	4.05	22.04	6.64	83.20	18.05
9.1	750	0.00	17.17	0.00	1.07	2.20	0.80	10.06	4.49	58.61	24.55	123.36	31.65	330.57	59.19
10.1	503	0.03	9.68	0.00	0.22	1.97	0.55	7.21	2.27	35.05	15.95	69.58	19.06	192.64	33.52
12.1	768	0.00	9.15	0.08	0.00	0.45	0.05	4.70	2.36	23.88	11.10	49.13	12.89	135.43	23.71
12.2	746	0.03	18.82	0.07	1.29	1.98	1.67	9.17	5.10	56.85	23.59	122.95	28.91	311.40	62.04
13.1	774	0.18	4.37	0.00	0.00	0.65	0.17	3.73	1.77	16.36	8.12	35.97	8.75	107.37	18.92
14.1	766	0.00	8.35	0.11	0.00	0.43	0.57	5.21	2.40	33.42	16.68	79.62	20.03	224.73	41.44
17.1	823	0.00	10.08	0.00	0.69	2.21	0.84	8.30	3.23	43.68	17.57	80.05	21.07	216.18	36.32
24.1	774	0.00	7.26	0.00	0.00	0.68	0.05	3.01	1.25	22.54	9.40	42.24	11.05	116.73	21.41
<hr/>															
11LJG7															
1.1	766	0.07	5.80	0.14	1.01	1.56	0.46	6.06	3.14	42.21	18.13	85.89	20.83	226.74	41.82
2.1	744	0.00	18.08	0.08	0.65	2.72	0.31	18.65	8.29	110.24	47.37	223.05	55.88	556.22	99.67
3.1	752	0.09	17.50	0.09	1.38	3.14	0.62	14.73	7.14	88.88	38.84	197.39	51.55	543.82	98.95
4.1	704	0.01	5.52	0.01	0.30	1.02	0.35	6.06	2.38	30.75	13.39	64.17	16.14	170.65	31.05
10.1	741	0.07	27.27	0.19	1.24	4.33	0.62	24.74	11.20	134.53	54.68	246.96	59.07	580.02	100.26
14.1	757	0.05	5.56	0.00	0.00	0.86	0.09	4.87	1.95	23.86	10.25	54.89	15.76	161.20	33.50

17.1	775	0.04	7.96	0.01	0.08	0.45	0.13	7.38	2.74	33.70	15.64	79.95	21.26	229.73	44.38
17.2	755	0.08	7.31	0.01	0.16	0.26	0.24	7.08	2.90	39.92	13.64	83.23	21.58	209.66	37.95
19.1	756	0.00	6.34	0.03	0.71	1.26	0.38	7.44	3.17	40.87	17.32	84.00	21.69	236.26	42.71
22.1	757	0.03	15.21	0.10	2.85	5.60	1.38	29.29	11.65	140.15	55.44	233.64	52.79	541.69	93.06
1209LJG5															
1.1	744	8.10	23.02	2.39	12.01	3.93	1.27	9.88	3.09	36.24	13.75	59.59	12.58	121.59	20.54
2.1	715	0.02	6.28	0.30	1.04	2.44	0.71	12.93	4.45	54.34	19.59	83.56	17.26	167.74	29.24
3.1	719	0.12	5.35	0.05	0.80	1.36	0.54	7.43	2.67	32.29	12.23	53.00	11.26	112.92	20.13
4.1	785	0.05	7.88	0.05	1.13	1.72	0.42	9.12	3.49	42.06	16.69	79.02	17.37	183.06	33.54
9.1	845	0.09	3.70	0.35	4.54	7.04	2.87	27.31	8.40	92.57	31.97	133.76	26.26	254.93	45.84
1202LJG3															
1.1	771	0.42	11.72	0.48	6.17	8.51	2.66	33.64	10.54	110.08	38.27	157.74	32.12	308.48	55.58
2.1	740	0.07	11.30	0.49	8.34	13.02	5.23	51.75	15.87	169.64	58.73	233.48	46.98	443.22	77.08
3.1	731	<0.01	4.44	0.12	2.18	2.28	0.81	9.90	3.58	40.93	15.88	76.43	17.86	191.16	38.75
4.1	750	0.19	12.33	0.20	3.54	5.17	1.37	24.75	8.57	93.47	34.53	146.95	30.25	299.98	52.71
9.1	760	0.20	24.51	1.13	19.45	27.05	9.90	102.12	29.57	304.04	100.81	397.44	76.58	695.61	118.29
11.1	837	0.05	10.07	0.38	6.28	9.53	3.59	41.40	12.45	133.20	45.85	187.42	37.81	350.54	61.25

Note: Ages are collected from Supplementary Table 7.

Supplementary Table 7

 Supplementary Table 7. SHRIMP zircon U-Pb isotope data for the **meta-basites** and meta-granitoids from Longjingguan.

Spot	Domain	Element (ppm)			Th/U	Isotopic ratio						Age (Ma)					
		U	Th	Pb		$^{207}\text{Pb}/^{206}\text{Pb}$	1 σ	$^{207}\text{Pb}/^{235}\text{U}$	1 σ	$^{206}\text{Pb}/^{238}\text{U}$	1 σ	$^{206}\text{Pb}/^{238}\text{U}$	1 σ	$^{207}\text{Pb}/^{206}\text{Pb}$	1 σ	$^{208}\text{Pb}/^{232}\text{Th}$	1 σ
11LJG2																	
1.1	C	25.3	8.2	10.3	0.33	0.1689	0.0046	10.9900	0.3847	0.4720	0.0109	2492	47	2547	45	2727	270
2.1	C	24.6	12.2	3.2	0.51	0.0560	0.0336	1.0600	0.6360	0.1382	0.0061	834	35	450	1300	675	430
3.1	M	86.8	34.7	10.8	0.41	0.1140	0.0100	2.2500	0.2025	0.1429	0.0030	861	17	1869	160	1733	170
4.1	C	351.9	177.9	130.0	0.52	0.1652	0.0014	9.7800	0.1858	0.4295	0.0073	2304	33	2510	14	2235	58
5.1	C	673.5	301.9	259.0	0.46	0.1602	0.0010	9.8880	0.0811	0.4478	0.0025	2385	11	2457	10	2334	39
6.1	M	46.5	37.2	13.3	0.83	0.1110	0.0178	4.9000	0.8330	0.3193	0.0089	1786	43	1820	300	1798	350
7.1	C	155.0	113.8	28.8	0.76	0.0811	0.0089	2.3700	0.2607	0.2115	0.0032	1237	17	1224	220	1225	130
9.1	C	343.0	210.0	39.3	0.63	0.0695	0.0067	1.2600	0.1222	0.1318	0.0013	798	7	914	200	807	68
10.1	C	472.1	184.3	92.5	0.40	0.0950	0.0013	2.9880	0.0478	0.2282	0.0015	1325	8	1528	27	1446	19
11.1	M	734.9	292.5	149.0	0.41	0.1320	0.0021	4.2960	0.0730	0.2359	0.0013	1366	7	2125	28	994	30
12.1	C	447.2	155.2	182.0	0.36	0.1661	0.0010	10.8080	0.0908	0.4719	0.0029	2492	13	2519	9	2481	42
13.1	C	139.4	111.8	16.4	0.83	0.0730	0.0168	1.3500	0.3105	0.1339	0.0029	810	17	1023	460	774	130
14.1	M	227.7	73.2	30.3	0.33	0.0948	0.0045	2.0020	0.0961	0.1532	0.0017	919	9	1524	88	1192	100
15.1	C	331.3	411.3	124.0	1.28	0.1596	0.0021	9.5600	0.1434	0.4346	0.0032	2327	14	2451	22	2223	41
16.1	C	204.6	145.2	62.9	0.73	0.1131	0.0054	5.4700	0.2680	0.3508	0.0039	1938	18	1849	87	1752	120
17.1	M	122.1	94.4	13.9	0.80	0.0770	0.0131	1.3500	0.2295	0.1263	0.0025	767	14	1128	330	934	100
18.1	M	30.1	24.3	4.1	0.83	0.1040	0.0582	2.0000	1.1200	0.1387	0.0096	837	54	1700	1000	--	--
19.1	C	814.6	613.6	242.0	0.78	0.1556	0.0009	7.3870	0.0554	0.3443	0.0017	1907	8	2409	9	1744	26
20.1	M	44.7	31.0	5.5	0.72	0.0800	0.0368	1.4400	0.6624	0.1307	0.0064	792	37	1201	910	1143	330
21.1	M	169.1	60.4	24.6	0.37	0.0784	0.0067	1.7700	0.1540	0.1635	0.0020	976	11	1157	170	954	110
23.1	M	77.7	58.8	22.8	0.78	0.1220	0.0031	5.6900	0.1707	0.3379	0.0054	1877	26	1986	45	1938	86

24.1	C	379.4	325.1	115.0	0.89	0.1247	0.0017	6.0240	0.0964	0.3504	0.0025	1936	12	2025	25	1895	55
25.1	C	497.8	37.7	212.0	0.08	0.1927	0.0015	13.1100	1.3110	0.4934	0.0031	2585	13	2765	13	2104	400
26.1	C	601.9	381.8	119.0	0.66	0.0855	0.0033	2.6900	0.1049	0.2281	0.0015	1325	8	1327	75	1209	54
27.1	C	401.6	301.3	123.0	0.78	0.1227	0.0033	5.9900	0.1677	0.3537	0.0027	1952	13	1996	47	1884	72
28.1	M	31.4	24.2	3.8	0.80	0.1360	0.0272	2.5000	0.5000	0.1336	0.0055	808	31	2172	350	1343	240
29.1	C	1715.1	229.4	429.0	0.14	0.1476	0.0007	5.9140	0.0337	0.2906	0.0010	1645	5	2318	7	1700	60
30.1	M	156.9	106.8	18.0	0.70	0.0660	0.0185	1.1400	0.3192	0.1245	0.0034	756	19	814	580	772	150
31.1	M	268.7	72.3	36.7	0.28	0.0760	0.0122	1.5900	0.2544	0.1524	0.0024	914	13	1085	310	692	310
32.1	M	147.8	94.0	17.9	0.66	0.0750	0.0135	1.4100	0.2538	0.1367	0.0026	826	15	1064	370	927	140
33.1	M	70.1	45.6	8.5	0.67	0.0650	0.0189	1.2200	0.3538	0.1355	0.0037	819	21	777	600	749	180
34.1	M	178.6	73.4	26.0	0.42	0.0780	0.0101	1.7700	0.2301	0.1638	0.0026	978	14	1158	260	1383	190
37.1	M	145.5	44.2	18.6	0.31	0.0950	0.0295	1.7400	0.5394	0.1321	0.0048	800	27	1534	580	1413	610
40.1	C	233.1	108.1	87.7	0.48	0.1674	0.0027	10.0600	0.1911	0.4358	0.0038	2332	17	2532	27	2331	110
32.2	C	421.0	333.9	48.7	0.82	0.0639	0.0062	1.1700	0.1147	0.1326	0.0013	803	8	737	210	738	50
35.1	M	44.0	34.4	5.6	0.81	0.1350	0.0297	2.6500	0.6095	0.1420	0.0054	856	30	2167	390	1431	310
36.1	M	121.4	75.7	12.6	0.64	0.0960	0.0269	1.4400	0.4032	0.1090	0.0034	667	20	1544	520	1027	210
38.1	M	112.6	68.6	13.2	0.63	0.0850	0.0170	1.5600	0.3120	0.1331	0.0025	805	14	1319	390	868	120
39.1	M	96.6	68.6	11.7	0.73	0.0720	0.0173	1.3200	0.3168	0.1338	0.0033	809	19	978	480	916	160
41.1	M	20.0	8.9	2.3	0.46	0.1360	0.0694	2.2000	1.1440	0.1200	0.0108	730	62	2174	890	1749	920
24.2	M	330.5	193.8	78.2	0.61	0.1240	0.0030	4.7000	0.1222	0.2750	0.0022	1566	11	2015	43	1694	39
30.2	C	504.9	499.2	56.9	1.02	0.0702	0.0037	1.2590	0.0680	0.1301	0.0010	788	6	934	110	775	24
11LJG3																	
1.1	M	140.4	86.3	16.0	0.64	0.0710	0.0107	1.2600	0.1890	0.1283	0.0019	778	11	966	310	827	120
2.1	M	141.5	80.4	14.8	0.59	0.0706	0.0054	1.1770	0.0906	0.1208	0.0017	735	10	947	150	739	55
3.1	M	778.5	475.2	82.0	0.63	0.0678	0.0018	1.1410	0.0319	0.1220	0.0007	742	4	863	57	737	20
4.1	C	657.9	472.6	71.6	0.74	0.0658	0.0022	1.1390	0.0387	0.1254	0.0008	762	4	801	71	711	19

5.1	M	527.1	361.2	58.5	0.71	0.0711	0.0018	1.2660	0.0329	0.1291	0.0009	783	5	961	52	802	16
6.1	C	308.2	171.1	34.6	0.57	0.0670	0.0154	1.1700	0.2691	0.1276	0.0026	774	15	826	480	737	180
7.1	M	188.7	106.6	21.1	0.58	0.0620	0.0112	1.0900	0.1962	0.1274	0.0022	773	12	679	380	721	120
8.1	M	415.2	292.8	44.4	0.73	0.0683	0.0010	1.1730	0.0188	0.1245	0.0009	757	5	878	30	776	12
9.1	C	1330.0	927.5	142.0	0.72	0.0625	0.0013	1.0620	0.0212	0.1233	0.0005	750	3	690	42	711	12
10.1	M	237.7	131.6	17.5	0.57	0.0550	0.0116	0.6100	0.1342	0.0812	0.0011	503	7	405	480	430	59
11.1	M	1138.3	881.6	123.0	0.80	0.0648	0.0020	1.1150	0.0346	0.1247	0.0007	758	4	769	65	755	20
12.1	M	777.7	511.8	84.8	0.68	0.0645	0.0032	1.1250	0.0563	0.1264	0.0008	768	5	759	100	733	29
13.1	M	648.8	452.7	71.9	0.72	0.0635	0.0058	1.1200	0.1030	0.1276	0.0012	774	7	724	200	727	52
14.1	M	622.0	404.1	68.0	0.67	0.0642	0.0044	1.1170	0.0771	0.1263	0.0009	766	5	747	140	730	36
17.1	C	148.4	84.5	18.2	0.59	0.0640	0.0205	1.2100	0.3872	0.1361	0.0034	823	19	756	680	871	230
18.1	C	735.1	657.0	82.3	0.92	0.0654	0.0033	1.1660	0.0583	0.1293	0.0008	784	5	788	100	758	22
19.1	C	260.8	168.9	28.8	0.67	0.0636	0.0062	1.1100	0.1077	0.1270	0.0014	771	8	729	200	744	65
20.1	C	677.0	815.5	12.6	1.24	0.0472	0.0066	0.1350	0.0189	0.0208	0.0002	133	1	60	340	131	9
21.1	C	36.8	29.6	4.8	0.83	0.0750	0.0608	1.4000	1.1340	0.1308	0.0085	793	48	1080	1600	693	420
22.1	M	400.0	286.3	45.6	0.74	0.0642	0.0077	1.1500	0.1380	0.1300	0.0014	788	8	750	260	794	62
6.2	M	201.2	130.3	22.3	0.67	0.0677	0.0081	1.1900	0.1428	0.1276	0.0018	774	11	859	260	727	78
4.2	M	2380.3	1485.2	258.0	0.64	0.0653	0.0065	1.1340	0.0147	0.1260	0.0010	765	6	783	21	729	9
12.2	C	2566.9	1856.4	271.0	0.75	0.0653	0.0065	1.1050	0.0111	0.1227	0.0004	746	2	785	21	710	5
23.1	C	3803.9	2568.4	73.6	0.70	0.0487	0.0030	0.1505	0.0093	0.0224	0.0001	143	1	133	140	144	6
24.1	M	526.9	320.2	58.1	0.63	0.0662	0.0015	1.1640	0.0279	0.1276	0.0009	774	5	812	48	728	15
5.2	C	968.1	1034.1	106.0	1.10	0.0639	0.0021	1.1200	0.0370	0.1271	0.0007	771	4	739	69	745	13
27.1	M	150.6	107.3	16.6	0.74	0.0710	0.0149	1.2200	0.2562	0.1235	0.0027	751	15	970	420	875	130
11LJG7																	
1.1	C	1380.3	1025.4	151.0	0.77	0.0640	0.0013	1.1140	0.0234	0.1262	0.0006	766	3	741	44	715	11
2.1	M	1493.7	925.5	158.0	0.64	0.0642	0.0026	1.0840	0.0444	0.1224	0.0006	744	4	749	86	716	26

3.1	C	1878.2	983.2	200.0	0.54	0.0646	0.0010	1.1020	0.0176	0.1237	0.0005	752	3	762	33	713	11
4.1	M	1424.2	931.4	142.0	0.68	0.0646	0.0012	1.0290	0.0185	0.1155	0.0005	704	3	763	38	673	10
5.1	M	1186.2	519.5	131.0	0.45	0.0628	0.0019	1.1050	0.0343	0.1277	0.0007	775	4	700	66	724	28
6.1	M	957.2	616.4	101.0	0.67	0.0651	0.0009	1.1010	0.0165	0.1226	0.0006	746	4	778	30	749	10
7.1	M	2184.0	1838.7	230.0	0.87	0.0633	0.0013	1.0650	0.0213	0.1220	0.0005	742	3	719	42	728	10
8.1	M	238.4	351.6	5.7	1.52	0.0970	0.0922	0.2800	0.2688	0.0209	0.0023	133	14	1560	1800	151	63
9.1	M	723.0	386.9	80.0	0.55	0.0649	0.0007	1.1520	0.0138	0.1288	0.0007	781	4	770	23	807	16
10.1	M	2808.3	2269.3	294.0	0.83	0.0669	0.0011	1.1230	0.0191	0.1219	0.0004	741	2	834	34	710	9
14.1	M	572.1	314.9	61.8	0.57	0.0671	0.0031	1.1540	0.0531	0.1246	0.0009	757	5	842	96	740	36
15.1	C	477.1	1364.0	8.8	2.95	0.0430	0.0323	0.1180	0.0885	0.0197	0.0007	126	5	-140	1900	118	10
17.1	C	1142.6	518.9	126.0	0.47	0.0681	0.0029	1.1990	0.0504	0.1277	0.0007	775	4	872	86	751	37
24.1	M	1674.6	1030.9	182.0	0.64	0.0660	0.0013	1.1510	0.0230	0.1265	0.0008	768	4	807	39	750	13
19.1	C	785.7	352.8	84.9	0.46	0.0641	0.0060	1.1000	0.1034	0.1244	0.0011	756	6	746	200	711	82
8.2	C	1611.5	4107.5	28.4	2.63	0.0451	0.0044	0.1260	0.0122	0.0202	0.0002	129	1	-49	240	121	2
22.1	M	2006.5	1767.6	216.0	0.91	0.0646	0.0006	1.1100	0.0222	0.1247	0.0021	757	12	760	20	723	13
17.2	M	651.2	358.1	70.2	0.57	0.0630	0.0020	1.0800	0.0356	0.1243	0.0015	755	9	708	66	707	22
25.1	M	1205.6	363.9	122.0	0.31	0.0628	0.0026	1.0060	0.0423	0.1163	0.0007	709	4	700	88	698	48
1303LJG2																	
1.1	C	301.4	252.9	34.8	0.87	0.0664	0.0009	1.2280	0.0184	0.1341	0.0012	811	7	820	26	776	10
2.1	C	194.8	311.4	22.3	1.65	0.0668	0.0018	1.2280	0.0356	0.1333	0.0013	807	7	831	57	774	10
3.1	C	312.7	147.1	32.4	0.49	0.0641	0.0012	1.0620	0.0223	0.1202	0.0011	732	6	745	39	853	16
4.1	M	352.2	388.5	42.4	1.14	0.0766	0.0034	1.4470	0.0666	0.1370	0.0012	828	7	1111	90	874	18
5.1	C	298.2	144.2	35.1	0.50	0.0638	0.0008	1.2030	0.0180	0.1367	0.0012	826	7	735	26	818	12
6.1	C	164.1	125.6	19.0	0.79	0.0625	0.0019	1.1580	0.0371	0.1343	0.0013	812	8	693	64	800	18
7.1	C	69.7	55.1	8.6	0.82	0.0620	0.0025	1.2170	0.0499	0.1424	0.0017	858	10	673	85	833	24
8.1	M	505.3	321.1	56.2	0.66	0.0650	0.0008	1.1570	0.0197	0.1292	0.0013	783	7	774	28	841	13

9.1	C	221.9	251.9	25.6	1.17	0.0657	0.0009	1.2150	0.0207	0.1342	0.0012	812	7	797	30	787	10
10.1	C	100.3	100.5	11.7	1.03	0.0649	0.0019	1.2150	0.0377	0.1357	0.0015	821	9	773	62	827	21
11.1	C	368.7	353.1	41.0	0.99	0.0660	0.0009	1.1750	0.0188	0.1291	0.0011	783	6	807	27	763	9
12.1	M	208.3	140.8	23.2	0.70	0.0645	0.0012	1.1530	0.0242	0.1296	0.0012	786	7	759	39	779	19
13.1	C	515.1	523.8	59.1	1.05	0.0640	0.0007	1.1760	0.0165	0.1334	0.0011	807	6	740	23	782	9
1202LJG3																	
1.1	C	221.0	78.7	24.2	0.37	0.0632	0.0015	1.1070	0.0277	0.1271	0.0010	771	6	715	50	769	22
2.1	C	166.9	152.9	17.5	0.95	0.0660	0.0020	1.1080	0.0343	0.1216	0.0010	740	6	808	62	734	15
3.1	C	139.3	34.1	14.4	0.25	0.0650	0.0016	1.0770	0.0280	0.1201	0.0012	731	7	776	52	682	28
4.1	C	373.9	55.0	39.8	0.15	0.0648	0.0011	1.1020	0.0187	0.1235	0.0007	750	4	767	35	712	33
5.1	C	214.5	55.0	23.7	0.27	0.0638	0.0021	1.1250	0.0383	0.1279	0.0009	776	5	735	70	670	38
6.1	C	38.4	56.8	4.4	1.53	0.0712	0.0056	1.3000	0.1027	0.1326	0.0024	802	13	963	160	854	31
7.1	C	82.8	73.6	9.0	0.92	0.0585	0.0041	1.0070	0.0715	0.1248	0.0015	758	9	550	150	769	29
8.1	C	195.4	42.5	20.1	0.22	0.0631	0.0015	1.0390	0.0260	0.1195	0.0009	728	5	711	50	746	32
9.1	M	68.0	35.2	7.4	0.54	0.0682	0.0049	1.1760	0.0858	0.1251	0.0016	760	9	874	150	812	56
10.1	M	98.7	106.8	10.4	1.12	0.0550	0.0253	0.7900	0.3634	0.1043	0.0023	640	14	400	1000	702	97
11.1	M	57.2	29.5	6.9	0.53	0.0656	0.0036	1.2540	0.0715	0.1387	0.0019	837	11	793	120	932	46
12.1	C	209.8	51.9	22.3	0.26	0.0649	0.0019	1.1040	0.0342	0.1233	0.0009	749	5	772	63	756	55
13.1	M	71.9	61.5	8.3	0.88	0.0648	0.0017	1.2030	0.0349	0.1347	0.0015	815	9	768	56	860	19
1209LJG5																	
1.1	M	19.1	10.6	2.0	0.57	0.0586	0.0064	0.9900	0.1089	0.1223	0.0028	744	16	554	230	651	65
2.1	M	147.4	145.1	14.9	1.02	0.0640	0.0014	1.0340	0.0238	0.1172	0.0008	715	5	741	47	682	10
3.1	M	46.5	38.8	4.7	0.86	0.0657	0.0031	1.0690	0.0513	0.1180	0.0014	719	8	797	98	747	18
4.1	M	117.9	47.9	13.2	0.42	0.0635	0.0023	1.1330	0.0419	0.1295	0.0010	785	6	724	76	800	55
5.1	C	121.1	107.1	14.4	0.91	0.0662	0.0019	1.2600	0.0365	0.1380	0.0012	833	7	813	58	841	17
6.1	M	55.8	30.7	12.6	0.57	0.1283	0.0021	4.6460	0.0976	0.2626	0.0032	1503	17	2075	29	1100	33

7.1	M	64.7	26.7	7.7	0.43	0.0680	0.0020	1.2950	0.0414	0.1381	0.0018	834	10	869	62	1071	32
8.1	M	61.8	45.3	20.9	0.76	0.1225	0.0018	6.6300	0.1193	0.3927	0.0043	2135	20	1994	26	2143	44
9.1	C	20.1	17.5	2.4	0.90	0.0769	0.0050	1.4900	0.1028	0.1401	0.0032	845	19	1118	130	906	40
10.1	C	581.2	725.1	184.0	1.29	0.1238	0.0006	6.2930	0.0422	0.3686	0.0017	2023	8	2012	9	2106	17
11.1	M	82.7	41.7	9.9	0.52	0.0694	0.0022	1.3280	0.0438	0.1389	0.0017	838	9	910	64	810	27
12.1	M	132.9	76.6	22.5	0.60	0.1013	0.0030	2.7280	0.0846	0.1953	0.0019	1150	10	1648	55	1198	53
13.1	M	27.8	18.8	3.3	0.70	0.0666	0.0041	1.2460	0.0797	0.1357	0.0028	820	16	825	130	805	39
14.1	C	926.4	371.1	277.0	0.41	0.1327	0.0006	6.3540	0.0343	0.3474	0.0010	1922	5	2133	8	1885	20
15.1	C	648.9	666.5	173.0	1.06	0.1209	0.0011	5.1610	0.0568	0.3095	0.0017	1738	8	1970	16	1612	26
6.2	C	198.9	27.8	73.7	0.14	0.1641	0.0018	9.7600	0.1269	0.4314	0.0030	2312	13	2498	19	2198	56
7.2	C	197.6	138.1	24.0	0.72	0.0647	0.0017	1.2590	0.0340	0.1410	0.0013	851	7	766	54	836	18

C: core; M: mantle; --: no data. Common Pb corrected using measured ^{204}Pb .

Supplementary Table 8

 Supplementary Table 8. MC-ICPMS zircon Hf isotope data for the **meta-basites and meta-granitoids** from Longjingguan.

Sample	$^{176}\text{Yb}/^{177}\text{Hf}$	$^{176}\text{Lu}/^{177}\text{Hf}$	$^{176}\text{Hf}/^{177}\text{Hf}$	$\pm(2s)$	Age (Ma)	$\varepsilon_{\text{Hf}}(t)$	$\pm(2\sigma)$	$T_{\text{DM1}}(\text{Ma})$	$\pm(2\sigma)$	$f_{\text{Lu/Hf}}$	$T_{\text{DM2}}(\text{Ma})$	$\pm(2\sigma)$
1303LJG2	0.0387	0.001604	0.282230	0.000043	783	-2.4	0.8	1466	61	-0.95	1853	95
	0.0806	0.001937	0.282118	0.000033	807	-6.5	0.6	1640	48	-0.94	2114	74
	0.0398	0.001477	0.282127	0.000033	783	-6.0	0.6	1607	47	-0.96	2079	73
	0.0988	0.002446	0.282211	0.000031	807	-3.5	0.6	1527	45	-0.93	1923	68
	0.0377	0.001614	0.282215	0.000030	811	-2.9	0.5	1488	43	-0.95	1889	67
	0.0593	0.002007	0.282092	0.000028	828	-7.5	0.5	1679	40	-0.94	2172	62
	0.0557	0.001634	0.282337	0.000023	858	1.4	0.4	1316	33	-0.95	1618	51
	0.0345	0.001251	0.282329	0.000019	811	1.3	0.3	1313	26	-0.96	1622	42
1202LJG3	0.1109	0.002578	0.282078	0.000041	749	-8.3	0.7	1727	59	-0.92	2213	91
	0.0269	0.001198	0.282069	0.000041	731	-7.9	0.7	1676	57	-0.96	2186	90
	0.0548	0.001727	0.282058	0.000039	802	-8.5	0.7	1715	55	-0.95	2227	86
	0.0238	0.000765	0.282017	0.000035	758	-9.5	0.6	1729	49	-0.98	2287	78
	0.0392	0.001070	0.282130	0.000032	728	-5.6	0.6	1585	45	-0.97	2047	71
	0.0490	0.001369	0.282025	0.000031	776	-9.5	0.6	1746	44	-0.96	2290	69
	0.0981	0.002896	0.282131	0.000034	771	-6.6	0.6	1663	49	-0.91	2104	75
1209LJG5	0.0226	0.000939	0.282059	0.000042	744	-8.1	0.8	1678	58	-0.97	2199	93
	0.0150	0.000460	0.281940	0.000028	715	-12.0	0.5	1820	39	-0.99	2446	62
	0.0295	0.001109	0.281978	0.000025	820	-11.0	0.5	1799	35	-0.97	2384	56
	0.0154	0.000590	0.282013	0.000024	845	-9.5	0.4	1726	33	-0.98	2289	52
	0.0241	0.000735	0.281304	0.000041	1738	3.3	0.8	2702	56	-0.98	2823	90

	0.0277	0.000773	0.281558	0.000039	2030	0.6	0.7	2359	54	-0.98	2574	86
	0.0266	0.000877	0.281363	0.000030	1922	5.1	0.6	2631	41	-0.97	2710	65
	0.0388	0.001323	0.282144	0.000024	798	-5.3	0.4	1575	34	-0.96	2023	54
	0.0136	0.000572	0.282078	0.000028	834	-7.2	0.5	1636	39	-0.98	2145	63
	0.0407	0.001459	0.282071	0.000026	810	-7.9	0.5	1685	36	-0.96	2191	57
11LJG2	0.0184	0.000737	0.281996	0.000029	837	-10.2	0.5	1756	41	-0.98	2332	65
	0.0740	0.002359	0.282219	0.000022	803	-3.2	0.4	1513	32	-0.93	1893	49
	0.0156	0.000652	0.281418	0.000022	2492	7.1	0.4	2542	30	-0.98	2506	48
	0.0067	0.000306	0.281316	0.000022	2304	4.1	0.4	2656	29	-0.99	2690	48
	0.0237	0.001066	0.281363	0.000019	1907	-6.6	0.4	2643	26	-0.97	3758	42
	0.009640	0.000425	0.282450	0.000019	778	5.6	0.3	1118	26	-0.99	1326	41
	0.031623	0.001417	0.282520	0.000018	746	7.6	0.3	1049	25	-0.96	1203	40
11LJG3	0.015560	0.000686	0.282458	0.000018	774	5.8	0.3	1114	26	-0.98	1316	41
	0.018829	0.000831	0.282519	0.000020	762	7.9	0.4	1033	28	-0.97	1184	45
	0.017119	0.000886	0.282411	0.000021	774	4.0	0.4	1187	30	-0.97	1429	48
	0.030741	0.001317	0.282453	0.000020	750	5.3	0.4	1140	29	-0.96	1347	45
	0.011368	0.000510	0.282476	0.000014	766	6.5	0.3	1085	20	-0.98	1271	32
	0.018567	0.000814	0.282433	0.000017	741	4.8	0.3	1153	24	-0.98	1377	39
11LJG7	0.027072	0.001152	0.282425	0.000018	775	4.3	0.3	1175	26	-0.97	1405	40
	0.023857	0.001042	0.282428	0.000019	744	4.5	0.3	1168	27	-0.97	1396	43
	0.041313	0.001769	0.282501	0.000020	752	6.7	0.4	1085	29	-0.95	1256	45

0.021598	0.000954	0.282501	0.000022	746	7.1	0.4	1062	30	-0.97	1229	48
0.031613	0.001363	0.282378	0.000018	742	2.6	0.3	1248	25	-0.96	1518	39
0.017878	0.000776	0.282469	0.000020	781	6.1	0.4	1101	28	-0.98	1294	44

$\epsilon_{\text{Hf}}(t)$ values are calculated at 780 Ma and 800 Ma for **meta-basites** and meta-granitoids, respectively, and at the zircon U-Pb ages for the older inherited zircon domains. Age data were obtained by in-situ zircon SHRIMP U-Pb analyses.

Supplementary Table 9Supplementary Table 9. Sr-Nd isotope compositions for the **meta-basites** from Longjingguan.

Sample	Rb (ppm)	Sr(ppm)	$^{87}\text{Rb}/^{86}\text{Sr}$	$^{87}\text{Sr}/^{86}\text{Sr}$	$(^{87}\text{Sr}/^{86}\text{Sr})_i$	Sm (ppm)	Nd (ppm)	$^{147}\text{Sm}/^{144}\text{Nd}$	$^{143}\text{Nd}/^{144}\text{Nd}$	$\epsilon_{\text{Nd}}(t)$	T_{DM1} (Ma)	T_{DM2} (Ma)
11LJG3	16.0	320	0.1423	0.705386	0.7049	9.64	35.9	0.1626	0.512559	-0.5	1768	1051
11LJG4	29.6	129	0.7176	0.708677	0.7063	4.15	13.1	0.1888	0.512532	-1.8	3773	1156
11LJG5	27	261	0.2865	0.707254	0.7063	4.54	16.8	0.1606	0.512674	1.8	1368	862
11LJG6	62.9	116	1.6997	0.709376	0.7038	4.17	16.3	0.1541	0.512511	-1.2	1634	1106
11LJG7	32.9	87	1.2153	0.706262	0.7023	4.53	17.5	0.1515	0.512546	-0.5	1483	1044
11LJG8	27.7	225	0.3828	0.707910	0.7067	5.32	19.8	0.1611	0.512634	1.0	1498	927

Supplementary Table 10. Pb isotopic compositions for the meta-basites from Longjingguan.

Sample	$^{206}\text{Pb}/^{204}\text{Pb}$	$^{207}\text{Pb}/^{204}\text{Pb}$	$^{208}\text{Pb}/^{204}\text{Pb}$	Pb(ppm)	Th(ppm)	U(ppm)	$(^{206}\text{Pb}/^{204}\text{Pb})_i$	$(^{207}\text{Pb}/^{204}\text{Pb})_i$	$(^{208}\text{Pb}/^{204}\text{Pb})_i$
11LJG3	17.127	15.403	38.119	9.34	1.91	0.70	16.959	15.394	37.969
11LJG4	17.046	15.397	38.149	10.20	1.27	0.60	16.914	15.391	38.058
11LJG5	17.192	15.424	38.209	4.83	1.73	0.38	17.015	15.415	37.946
11LJG6	17.216	15.405	38.304	3.45	2.34	0.57	16.843	15.386	37.806
11LJG7	17.308	15.440	38.344	2.36	1.65	0.34	16.982	15.424	37.829
11LJG8	17.235	15.467	38.190	7.48	1.80	0.43	17.105	15.460	38.013